Why Molecules Look the Way They Do in STM: A Systematic Functional Group Approach

Thesis by

Christopher L. Claypool

Submitted in Partial Fulfillment of the Requirements for the

Degree of Doctor of Philosophy

California Institute of Technology

Pasadena, California

1999

(Submitted August 24, 1998)

Acknowledgments

One of the great things about Caltech is the eagerness of people to work together, and this thesis is certainly another example of that. This work represents the combined efforts of several people, including Rudy Marcus, Harry Gray, Cecco Faglioni, Bill Goddard, Adam Matzger, and Nate Lewis. Many thanks go to them for their help and guidance along the way. Rudy was instrumental in helping me get started with this project, and contributed throughout with helpful discussions and great ideas. He is also responsible for the work on the image symmetry with respect to bias polarity. Harry came up with the HOMO-IP idea that pretty much guided our thoughts for the entire project. Cecco performed all of the calculations, and was an integral part of this work. Bill was a great person to have around during some of our round table discussions and really contributed some great ideas, and Adam recently joined the project and made the molecules in Chapter 3. Most of all, this was just a fantastic group of people to interact with.

Nate deserves his own paragraph--he is a tremendous advisor and a great person. His enthusiasm is contagious and his scientific intuition is really a neat thing to observe. I have learned a lot from him, and for that I owe him a great deal. There is one major fault with Nate, though--his taste in football teams is awful! One other thing: never, never bet Nate a six pack of Diet Coke.

The Lewis group was a fine bunch to work and interact with. There are too many people to list individually, so many thanks goes to everyone in the group, past and present. From the EXAFS project to group meetings to Ragers, the group could always be counted on for some interesting times.

I wish also to acknowledge Professors Jack Beauchamp and Mitchio Okumura for what they taught me about building instruments while I was a TA for Chem 6. I

especially enjoyed lunches with Jack when he would take me flying, and I owe Mitchio many thanks for his part in helping me get my foot in the door at Bell Labs.

Another excellent aspect of Caltech is the many interesting people it attracts, and activities outside of work have introduced me to some truly great people on the campus. So thanks goes to all the guys on the Caltech Hockey team and Motorcycle Club for all the good times. Thanks also goes to Mike, Ray, and Guy in the Chemistry shop for helping with some of my extracurricular activities in their spare time.

One special note to George--it looks like I have won the bet.

Abstract

A series of functionalized alkanes and/or alkyl alcohols have been prepared and imaged by scanning tunneling microscopy (STM) methods on graphite surfaces. The stability of these ordered overlayers has facilitated reproducible collection of STM images at room temperature with sub-molecular resolution, in most cases allowing identification of individual hydrogen atoms in the alkane chains, but in all cases allowing identification of molecular length features and other aspects of the image that can be unequivocally related to the presence of functional groups in the various molecules of concern. Functional groups imaged in this study include halides (X=F, Cl, Br, I), amines, alcohols, nitriles, alkenes, alkynes, ethers, thioethers, allenes, and disulfides. The dominance of molecular topography in producing the STM images of alkanes and alkanols was established experimentally and also was consistent with quantum chemistry calculations. For molecules in which electronic effects overwhelmed topographic effects in determining the image contrast, a simple model is presented to explain the variation in the electronic coupling component that produces the contrast between the various functional groups observed in the STM images. Additionally, a theoretical model based on perturbation theory has been developed to predict the scanning tunneling microscopy (STM) images of molecules adsorbed on graphite. The model is applicable to a variety of different molecules with reasonable computational effort and provides images that are in qualitative agreement with experimental results. The computations correlate well with the STM data of functionalized alkanes and allow assessment of the structure and orientation of most of the functionalized alkanes that have been studied experimentally. In addition, the computations suggest that the highly diffuse virtual orbitals of the adsorbed molecules, despite being much farther in energy from the Fermi level of the graphite than the occupied orbitals, may play an important role in determining the STM image contrast of such systems.

Table of Contents

List of Figures

Chapter 1

Chapter 2

Chapter 3

List of Tables

Chapter 1

Chapter 2

Chapter 1

The Source of Image Contrast in STM Images of Functionalized Alkanes on Graphite: A Systematic Functional Group Approach

Abstract

A series of functionalized alkanes and/or alkyl alcohols have been prepared and imaged by scanning tunneling microscopy (STM) methods on graphite surfaces. The stability of these ordered overlayers has facilitated reproducible collection of STM images at room temperature with sub-molecular resolution, in most cases allowing identification of individual hydrogen atoms in the alkane chains, but in all cases allowing identification of molecular length features and other aspects of the image that can be unequivocally related to the presence of functional groups in the various molecules of concern. Functional groups imaged in this study include halides (X=F, Cl, Br, I), amines, alcohols, nitriles, alkenes, alkynes, ethers, thioethers, and disulfides. Except for -Cl and -OH, all of the other functional groups could be distinguished from each other and from -Cl or -OH through an analysis of their STM metrics and image contrast behavior. The dominance of molecular topography in producing the STM images of alkanes and alkanols was established experimentally and also was consistent with quantum chemistry calculations. Unlike the contrast of the methylene regions of the alkyl chains, the STM contrast produced by the various functional groups was not dominated by topographic effects, indicating that variations in local electronic coupling were important in producing the observed STM images of these regions of the molecules. For molecules in which electronic effects overwhelmed topographic effects in determining the image contrast, a simple model is presented to explain the variation in the electronic coupling component that produces the contrast between the various functional groups observed in the STM

images. Additionally, the bias dependence of these STM images has been investigated and the contrast vs. bias behavior is related to factors involving electron transfer and hole transfer that have been identified as potentially being important in dominating the electronic coupling in molecular electron transfer processes.

I. Introduction

Scanning tunneling microscopy (STM) images of molecules, obtained at the resolution of individual atoms and/or functional groups, has potential for providing spatial information on electronic coupling matrix elements that are important in a variety of heterogeneous and homogeneous electron transfer processes. Although the scanning tunneling microscope[1] (STM) has been used to investigate a rapidly growing list of organic materials at surfaces and interfaces,[2] the mechanisms of electron transport through insulating organic materials are still under debate. It is thus of great theoretical and experimental interest to understand, in a systematic fashion, the factors that control the spatial image contrast in a molecular-resolution STM image.

A significant experimental barrier to advancing this subject is the lack of a controlled method of sample preparation which allows the collection of reproducible STM images that can be unequivocally assigned to the molecule of interest. At room temperature, isolated molecules are generally mobile on surfaces, and such mobility during a lateral scan with the STM tip is thought to prevent collection of reproducible STM images. In cases where individual, isolated STM images assignable to molecular features have been obtained,[3] there is a question as to whether the image actually corresponded to a region of the surface where the molecule of interest resided or whether it corresponded to a surface defect and/or tip-related imaging artifact.[4] In some cases, molecules apparently migrate to step edge sites and must be located by sorting through a large number of images that do not display the molecule of interest.[5] In other cases, defects have been shown to produce STM images that resemble biomolecules or other possible molecular species.[6a] Approaches to obviate this problem include preparation of

molecular corrals[6b] in which molecules might be immobilized, or the development of strategies to attach molecules covalently in a reproducible, defined fashion to smooth, STM-compatible substrates.

Another approach to circumvent this problem is to study surface/molecular overlayer combinations that spontaneously yield ordered domains of well-defined molecular monolayers. In this fashion, the same molecular structure can be reliably prepared, and observed experimentally, over a variety of experimental trials. In such systems, the STM data can be assigned with confidence to the molecule of concern. Systematic variation of the molecular size can then be used to lend confidence to the association between the object in the image and the molecule of interest; additionally, systematic variation in the identity of individual functional groups can be used to establish a relative contrast scale for probing the variation in tunneling current between sections of a molecule and/or between various types of molecules. We have adopted this strategy in this study, which was designed to elucidate several aspects of STM image contrast and to relate these features to factors thought to control electron transfer matrix elements in intramolecular and intermolecular donor/acceptor charge transfer reactions.

The basis for our work is the demonstration that long chain alkanes and alcohols adsorb from non-polar solutions to form single, close-packed monolayers on graphite. This process has been investigated through measurement of adsorption isotherms, enthalpies of adsorption, and adsorbed surface mass measurements.[7-10] Only a single monomolecular layer of alkanes absorbs onto highly ordered pyrolytic graphite surfaces at room temperature, and the measured heat of adsorption increases uniformly with the chain length (~ 0.94 kJ/mol for each methylene unit), reaching 209 kJ mol^{-1} for dotriacontane ($C_{32}H_{66}$).[10, 11] There has been some debate about whether the alkane adsorption is driven by adsorbate-substrate interactions or by lateral intermolecular interactions, but recent evidence tends to point toward the latter.[12, 13] These reproducibly prepared, ordered overlayers have proven to be very amenable to study with the STM.

Since the first report of imaging an alkane monolayer on graphite with a scanning tunneling microscope,[14] several reports have described images of functionalized alkanes, including alcohols,[12, 15-17, 19, 20] carboxylic acids,[12] dialkyl-substituted benzenes, [12, 18] disulfides,[19] thiols,[20] amines,[20b] and halides.[20] X-ray diffraction studies of alkane and alkanol monolayers on graphite confirm that the STM images of these organic molecules have revealed the actual arrangements of the molecules adsorbed on graphite.[21]

Unlike several other systems in the literature we have tried to reproduce, we have found that monolayers of these simple alkanes and alkanols on graphite yield highly reproducible STM images. Based on the reproducibility of this system and its simplicity, we have chosen this class of organic molecules to study the mechanisms underlying STM image contrast. Towards this end, a series of functionalized alkanes and/or alkyl alcohols have been prepared and imaged on graphite surfaces. We have stored over 500 images and have observed reproducible behavior during over 100 imaging sessions with almost 20 different molecules in this system. The stability of these ordered overlayers has facilitated collection of STM images at room temperature with sub-molecular resolution, in most cases allowing identification of individual hydrogen atoms in the alkane chains, but in all cases allowing identification of molecular length features and other aspects of the image that can be unequivocally related to the presence of functional groups in the various molecules of concern. This combination of reproducibility and sub-molecular resolution has allowed us to establish a contrast scale of the tunneling current for individual functional groups relative to the tunneling current over methylene groups in an alkane chain, and to relate these relative contrast features to matrix elements used to compute electronic coupling terms in electron transfer reactions. Functional groups investigated in this study include halides (X=F, Cl, Br, I), amines, alcohols, nitriles, alkenes, alkynes, ethers, thioethers, and disulfides. Additionally, we have investigated the bias dependence of these images to probe issues related to electron transfer vs. hole transfer that have been

identified as potentially being important in dominating the electronic coupling in molecular electron transfer processes.

II. Experimental

Samples were prepared by placing a 6 μl droplet of a solution of the organic compound (typically 1-10 mg/ml) in phenyloctane (except for decanol, which was used neat) onto a freshly cleaved, highly oriented pyrolytic graphite surface (HOPG, Union Carbide). A mechanically prepared Pt/Ir tip was then immersed into the liquid droplet and the imaging (Nanoscope III, Digital Instruments, Santa Barbara, CA) was performed at the liquid/graphite interface. All of the images presented were obtained at constant current in the variable height mode. Bright portions of the images displayed herein correspond to points at which the tip retracted away from the surface in order to maintain a constant current. Nearly every prepared sample yielded evidence of the adsorbed monolayer in the STM image; however, several different tips were sometimes necessary to achieve high resolution images.

The lattice spacing of graphite (2.46 Å) was used as the calibration standard for the x and y piezo dimensions. The height of a step edge on a graphite surface was determined to be 3.4 Å using the manufacturer's specifications for the z-piezoelectric coefficient of the ceramic. Since the separation between graphite layers is 3.35 Å, the manufacturer's specification for the z-piezo dimension was used in computing all z-corrugation values reported in this work. Metrics were determined using Nanoscope III software, and the apparent heights of heteroatoms and groups are reported with respect to the average height of the image over the methylene portion of the adsorbed molecule. Errors in the distances quoted in this manuscript include our estimates of the measurement errors associated with determining the metrics from the images as well as the reproducibility of these metrics over various experiments. Images that displayed excessive thermal drift were not analyzed. To reduce noise, after data collection the images were filtered using Nanoscope III software. The filtering was primarily performed

to enhance the visual presentation of the printed images, but the filtering was performed in such a way that it did not distort any of the primary metrics evident in the original data nor did the filtering procedure introduce any new spot patterns or new topographic features into an image.

Pentatriacontane (TCI), tetradecanol (Aldrich), dodecanol (Aldrich), decanol (Aldrich), 1, 12-dodecanediol (Aldrich), 1, 14-tetradecanediol (Aldrich), 12-bromo-1-dodecanol (Aldrich), hexadecyldisulfide (Lancaster), tetradecyl sulfide (TCI), hexadecyl ether (TCI), stearone (TCI), trans-17-pentatriacontene (Aldrich), 7-hexadecyn-1-ol (Lancaster), and dioctadecylamine (Pfaltz & Bauer) are commercially available and were used as received. The molecules containing fluoro-, chloro-, iodo-, and nitrile- groups were synthesized as described below.[22]

Synthesis of $\mathbf{CF_3(CF_2)_3(CH_2)_{10}OH}$. After flushing with nitrogen, perfluorobutyl iodide, 9-decen-1-ol, and a catalytic amount of azo-bis-isobutyronitrile, AIBN, were added to an ampoule fitted with a Teflon stopcock. The ampoule was sealed and heated to 70 °C for 24 h. The resulting solution was transferred to a flask equipped with a condenser and a catalytic amount of AIBN. After heating to 60 °C, tributyltin hydride was added over a period of 40 minutes, and the solution was allowed to stir for 4 h. Multiple distillations at 164 °C and 3 mm Hg gave the desired product. ^{1}H NMR ($CDCl_3$) 1.39 (s, 14 H), 1.58-1.69 (m, 2 H), 1.98-2.18 (m, 2 H), 2.34 (s, 1 H), 3.65 (t, 2 H). ^{13}C NMR ($CDCl_3$) 13.4, 16.8, 20.1, 26.7, 27.1, 28.8-28.9 (m, 2 C), 31.8-32.0 (m, 1 C), 33.2, 63.6, 120.8 (m, 4 C). Anal. Calcd. for $C_{14}H_{21}F_9O$: C, 44.68 ; H, 5.63. Found: C, 44.33; H, 6.12.

Synthesis of $\mathbf{CF_3(CH_2)_{11}OH}$. Using a similar procedure, an ampoule was filled with undecylenyl alcohol, trifluoromethyl iodide, and a catalytic amount of AIBN. The ampoule was sealed and heated to 70 °C for 24 h. The resulting solution was transferred to a flask equipped with a condenser and a catalytic amount of AIBN. After heating to 60 °C, tributyltin hydride was added over a period of 40 minutes and the solution was

allowed to stir for 4 h. Multiple distillations at 50 mm Hg and 86 °C gave the desired product, m.p. 27 °C. ^{1}H NMR ($CDCl_3$) 1.38 (s, 22 H), 1.58-1.62 (m, 2 H), 1.78 (s, 1 H), 2.02-2.21 (m, 2 H), 2.72 (t, 2 H). Anal. Calcd. for $C_{12}H_{23}F_3O$: C, 59.98; H, 9.65. Found: C, 58.21; H, 9.17.

Synthesis of **$Cl(CH_2)_{12}OH$**. 2 g of 1,12-dodecanediol were refluxed for 24 h in the presence of petroleum ether (2 ml) and concentrated HCl (26.3 ml). Petroleum ether (13 ml) was then added to the hot reaction mixture, and the organic layer was removed. Another 10 ml of petroleum ether was added to the reaction mixture, and the organic layer was removed and combined with the previous extract. The combined extract was cooled, and the precipitated diol was removed. Distillation of the resulting oil at 2 mm Hg and 95 °C gave the dichloride, and the desired product was collected at 2 mm Hg and 100 °C. ^{1}H NMR ($CDCl_3$) 1.38 (s, 16 H), 1.53-1.64 (m, 2 H), 1.78-1.89 (m, 2 H), 3.58 (t, 2 H), 3.72 (t, 2 H). Anal. Calcd. for $C_{12}H_{25}ClO$: C, 65.28; H, 11.41. Found: C, 64.29; H, 11.48.

Synthesis of **$I(CH_2)_{12}OH$**. 1 g of 12-bromododecanol was dissolved in 25 ml of butanone. 0.75 g of NaI was added to this solution, and the mixture was refluxed for 1 h. The mixture was then filtered and the solvent removed. The product was purified by dissolving in pentane, removal of solvent, and filtering the resulting solid. ^{1}H NMR ($CDCl_3$) 1.38 (s, 16 H), 1.56-1.68 (m, 2 H), 1.81-1.95 (m, 2 H), 3.22 (t, 2 H), 3.72 (t, 2 H). Anal. Calcd. for $C_{12}H_{25}IO$: C, 46.16; H, 8.07. Found: C, 46.21; H, 8.12.

Synthesis of **$NC(CH_2)_{12}OH$**. In a three necked flask, 1 ml of water was added to 0.96 g of NaCN, and the solution was heated until the mixture dissolved. A solution of 12-bromododecanol in 50 ml of methanol was added to the NaCN solution over a period of five minutes, and the mixture was refluxed for 24 h. The solvent was removed and the product was purified by column chromatography (30% ethyl acetate, 70% hexane). ^{1}H NMR ($CDCl_3$) 1.37 (s, 16 H), 1.40-1.51 (m, 2 H), 1.64-1.77 (m, 2 H), 2.39 (t, 2 H), 3.69 (t, 2 H). ^{13}C NMR ($CDCl_3$) 17.7, 36.1, 36.7, 38.0, 39.7, 43.6, 63.9, 120.4. Anal. Calcd. for $C_{13}H_{25}NO$: C, 73.88; H, 11.92; N, 6.63. Found: C, 73.94; H, 11.86; N, 6.57.

III. Results

1. STM Images of Alkanes and Alkanols

Figure 1a-c displays representative STM images for three different molecular monolayers on highly ordered pyrolytic graphite: $C_{10}H_{21}OH$, $C_{12}H_{25}OH$, and $C_{14}H_{29}OH$. For comparison, Figure 1d displays a representative STM image obtained, under nominally identical conditions, from a monolayer of pentatriacontane ($C_{35}H_{72}$) adsorbed on graphite. These images were highly reproducible under our conditions, and are representative of the many hundreds of images obtained of these monolayers over numerous independent trials.

The prominent features of these images clearly can be assigned to the structure of the molecules in the graphite overlayer. In each case, lamellae were observed. In images of the alkane and alkanol overlayers, molecules in adjacent lamellae are staggered by half a molecular width.[14, 21] The metrics of interest in the images are schematically indicated in Figure 1e. Figure 1f shows average line scans for these three images taken perpendicular to the lamellae. The mean length, *a*, of the lamellae was 26.7, 32.4 and 38.0 (±0.5) Å for the C_{10}, C_{12}, and C_{14} alkanol overlayer, respectively . For the overlayer derived from the $C_{35}H_{72}$ alkane, the lamellae had a mean length of 47.5±0.5 Å, while those of $C_{36}H_{74}$ had a mean length of 48.8±0.5 Å. The mean molecular lengths of 14.7, 17.6 and 19.9 Å for the C_{10}, C_{12}, and C_{14} alkanols, respectively, and 47.5 Å for $C_{35}H_{72}$ and 48.8 Å for $C_{36}H_{74}$ correspond quite well with the lengths of the all trans- conformations that are calculated using the standard bond length values and van der Waals radii for the terminal atoms of these molecules. These lengths are 14.1, 16.7, 19.2 Å for the C_{10}, C_{12}, and C_{14} alkanols, respectively, and 45.4 Å for $C_{35}H_{72}$ and 46.7 Å for $C_{36}H_{74}$. Additionally, the unit cell dimensions determined from the STM data are in excellent agreement with the unit cell dimensions observed in previous low angle X-ray diffraction studies of alkanol monolayers on graphite (Table 1).[21]

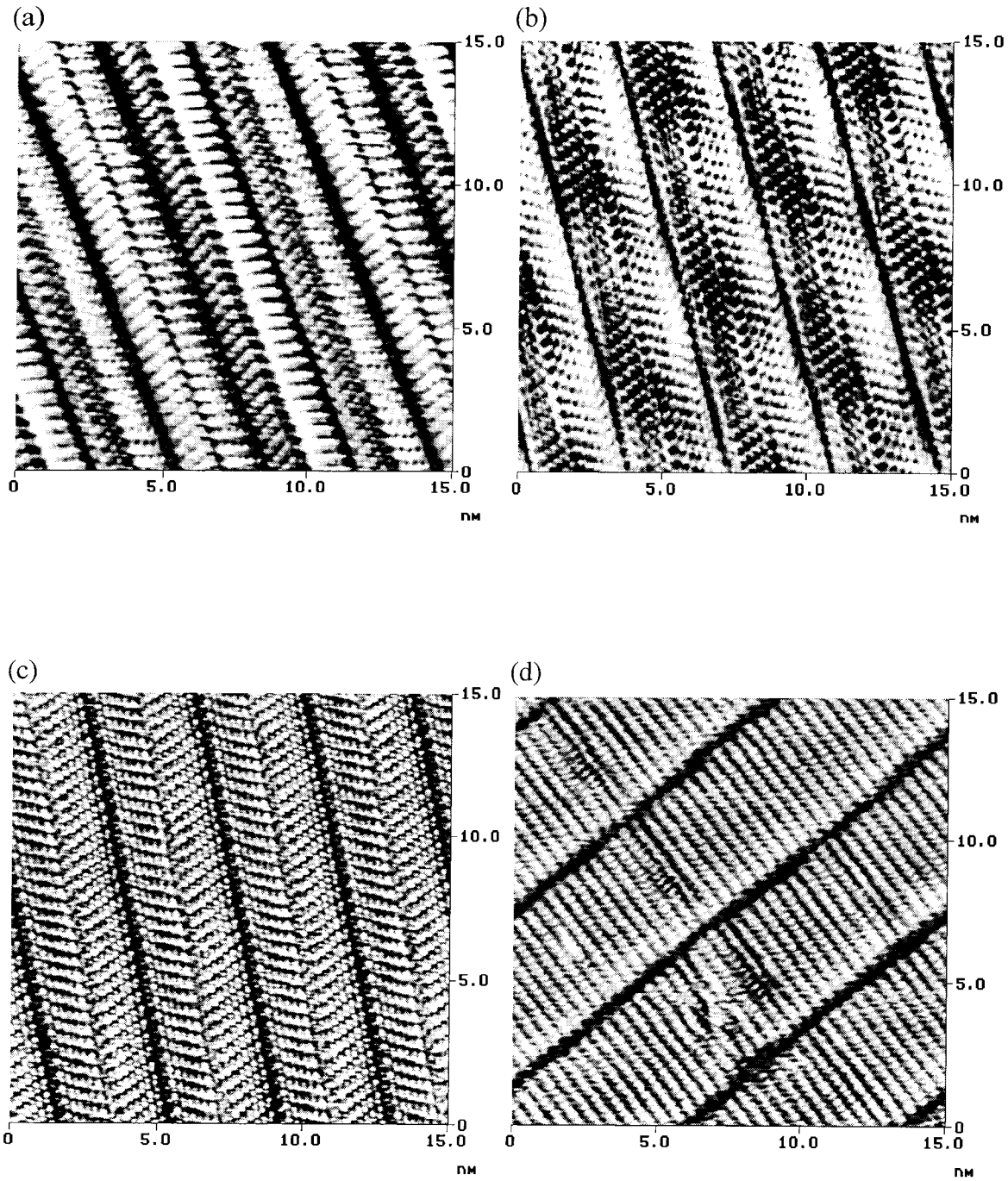
(a)
(b)
(c)
(d)
15.0
10.0
5.0
0
0
5.0
10.0
15.0
nm

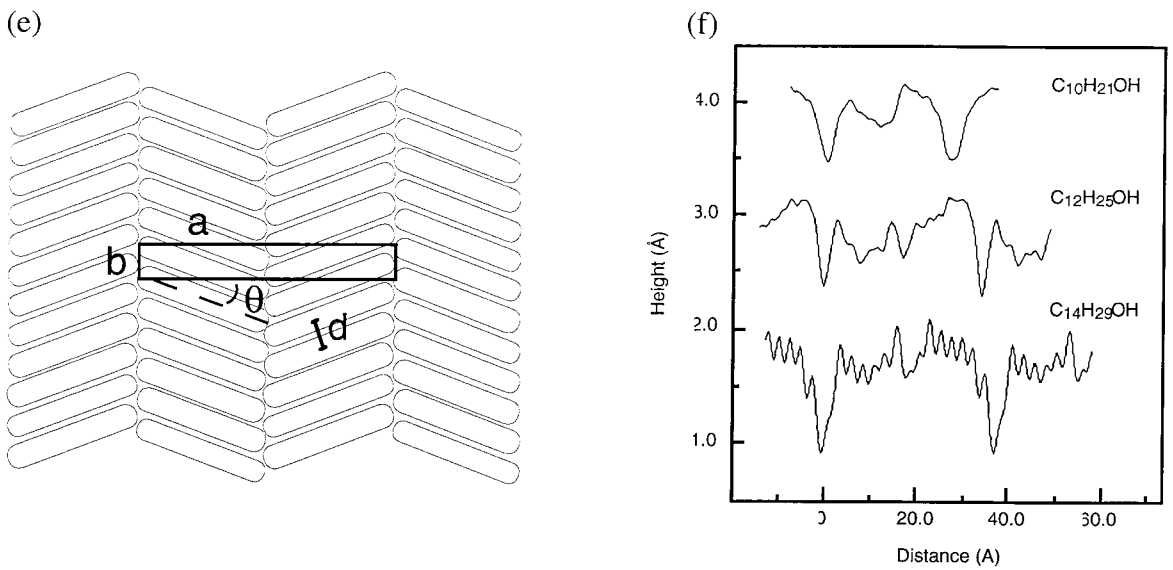

Figure 1. (a) Constant current STM image of a monolayer of decanol ($C_{10}H_{21}OH$) molecules adsorbed on a graphite surface (V=1.015 volt, I=650 pA, line direction=left, frame direction=down). (b) STM image of a monolayer of dodecanol ($C_{12}H_{25}OH$) molecules adsorbed on graphite (V=1.210 volt, I=650 pA, line direction=down, frame direction=left). (c) STM image of a monolayer of tetradecanol ($C_{14}H_{29}OH$) molecules adsorbed on graphite (V=1.127 volt, I=650 pA, line direction=right, frame direction=up). (d) STM image of a monolayer of pentatriacontane ($C_{35}H_{72}$) molecules on graphite (V=-1.611 volt, I=650 pA, line direction=left, frame direction=down). The images are dominated by the structure of the adsorbate molecules, and clearly show the herringbone structure of the alcohol monolayers and the parallel packing structure of the alkane monolayer. (e) Schematic diagram depicting the unit cell of an alkanol monolayer on graphite. (f) Averaged line scans across the lamellae for decanol, dodecanol, and tetradecanol monolayers. As expected, the size of the lamellae increases with increasing chain length of the adsorbed molecules.

Table 1

Molecule	Unit Cell by STM		Unit Cell by X-Ray Diffraction[21]	
	a (Å)	*b* (Å)	*a* (Å)	*b* (Å)
$C_{10}H_{21}OH$	26.7 ± 0.5	5.0 ± 0.2	26.5 ± 0.3	5.17 ± 0.02
$C_{12}H_{25}OH$	32.4 ± 0.5	5.2 ± 0.2	32.0 ± 0.4	5.04 ± 0.02
$C_{14}H_{29}OH$	38.0 ± 0.5	5.2 ± 0.2	-	-

The lamellae observed for alkanol overlayers were observed to form a herringbone structure. In the STM images the angle θ of Figure 1e was 23°, 24°, 25° for decanol, dodecanol, and tetradecanol, respectively, compared to an orientation angle determined by X-ray diffraction methods of ≈26° for alkanol monolayers on graphite.[21] The herringbone structure of the alkanol overlayer is consistent with expectations based on hydrogen bonding interactions driving the intermolecular packing geometries of these systems. The distance *d* between molecules determined from the X-ray diffraction data was 4.5-4.6 Å,[21] and that from STM data was 4.4-4.6 Å. The STM observations are thus in excellent agreement with the low angle X-ray diffraction data on these overlayers, lending confidence to the assignments of the STM images described herein.

The molecular-resolution features described above are similar to the qualitative features of STM images of related alkane or alkanol molecular overlayers that have been reported previously.[12-19] In this work, additional important information was obtained from a detailed analysis of higher resolution STM images. These highly resolved images were repeatable, but not always predictable. Higher magnification images (Figure 2a) of a representative alkanol containing 14 carbon atoms in its backbone, $C_{14}H_{29}OH$, showed

that each molecule exhibited 14 alternating bright spots that were separated by a mean distance of 2.57±0.02 Å in the direction along the molecule (a to b). The angle between adjacent bright spots (angle acb) in an individual molecule was measured to be 61°, and the distance between these spots was 2.36±0.02 Å (a to c and b to c). In addition, the distance between alternating spots in adjacent molecules was 2.76±0.02 Å (c to d).

These distances do not correspond to the lattice spacing of the underlying graphite substrate. Specifically, the distance between adjacent β site carbon atoms in a graphite lattice is 2.46 Å and that between β site carbon atoms located in every second carbon row of the graphite structure is 4.26 Å.[23] The origin of the bright spots in the STM data therefore cannot be explained in terms of enhanced imaging of graphite lattice atoms by the presence of the adsorbed alkanol, since any orientation of an alkanol having the overlayer commensurate with certain graphite atoms (to match some of the observed spot positions) would produce equivalently-imaged spots in positions that cannot be overlaid onto any corresponding graphite lattice atom or lattice site. Additionally, the spots cannot be attributed to the carbon atoms in the adsorbed tetradecanol molecules because the separations and angles observed for the spots do not correspond well to the expected C-C distance and angle of 1.55 Å and 109.5° for a trans- alkane.[24] The observed distances do, however, correspond closely to the H-H distances expected for hydrogens attached to adjacent (2.52 Å) and next-nearest (2.56 Å) methylene units in trans- alkanes.[24] The measured bond angle of 61° between adjacent spots in an alkanol lamella is also in accord with the H-H angles of 61.3° expected for hydrogens on adjacent methylene units in a trans- alkane. Thus, the metrics obtained from the experimental data indicate that the bright spots in individual alkanol molecules are primarily related to the locations of the individual hydrogen atoms on the methylene units of an alkanol chain. This assignment also implies that the plane containing the carbon-carbon skeleton in the alkanols lies in a parallel orientation to the graphite surface plane (Figure 2b).

(a)

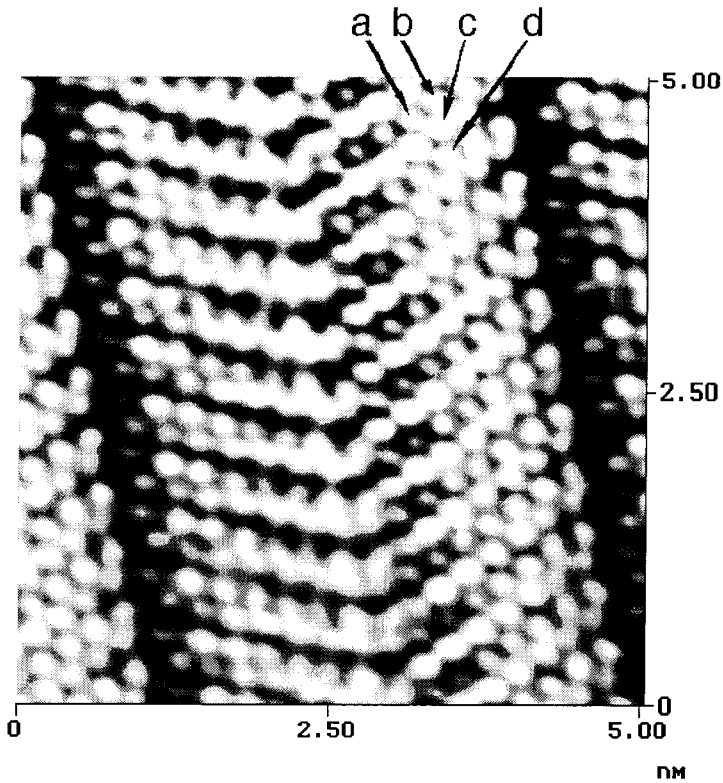

(b)

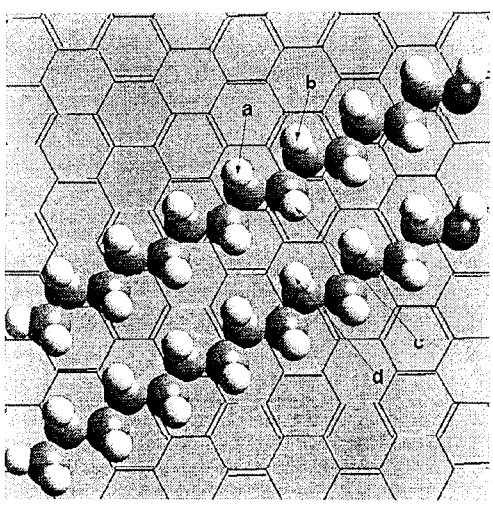

Figure 2. (a) High resolution STM image of tetradecanol molecules on graphite (V=1.127 volt, I=650 pA, line direction=right, frame direction=up). Individual tetradecanol molecules produce 14 bright spots in the STM image, which correspond closely to the locations of the 14 hydrogen atoms nearest to the tip. (b) Schematic diagram of individual tetradecanol molecules adsorbed onto graphite.

Low resolution images of alkanes exhibited bright spots that appeared to be associated with alternating methylene units in the alkane chain. For example, images of $C_{35}H_{72}$ showed 17 spots of mean separation 2.57±0.02 Å (Figure 1d). These images are in accord with the images of alkane overlayers on graphite presented previously in the literature.[12, 14] However, high resolution STM images of the alkanes (Figure 3), which were obtained using nominally the same experimental parameters as those that produced the lower resolution images, displayed alternating spot patterns that are very similar to those observed in the alkanol images. Images of $C_{35}H_{72}$ displayed bright spots which are separated by a mean distance of 2.54±0.02 Å in the direction along a molecule (a to c) and by a distance of 2.35±0.02 Å between adjacent spots within a molecule (a to b and b to c). These data are nearly identical to those for the alkanol overlayers, and indicate that the positions of the bright spots in images of the alkanes are dominated by the locations of individual hydrogen atoms on methylene units in a trans- alkane chain. These metrics also imply that the alkanes, like the alkanols, are adsorbed under our imaging conditions such that the bonds in the carbon-carbon skeleton are oriented in a plane parallel to the graphite surface. These high resolution images of the alkanes appear to be in accord with a previously published STM image of a $C_{36}H_{74}$ overlayer on graphite,[25] but a detailed determination of the important metrics of high resolution STM images of alkane overlayers such as that described above has not, to our knowledge, been reported previously in the literature.

Many of the STM images for the alkanes and alkanol overlayers also contained a larger scale modulation of the image contrast. This regular modulation in the image contrast is likely due to a Moiré pattern between the lattices of the graphite and of the monolayer.[26, 27] In fact, this pattern changes as the chain length of the molecule changes, and it is also a function of bias voltage and tip condition (vide infra). As a result of this superstructure, the contrast of the bright regions assigned to the hydrogen atoms sometimes varied slightly from one end of a molecule to the other.[28] Moiré patterns can

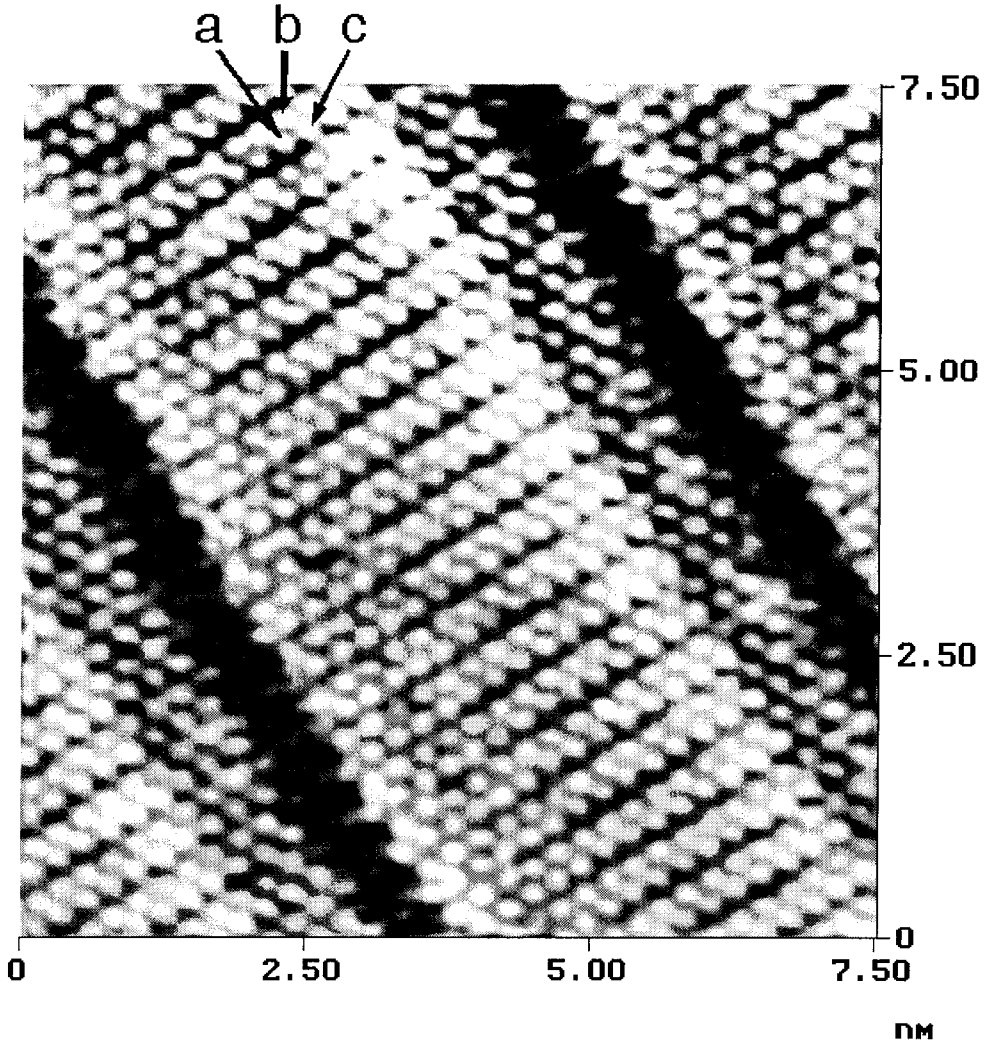

Figure 3. High resolution STM image of pentatriacontane molecules on graphite (V=1.210 volt, I=650 pA, line direction=left, frame direction=down). Unlike the lower resolution image in Figure 1d that seems to show every other methylene group (17 bright spots), the high resolution image shows 35 bright spots which correspond closely to the positions of the 35 upward-facing hydrogen atoms in the alkane chain. Similar to the alkanol overlayers, the molecules appear to be oriented with their carbon-carbon skeleton parallel to the graphite surface plane. The slight variation in contrast visible along the alkane chains was observed to be very tip dependent, and changed with time.

arise from the presence of two or more monolayers of an organic species adsorbed onto a substrate,[29] but prior calorimetric and X-ray diffraction data indicate that only single monolayers of alkanes and alcohols are absorbed onto graphite from the dilute solutions of these adsorbates that were used in our work.[21]

2. STM Images of Diols

The molecular resolution STM image of dodecanol displayed in Figure 1b is similar to other alkanol images reported previously,[12, 15, 16] and does not allow immediate identification of the location of the -OH group in the alkanol. The dark trough of mean length 4.3±0.1 Å that seemingly separates each lamella, corresponding to a 0.46±0.05 Å tip-sample decrease (relative to the average methylene height) required to maintain a constant 650 pA current at a sample bias of +1.210 V, could either contain two -OH groups hydrogen-bonded to each other, or could be the site of two terminal -CH_3 groups, one on each alkanol chain. However, since the positions of the individual spots were assigned in this work to be dominated by the locations of H atoms on methylene units in the alkanol chains, and since high resolution images of the alkanols showed no troughs between molecules on one side and troughs on the other (Figure 2), it is very reasonable to associate these troughs with the location of the -OH groups.

To validate this hypothesis without relying on such spot assignments, STM data were collected on overlayers of α, ω-alkanediols on graphite and the images compared to those of the corresponding alcohol. Figure 1b shows a STM image of dodecanol and Figure 4a displays an image of the corresponding diol, $HO(CH_2)_{12}OH$. The image of the diol exhibits lamellae of mean length of 34.5±0.5 Å, as compared to a mean lamellar length of 32.4±0.5 Å for dodecanol (Figure 4b and 1f). Identically-sized troughs are apparent at both ends of the molecules in the dodecanediol image, with the troughs having an average width of 4.3±0.1 Å and an average depth of 0.42±0.05 Å. Since the trough at the end of the dodecanol molecule is identical to the dark regions at the terminal areas of the diol molecules, these dark regions can be clearly assigned to -OH groups.

(a)

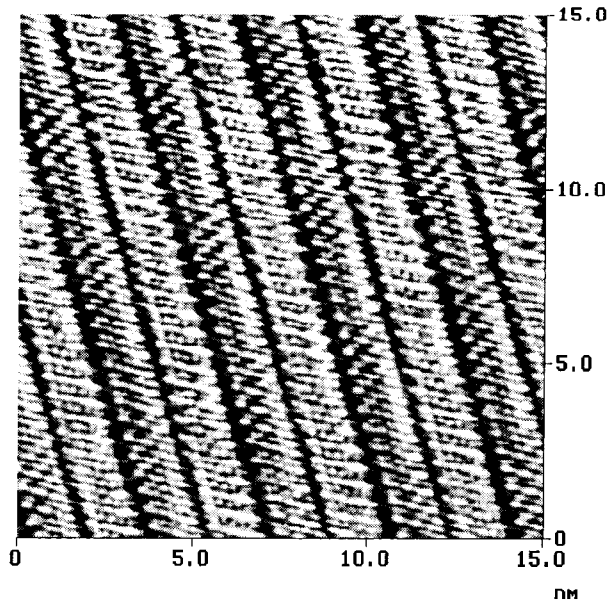

(b)

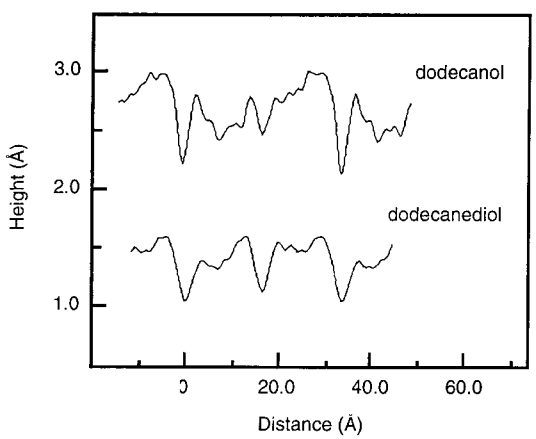

Figure 4. (a) STM image of a 1, 12-dodecanediol monolayer on graphite (V=1.318 volt, I=650 pA, line direction=left, frame direction=up). Unlike the image of dodecanol in Figure 1b, in which troughs are apparent on only one side of the molecules, in this image identical troughs are visible on both sides of the diol molecules. (b) Averaged line scans taken perpendicular to the lamellae (parallel to the a axis of the unit cell) for dodecanol and dodecanediol. Note that twice as many troughs are apparent in the line scan of dodecanediol as compared to dodecanol. This comparison shows that the hydroxyl functionalities are dark relative to the methylene groups, i.e., have a lower tunneling probability relative to the methylene groups in the alkane chain.

(a)

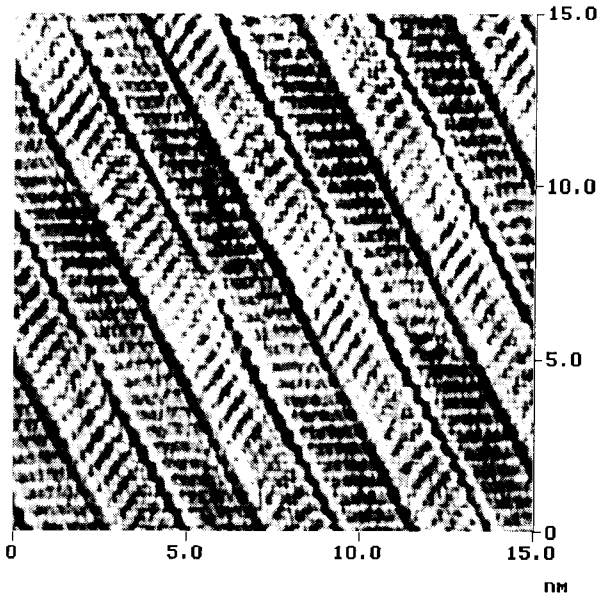

(b)

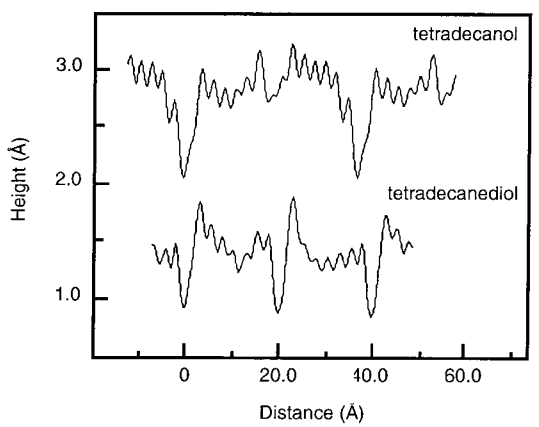

Figure 5. (a) STM image of 1,14-tetradecanediol molecules on graphite (V=1.095 volt, I=650 pA, line direction=down, frame direction=right). Troughs are apparent at both ends of the molecules, as compared to only on one side for tetradecanol (Figure 1c), indicating that the hydroxyl groups are dark relative to the methylene groups in the alkane chain. (b) Averaged line scans taken perpendicular to the lamellae (parallel to the a axis of the unit cell) for tetradecanol and tetradecanediol. Note that twice as many troughs are apparent in the line scan of tetradecanediol as compared to tetradecanol. Like the image of dodecanediol, twice as many troughs are apparent in the line scan of tetradecanediol as compared to tetradecanol (Figure 1f).

A similar comparison was performed between the STM images of tetradecanol and 1,14-tetradecanediol (Figures 1c and 5a). The mean length of the lamellae in images of tetradecanol was 38.0±0.5 Å while the mean lamellar length in images of 1, 14-tetradecanediol was 39.3±0.5 Å (Figure 1f and 5b). The trough at the end of the molecule in the image of tetradecanol had a mean length of 4.3±0.1 Å and a mean depth of 0.82±0.05 Å. As was the case for images of $HO(CH_2)_{12}OH$, the troughs at both ends of the lamellae in the images of 1, 14-tetradecanediol were identical, having an average length of 4.1±0.1 Å and an average depth of 0.61±0.05 Å. These data are also consistent with the assignments made above regarding the location of the hydroxyl functionality, and suggest that, in general, hydroxyl groups in alkanols will appear dark; i.e., will comprise regions of lower tunneling probability relative to methylene or methyl units in an alkane chain. The data also clearly show, contrary to earlier suggestions in the literature, that -OH groups can be distinguished by STM methods from terminal methyl groups in images of alkanol overlayers on graphite.[16, 20]

3. Bias Dependence of the STM Images of Alkanes and Alkanols on Graphite

In accord with other reports in the literature,[12, 14, 15, 18, 19] we have observed that the image contrast for alkanes and alkanols adsorbed on graphite depended on the tunneling bias. Figure 6a-c shows a series of STM images of decanol adsorbed on graphite as a function of bias voltage that were obtained over the same spatial region of the graphite surface. At low bias (i.e., at a tunnel gap resistance $R_{gap}=V/I=76$ MΩ), the STM height image is dominated by the graphite substrate. At an intermediate bias voltage ($R_{gap}=1975$ MΩ), the height image is comprised of features that can be associated with a combination of the substrate and adsorbate. At high biases, generally 1 V in magnitude ($R_{gap}=2020$ MΩ), the height image is dominated mostly by the adsorbate, and the herringbone structure of the decanol molecules is clearly observed. The transition between these various images was observed for several runs and was independent of the sequence in which the data were collected; only the bias voltage and setpoint current

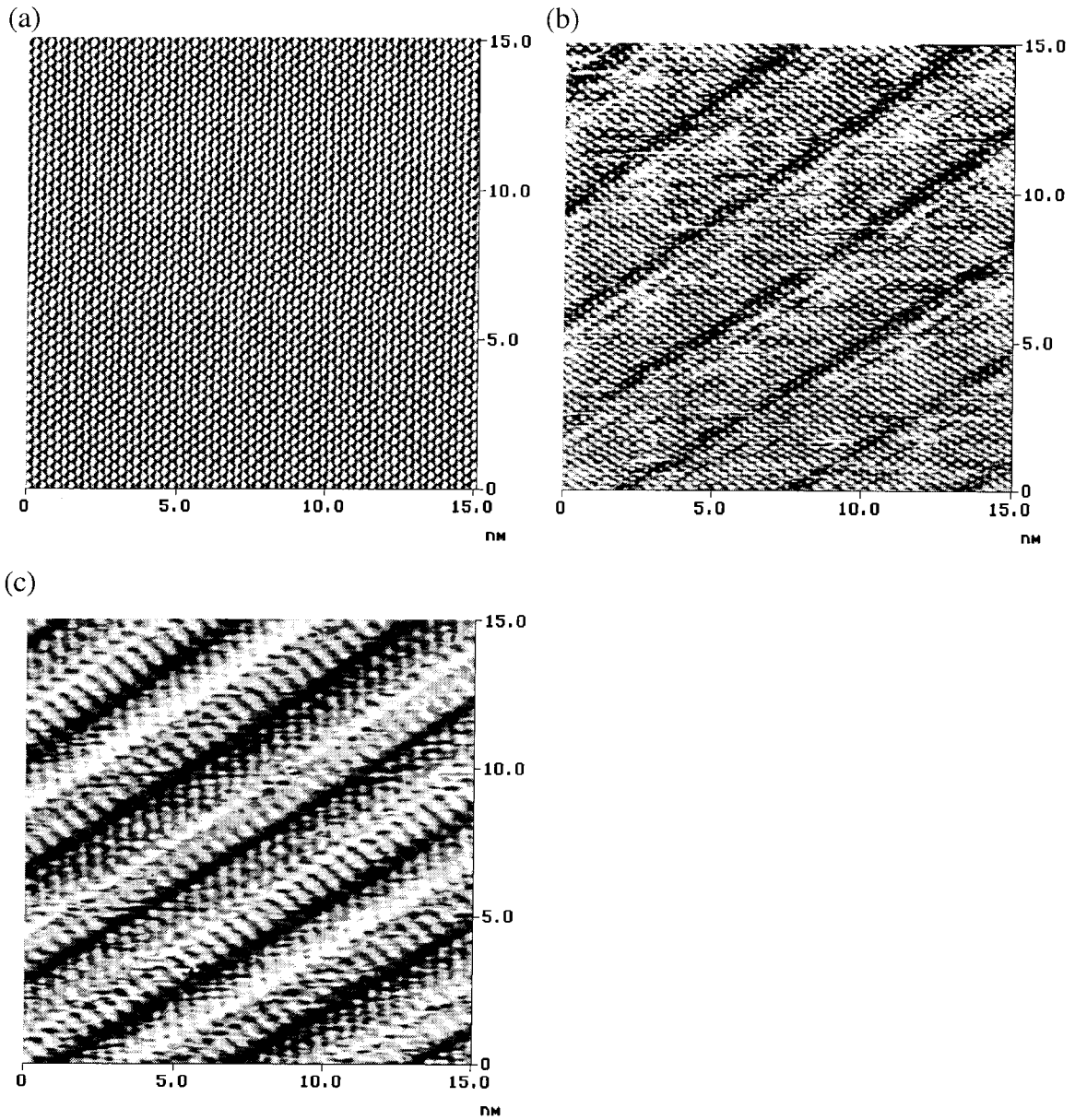

Figure 6. STM images of decanol on graphite. (a) The STM image is dominated by the substrate at low bias (V=0.050 volt, I=660 pA, line direction=left, frame direction=up). (b) At an intermediate bias, the image is comprised of features associated with both the substrate and the adsorbate (V=0.855 volt, I=433 pA, line direction=left, frame direction=down). (c) At high biases, the image is dominated by the adsorbate (V=1.160 volt, I=574 pA, line direction=left, frame direction=down).

determined which image was observed over a specific region of the sample. During the course of this study, we never reproducibly observed a "contrast reversal" during, or between, successive STM scans, in which the features in an image spontaneously reversed in contrast and could then be reproducibly imaged in this other image format. The simultaneous observation of features that can be associated with both the molecule and the graphite surface structure (Figure 6b) strongly suggests that the observed bias dependence of the images is not predominantly a result of physical displacement of molecules from the substrate by the tip at low or intermediate bias voltages. The data of Figure 6b also reveals that the decanol lamellae in the overlayer are aligned with the underlying graphite lattice.

The bias dependence of the images was observed not to depend on the polarity of the bias voltage; the bias dependence was thus symmetrical about zero volts between the tip and sample. Figure 7 shows I/V curves for the bare graphite surface and for the adsorbate covered surface. The curves are symmetrical with respect to bias polarity, and the tunneling current observed for the adsorbate covered surface increases slightly more rapidly with bias than for the bare graphite surface (Figure 7). The dependence of image contrast on bias is not unique to alkanes and alkanols adsorbed onto graphite; it has also been observed for phthalocyanine molecules,[30] cytochrome c_3,[31] and a variety of liquid crystals.[32, 33] However, it is especially interesting to note that the images were essentially symmetrical with respect to the zero bias position, set in this case by the Fermi level of the graphite.

4. STM Images of Alkanols with Perfluorinated Methyl and Methylene Functionalities

Since prior calorimetry measurements have shown that alkanols exhibit significantly more negative enthalpies of adsorption on graphite than the corresponding alkanes,[11] further STM data were collected on functionalized alkanols generally having 10-14 carbons in the alkane chain. The use of substituted alkanols having terminal hydroxyl

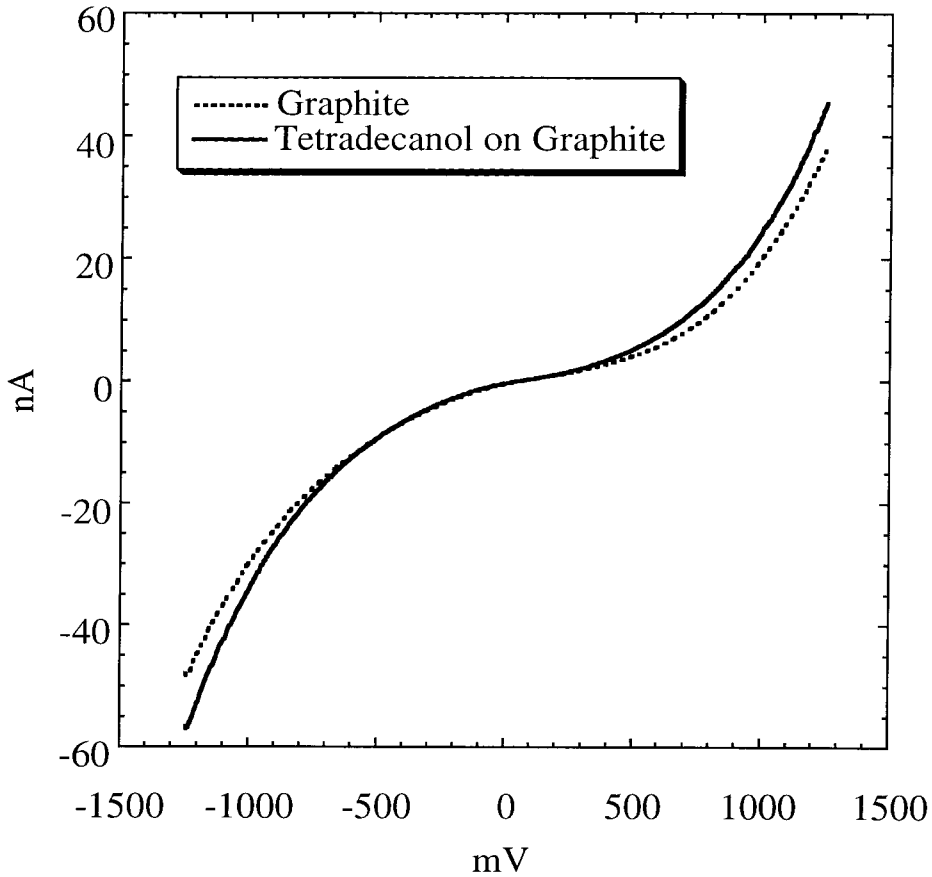

Figure 7. I/V curves of graphite and tetradecanol adsorbed on graphite with the tip sample separation defined by a sample bias of 100 mV and setpoint current of 650 pA.

groups allowed reproducible preparation of ordered monolayers of the molecular species on the graphite surface. In addition, the presence of the terminal hydroxyl group served as a convenient reference for establishing the relative contrast of other functional groups in the STM data. The section below describes STM images of alkanols that contain perfluorinated methyl and/or perfluorinated methylene groups.

We were unable to observe STM images of completely fluorinated alkanols such as hexadecafluoro-1,10-decanediol, most likely because a crystalline monolayer is not formed at room temperature on the graphite substrate. We did, however, observe STM images for partially fluorinated alkanols on graphite substrates. A STM image of $CF_3(CH_2)_{11}OH$ on highly ordered pyrolytic graphite is shown in Figure 8. The average length of the lamellae is 33.6±0.5 Å, and the average molecular length is 17.9±0.5 Å. This mean molecular length is in good agreement with the molecular length of 17.2 Å obtained from molecular modeling using Cerius 2 software for the all trans- conformation of the molecule. Troughs were apparent at both ends of the molecules, with one trough being longer and deeper than the other. The smaller trough has a width of 3.9±0.1 Å and a depth of 0.49±0.5 Å, and this is assigned to the -OH groups due to its similarity to the troughs observed in STM images of alkanols and alkanediols (Figures 4 and 5). The larger trough, assigned to the regions containing $-CF_3$ groups, has an average width of 8.2±0.1 Å and depth of 1.32±0.05 Å. Thus, like the -OH functionality, the $-CF_3$ group is dark relative to the methylene groups. The contrast in the images of this molecule was similar at positive and negative sample biases, as was observed for the alkanes and alkanols.

Figure 9 shows the STM image of $CF_3(CF_2)_3(CH_2)_{10}OH$ at positive sample bias. The image is not as clearly resolved as images of the alkanol molecules described above, and this may be due to the dynamics of the fluorinated ends of the molecule in these room temperature images (which may also explain the large width of the $-CF_3$ regions in the images of Figure 8). Lamellae of mean length 38.8±0.5 Å are observed, and the average length of the molecules is 19.9±0.5 Å. This length is in excellent agreement with the

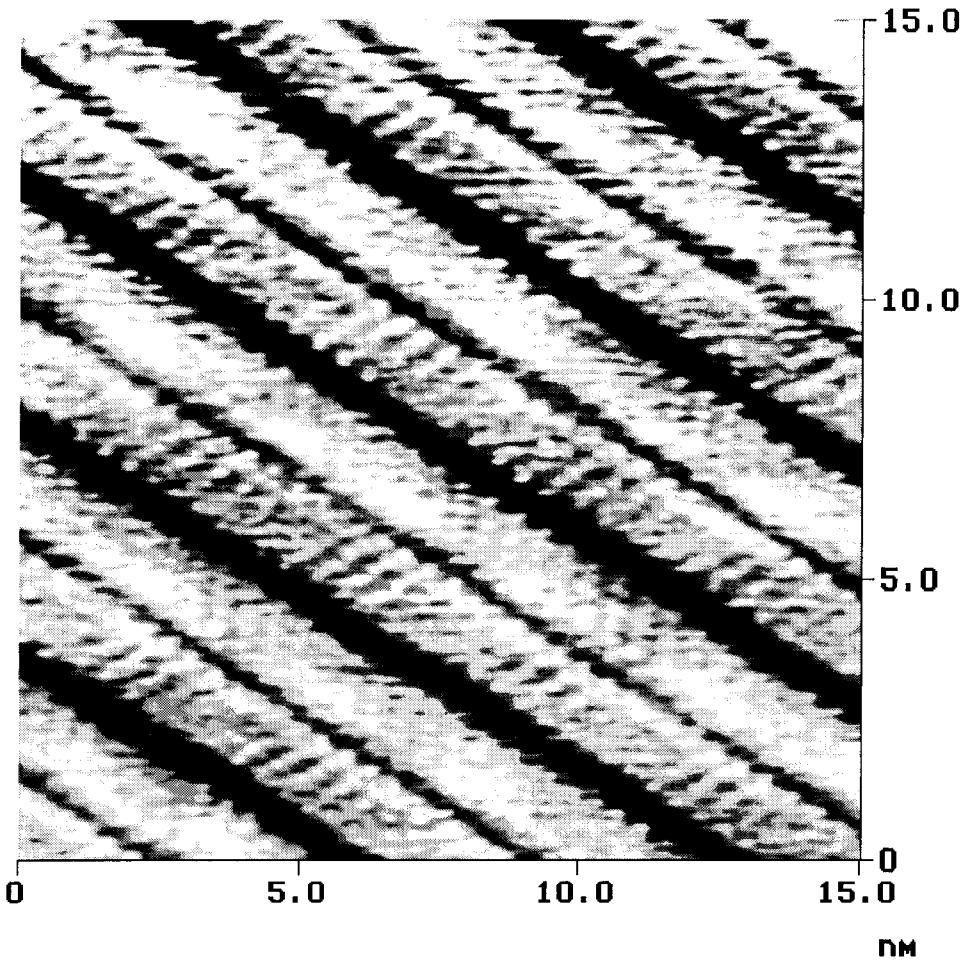

Figure 8. STM image of $CF_3(CH_2)_{11}OH$ molecules on graphite (V=-0.410 volt, I=650 pA, line direction=left, frame direction=down). The smaller trough is assigned to the -OH groups, while the larger trough is assigned to the regions containing terminal $-CF_3$ groups.

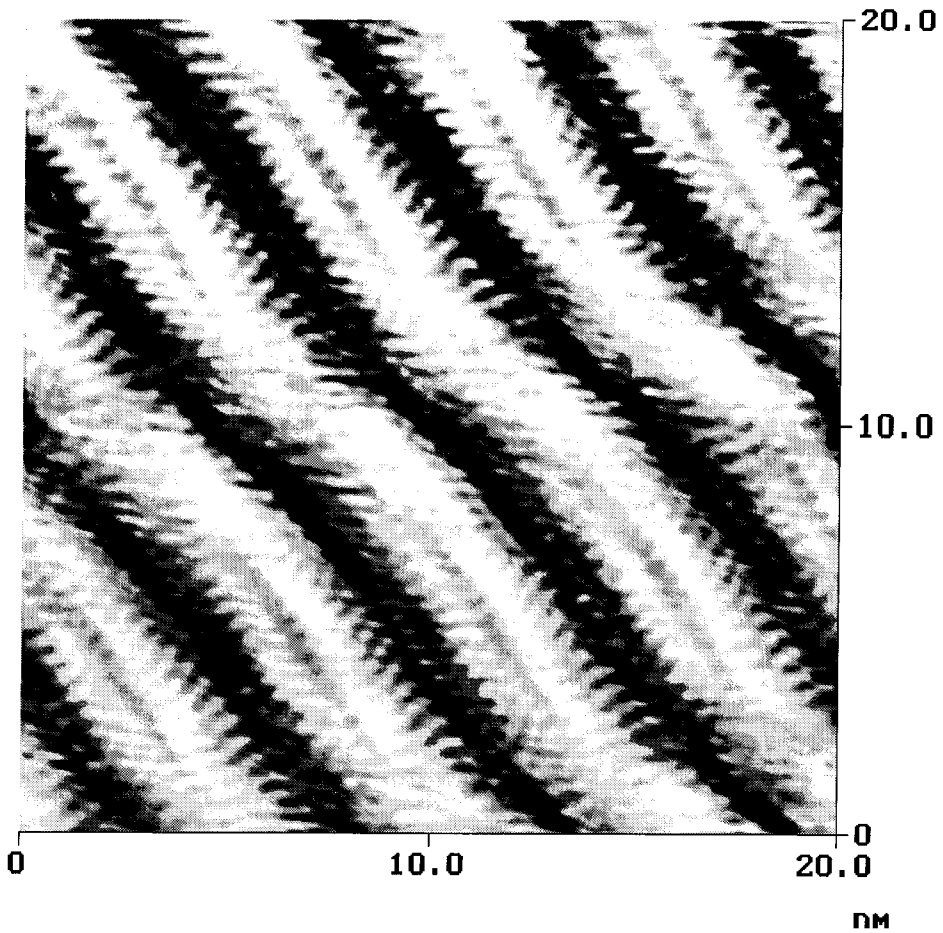

Figure 9. STM image of $CF_3(CF_2)_3(CH_2)_{10}OH$ molecules on graphite (V=0.185 volt, I=650 pA, line direction=right, frame direction=down). The smaller trough is assigned to the -OH groups, while the larger trough is assigned to the regions containing terminal - $CF_3(CF_2)_3$ groups. Like the hydroxyl group, fluorinated groups are found to be dark relative to the methylene groups.

length of 19.8 Å for the all trans- conformation of this molecule obtained from molecular modeling. Additionally, the STM images showed dark regions of mean length 4.3±0.1 Å and depth 0.30±0.05 Å that are assigned to the -OH groups. The longer trough can be assigned to the fluorinated region of the molecule, and has an average length of 16.0±0.5 Å and a mean depth of 1.32±0.05 Å. The large scale periodicity in the image is likely due to a packing effect or to a Moiré pattern between the monolayer and substrate. As was the case for the -OH group, we conclude that the fluorinated part of the molecule is dark relative to the methylene groups in such STM images at both positive and negative sample bias.

5. STM Images of Alkanol Halides

This approach was readily extended to a variety of functional groups. Figures 10-12 display representative STM data for the halides 12-bromo-1-dodecanol, $Br(CH_2)_{12}OH$, 12-chloro-1-dodecanol, $Cl(CH_2)_{12}OH$, and 12-iodo-1-dodecanol, $I(CH_2)_{12}OH$; the topographic metrics of these images are summarized in Table 2. Similar to the previous molecules, the STM contrast of the functional groups was independent of the bias polarity. The STM image of 12-bromo-1-dodecanol, $Br(CH_2)_{12}OH$, at negative sample bias is shown in Figure 10. The average length of the molecules in the 12-bromo-1-dodecanol overlayer is 17.8±0.3 Å, which compares well with the predicted length obtained from molecular modeling of 17.5 Å for an all trans- conformation of this molecule. Dark regions are observed on both ends of the molecule, indicating that bromine, like fluorine and oxygen, is dark relative to the methylene groups of these overlayers. A recent STM study of 1-bromodocosane (n-$C_{22}H_{45}Br$) adsorbed on graphite observed that the bromide functionality was generally dark in contrast relative to the alkyl chain,[20b] in accord with our data for $Br(CH_2)_{12}OH$. However, the STM images of $C_{22}H_{45}Br$ did not allow unambiguous identification of location of the Br group.[20b] The use of brominated alkanols, which adsorb more strongly onto graphite than brominated alkanes, enables higher resolution STM images to be obtained and permits location of the

Table 2

Molecule	Bias	-OH Features		Halide Features	
		length (Å)	height (Å)	length (Å)	height (Å)
$BrC_{12}H_{24}OH$	(+)	4.4 ± 0.1	-0.42 ± 0.05	5.9 ± 0.1	-0.63 ± 0.05
$BrC_{12}H_{24}OH$	(-)	4.1 ± 0.1	-0.41 ± 0.05	4.1 ± 0.1	-0.41 ± 0.05
$ClC_{12}H_{24}OH$	(+)	4.4 ± 0.1	-0.56 ± 0.05	4.4 ± 0.1	-0.56 ± 0.05
$ClC_{12}H_{24}OH$	(-)	4.7 ± 0.1	-0.63 ± 0.05	4.7 ± 0.1	-0.63 ± 0.05
$IC_{12}H_{24}OH$	(+)	4.3 ± 0.1	-0.80 ± 0.05	9.0 ± 0.1	1.91 ± 0.05
$IC_{12}H_{24}OH$	(-)	3.9 ± 0.1	-0.56 ± 0.05	8.8 ± 0.1	2.06 ± 0.05

Br functionality through reference to the position of the characteristic -OH trough in the STM images of substituted alkanols. Thus, for $Br(CH_2)_{12}OH$, the metrics of the STM images in positive bias allowed differentiation between the position of the -OH group and that of the Br functionality (Table 2).

The STM image of 12-chloro-1-dodecanol, $Cl(CH_2)_{12}OH$, also shows dark troughs on either side of the molecule, indicating that chlorine is dark as well (Figure 11). Under the imaging conditions of this work, the locations of the -Cl groups could not be distinguished from those of the -OH functionalities. The average length of the molecules in the 12-chloro-1-dodecanol overlayer is 17.3±0.3 Å, which is in excellent agreement with the length of 17.4 Å predicted for the all trans- conformation of this molecule by molecular modeling. The STM image of 12-iodo-1-dodecanol, $I(CH_2)_{12}OH$, is shown in Figure 12. The average length of the molecules is 18.1±0.3 Å, as compared with the predicted length of 17.8 Å from molecular modeling of the all trans- conformation. Unlike the previous molecules described above, images of this molecule show a slightly different

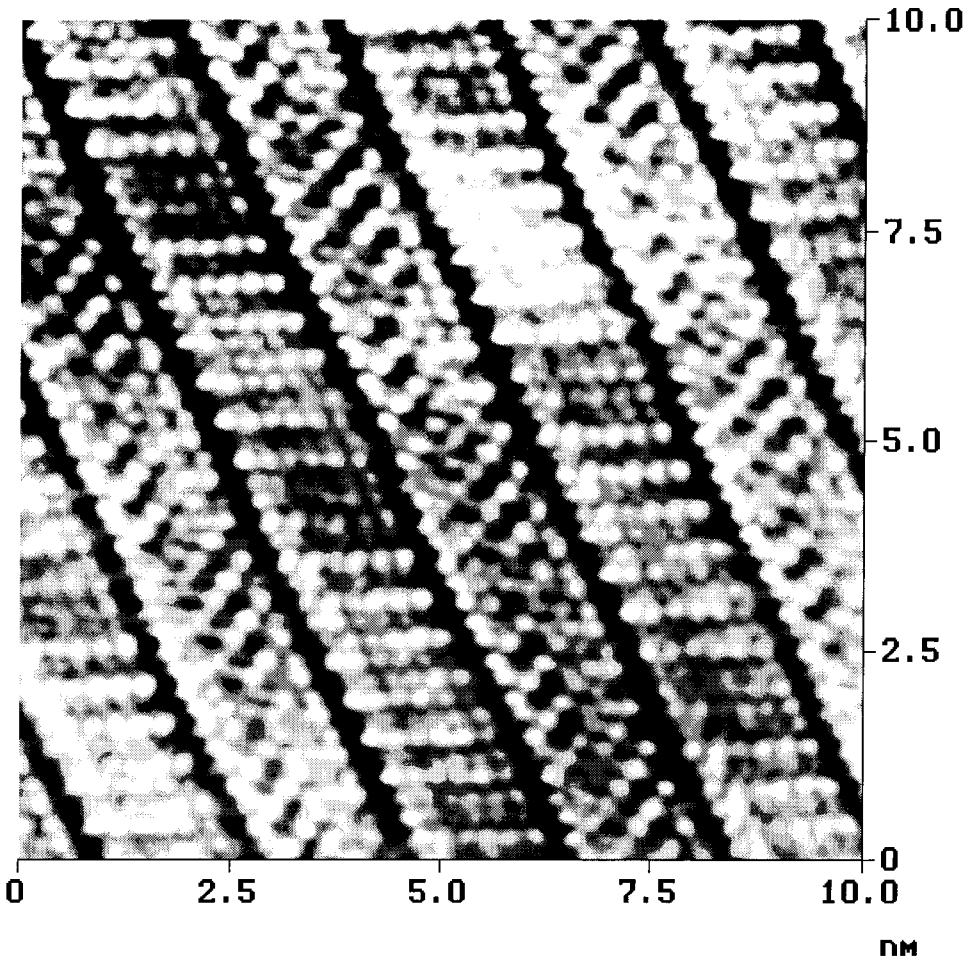

Figure 10. STM image of $Br(CH_2)_{12}OH$ molecules on graphite (V=-1.243 volt, I=650 pA, line direction=right, frame direction=up). Similar troughs are located at both ends of the molecules, indicating that the bromine is dark relative to the methylene groups.

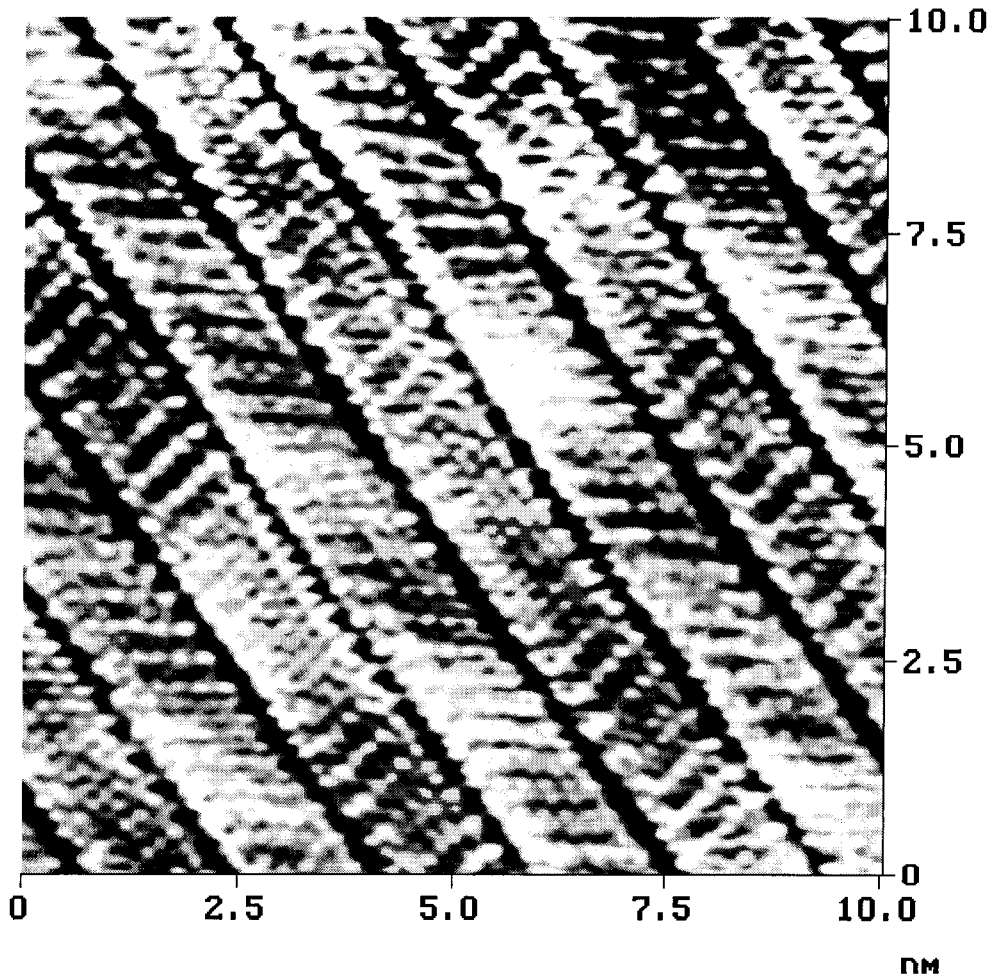

Figure 11. STM image of $Cl(CH_2)_{12}OH$ molecules on graphite (V=1.095 volt, I=650 pA, line direction=right, frame direction=up). Similar to 12-bromo-1-dodecanol, both ends of the molecules are dark, indicating that the chlorine is dark relative to the methylene groups.

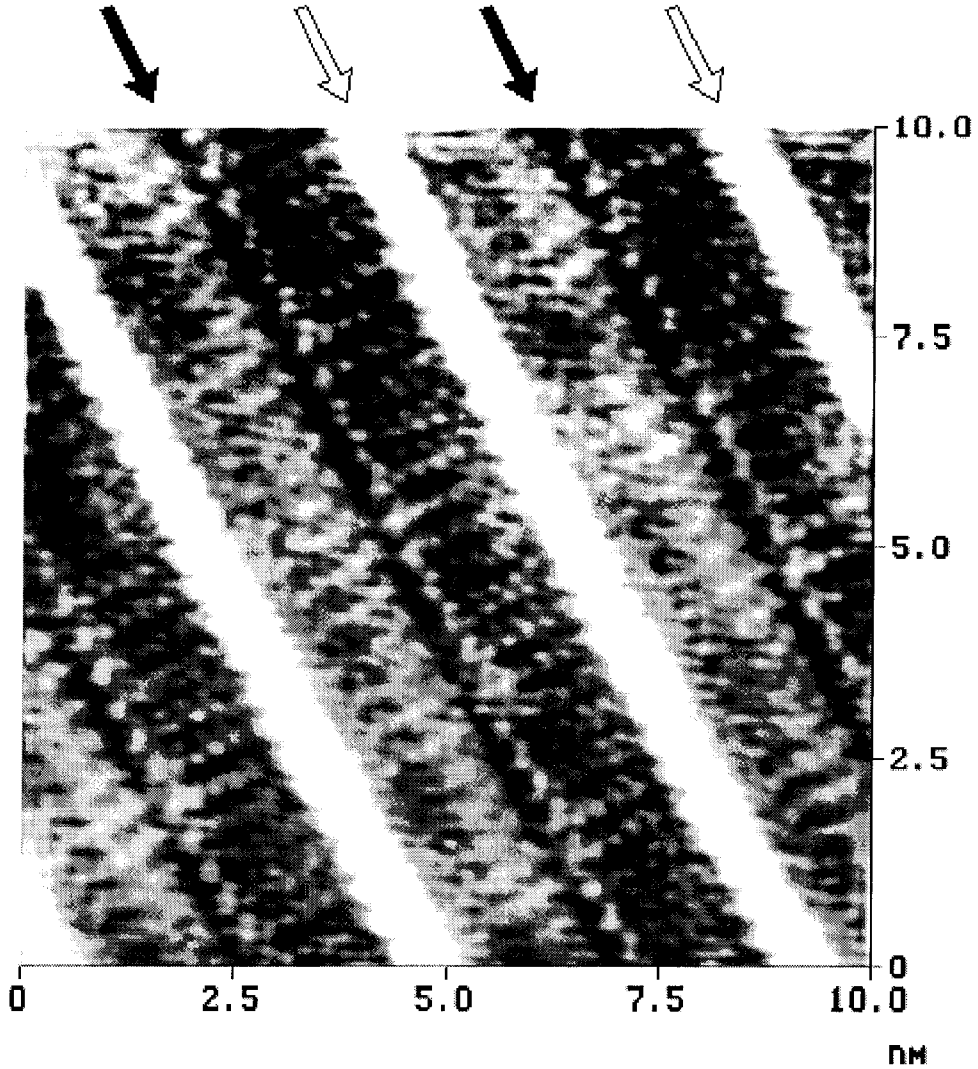

Figure 12. STM image of $I(CH_2)_{12}OH$ molecules on graphite (V=-0.177 volt, I=650 pA, line direction=right, frame direction=down). Using the dark trough associated with the terminal hydroxyl groups as a reference (black arrows), the bright region at the other end of the molecules is assigned to the region containing the iodine heteroatoms (white arrows).

packing arrangement, and reveal that one end is dark while the other is bright. Knowing that the -OH functionality is dark, we logically conclude that the iodine-containing regions are bright relative to the methylene groups in such STM images. This conclusion is in accord with recent STM images of 1-iodooctadecane on graphite, which also display bright iodide groups relative to the alkyl portions of the molecular overlayer.[20b]

6. Disulfides, Thioethers, Ethers and Amines

Figure 13 depicts the STM image of a dialkyldisulfide. Rabe *et al.* have reported a STM image of hexadecyldisulfide, $(C_{16}H_{33})_2S_2$, under positive bias;[26] similar to their report, we have found that hexadecyldisulfide adopts a V-shaped conformation about the sulfur atoms, (Figure 13) with the alkyl chains forming an angle of 130∞. The mean length of the lamellae is 43.9±0.5 Å. In accord with their report, we observe that the sulfur atoms are brighter than the methylene groups in positive bias. We additionally observe the same contrast between the sulfur atom locations and the methylene units for images obtained under negative sample bias.

Figure 14 presents the STM image of a thioether, tetradecyl sulfide, $(C_{14}H_{29})_2S$. The molecule is observed to be linear about the thioether functionality, and the average length of the molecules is 39.2±0.5 Å, as compared to the predicted length of 38.3 Å from molecular modeling. Since the sulfur atoms of the disulfide are brighter than the methylene units (Figure 13), a similar assignment of a bright sulfur-containing functionality can be made for the thioether. This assignment is consistent with recent images of thiols on graphite, in which the terminal -SH group was bright compared to the alkyl portion of 1-docosanethiol ($C_{22}H_{45}SH$).[20b] The width of the bright region associated with the thioether functionality was ~7 Å, indicating that the tip height was strongly affected over regions assigned to methylene groups located adjacent to the sulfur atom.

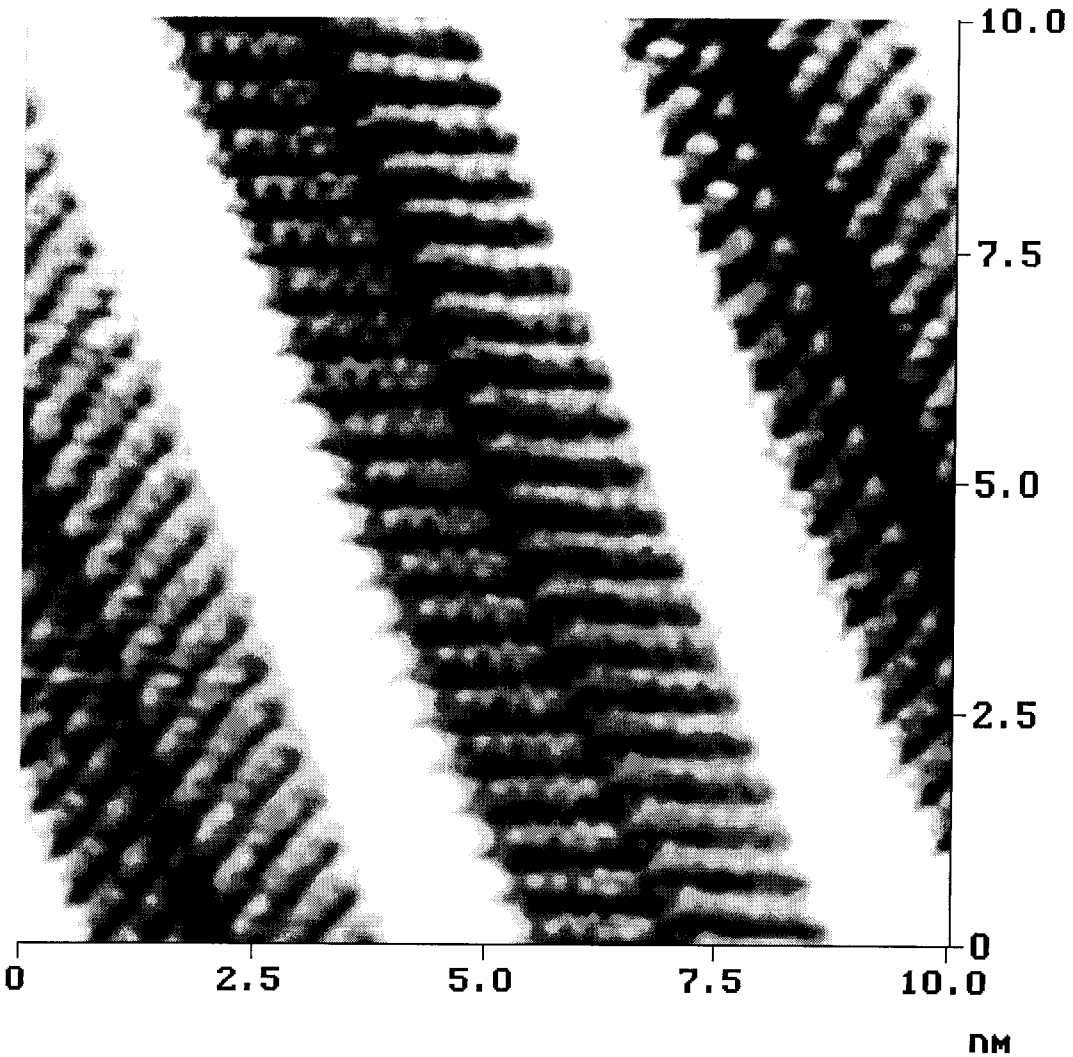

Figure 13. STM image of $(C_{16}H_{33})_2S_2$ molecules on graphite (V=1.556 volt, I=650 pA, line direction=right, frame direction=down). The disulfide molecules adsorb in a V-shaped conformation about the sulfur atoms, and the sulfur-containing region of the molecule is brighter than the surrounding methylene groups.

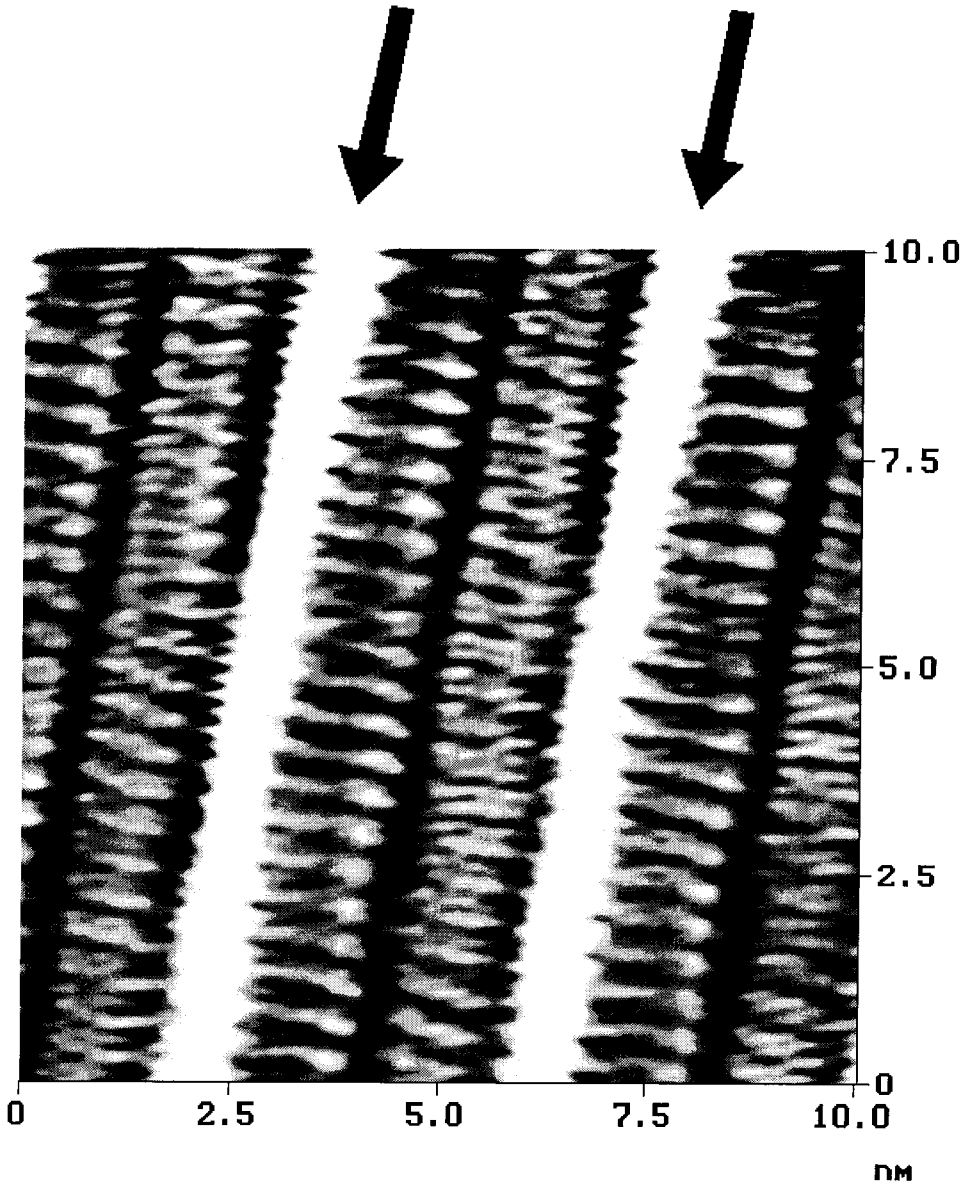

Figure 14. STM image of $(C_{14}H_{29})_2S$ molecules on graphite (V=-1.331 volt, I=650 pA, line direction=left, frame direction=up). The sulfur-containing region in the middle of the molecule is bright relative to the methylene groups (black arrows).

Figure 15 depicts the dramatic change in the image contrast that was observed when the thioether functionality was replaced by an ether functionality, through use of the molecule hexadecyl ether, $(C_{16}H_{33})_2O$. Comparison of the STM image of the ether (Figure 15) with that of tetradecyl sulfide (Figure 14) shows that the ether functionality appears dark relative to the methylene groups. This change in contrast was observed at both positive and negative bias voltages. The molecules were observed to be linear and staggered by half a molecular width across adjacent lamellae. The average length of the molecules is 43.4±0.5 Å, which compares well with the expected length of 43.0 Å obtained from molecular modeling of the all trans- conformation of hexadecyl ether. The width of the dark, oxygen-containing, region in the ether was ~5 Å, and, as is the case for most of the other functional groups studied under our conditions, the apparent length of the trough containing the region assigned to the ether functionality is much larger than the expected distance for an oxygen atom, indicating that the tip height is lowered over neighboring methylene groups as well as over the ether functionality itself.

The contrast of an amine functionality is shown in the STM image of dioctadecylamine, $(C_{18}H_{37})_2NH$ (Figure 16). The average length of the molecules is 47.5±0.5 Å, as compared to the expected length of 43.0 Å obtained from molecular modeling of the all trans- form of the amine. This discrepancy is most likely due to drift, which was exacerbated in this image relative to the other images obtained in this work because the amine molecules were aligned in the slow scan direction during this particular experiment. However, we observe the amine group to be bright relative to the methylene groups. This finding is in accord with a recent STM study of 1-octadecylamine ($C_{18}H_{37}NH_2$) overlayers on graphite, in which the amine group was bright relative to the alkyl chain.[20b] The topographic metrics of these functionalities are summarized in Table 3.

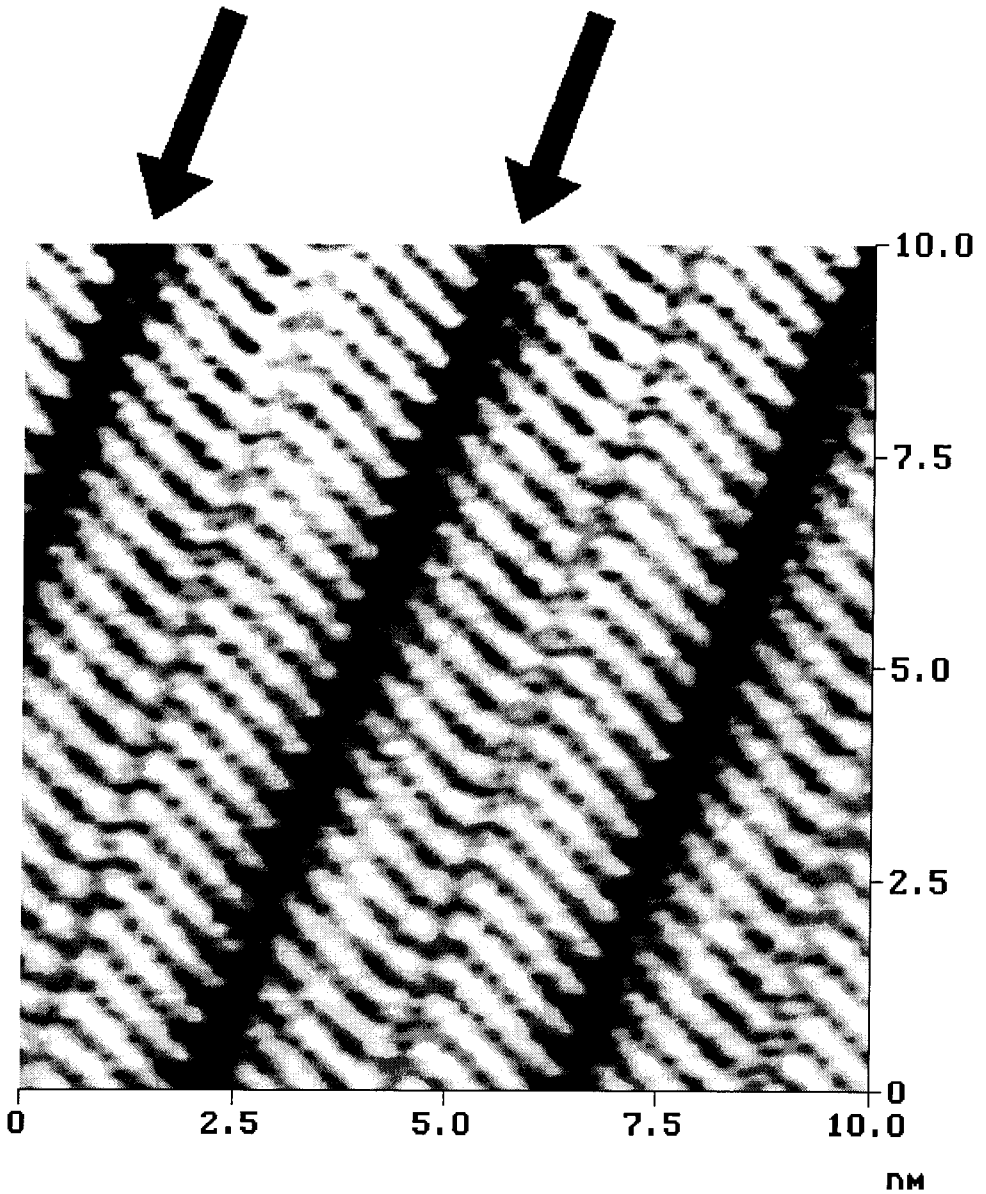

Figure 15. STM image of $(C_{16}H_{33})_2O$ molecules on graphite (V=-1.414 volt, I=650 pA, line direction=right, frame direction=up). Comparison of this image with that of $C_{35}H_{72}$ (Figure 1d) and with the thioether (Figure 14) leads to the conclusion that the dark trough in the middle of the molecular rows is due to the ether functionality (black arrows).

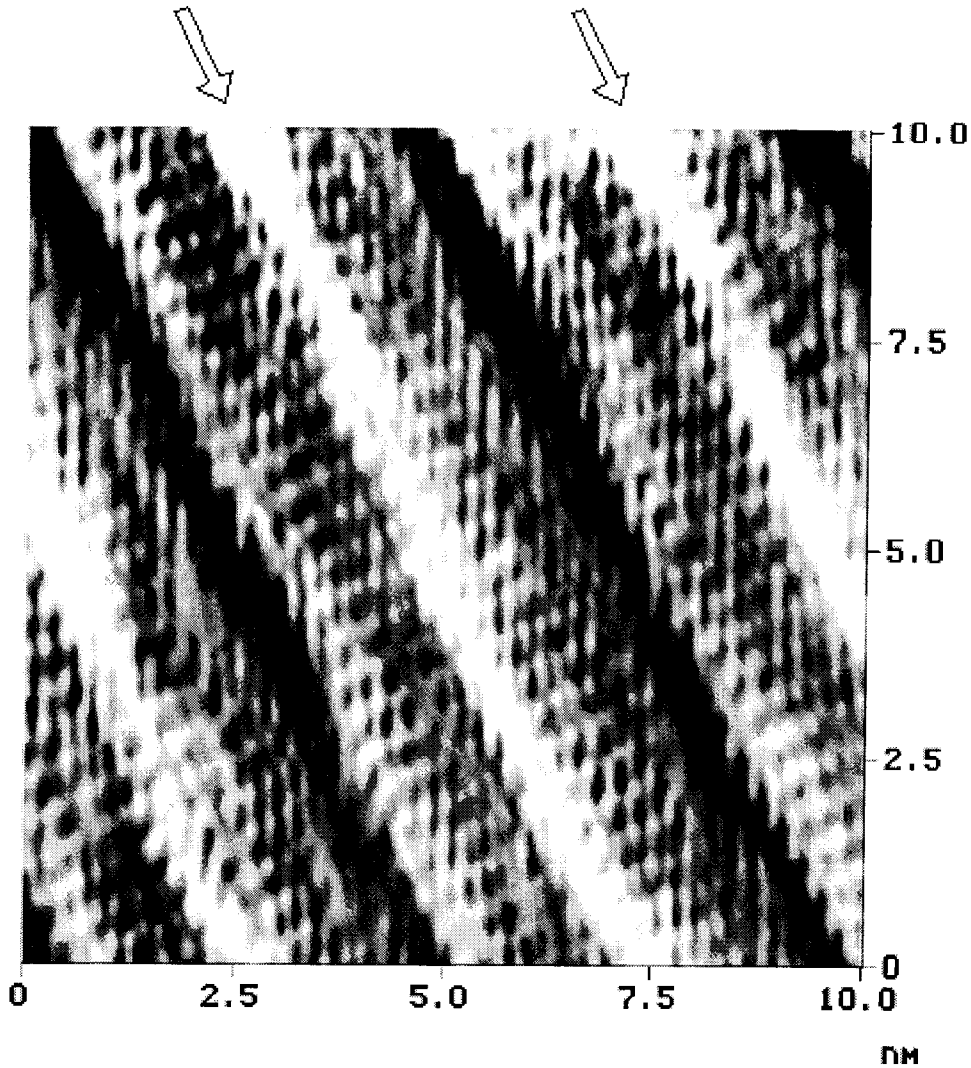

Figure 16. STM image of $(C_{18}H_{37})_2NH$ molecules on graphite (V=1.331 volt, I=650 pA, line direction=down, frame direction=left). The bright region in the middle of the molecular rows is assigned to the amine group (white arrows).

Table 3

Molecule	Bias	Heteroatom Features	
		length (Å)	height (Å)
$(C_{16}H_{33})_2O$	(+)	5.5 ± 0.1	-0.74 ± 0.05
$(C_{16}H_{33})_2O$	(-)	5.1 ± 0.1	-0.66 ± 0.05
$(C_{14}H_{29})_2S$	(+)	6.5 ± 0.1	0.80 ± 0.05
$(C_{14}H_{29})_2S$	(-)	6.7 ± 0.1	1.54 ± 0.05
$(C_{16}H_{33})_2S_2$	(+)	11.6 ± 0.1	1.25 ± 0.05
$(C_{16}H_{33})_2S_2$	(-)	12.6 ± 0.1	1.38 ± 0.05
$(C_{18}H_{37})_2NH$	(+)	7.7 ± 0.1	0.54 ± 0.05

7. Alkenes, Alkynes, and Nitriles

We observed a carbon-carbon double bond in the STM image of trans-17-pentatriacontene, $C_{16}H_{33}HC{=}CHC_{17}H_{35}$ (Figure 17a). The average length of the molecules is 44.9±0.5 Å, which compares well with the expected length of 45.0 Å obtained from molecular modeling of the all trans- conformation of the molecule. The double bond is located towards the center of the molecule, offset by one carbon, and in the STM image a bright feature appears at both positive and negative bias that is on average 21.8 Å from one end of the molecule and 23.1 Å from the other (Figures 17 a,b). Molecular modeling of an all trans- alkane with a trans- olefin functionality predicts that the center of the double bond should be located at 21.9 Å from one end of the molecule and 23.1 Å from the other, which compares well with experimental observations. Thus, we conclude that the double bond is bright in contrast. A carbon-carbon triple bond was observed in the image of 7-hexadecyn-1-ol, $H_3C(CH_2)_7C{\equiv}C(CH_2)_6OH$ (Figure 18), and

(a)

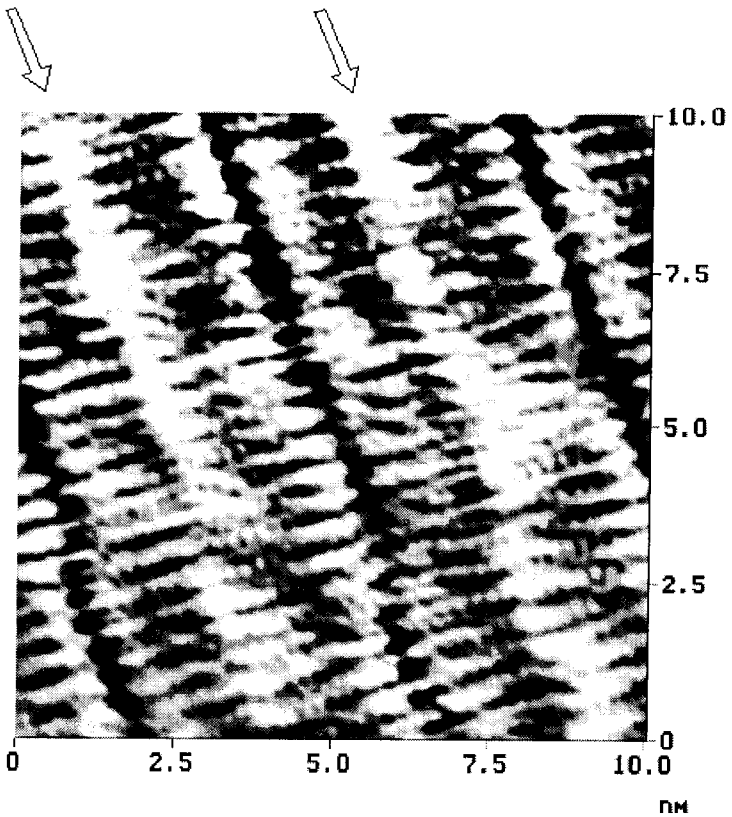

(b)

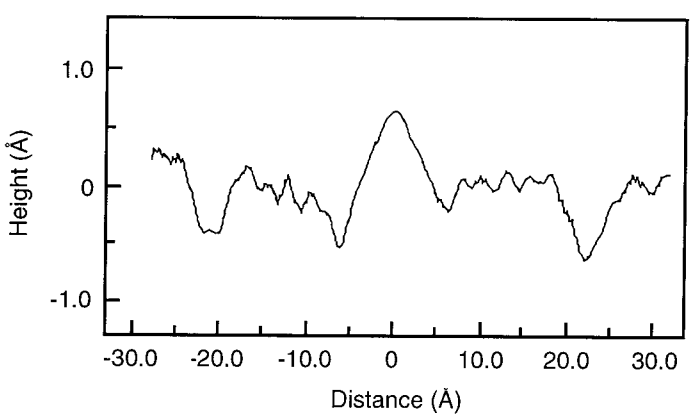

Figure 17. (a) STM image of *trans*- $C_{16}H_{33}HC{=}CHC_{17}H_{35}$ molecules on graphite (V=1.193 volt, I=650 pA, line direction=left, frame direction=up). The bright region located towards the center of the molecular rows is assigned to the carbon-carbon double bond (white arrows). (b) Single line scan along the length of the molecule; note the asymmetric location of the peak assigned to the double bond relative to the ends of the molecule.

(a)

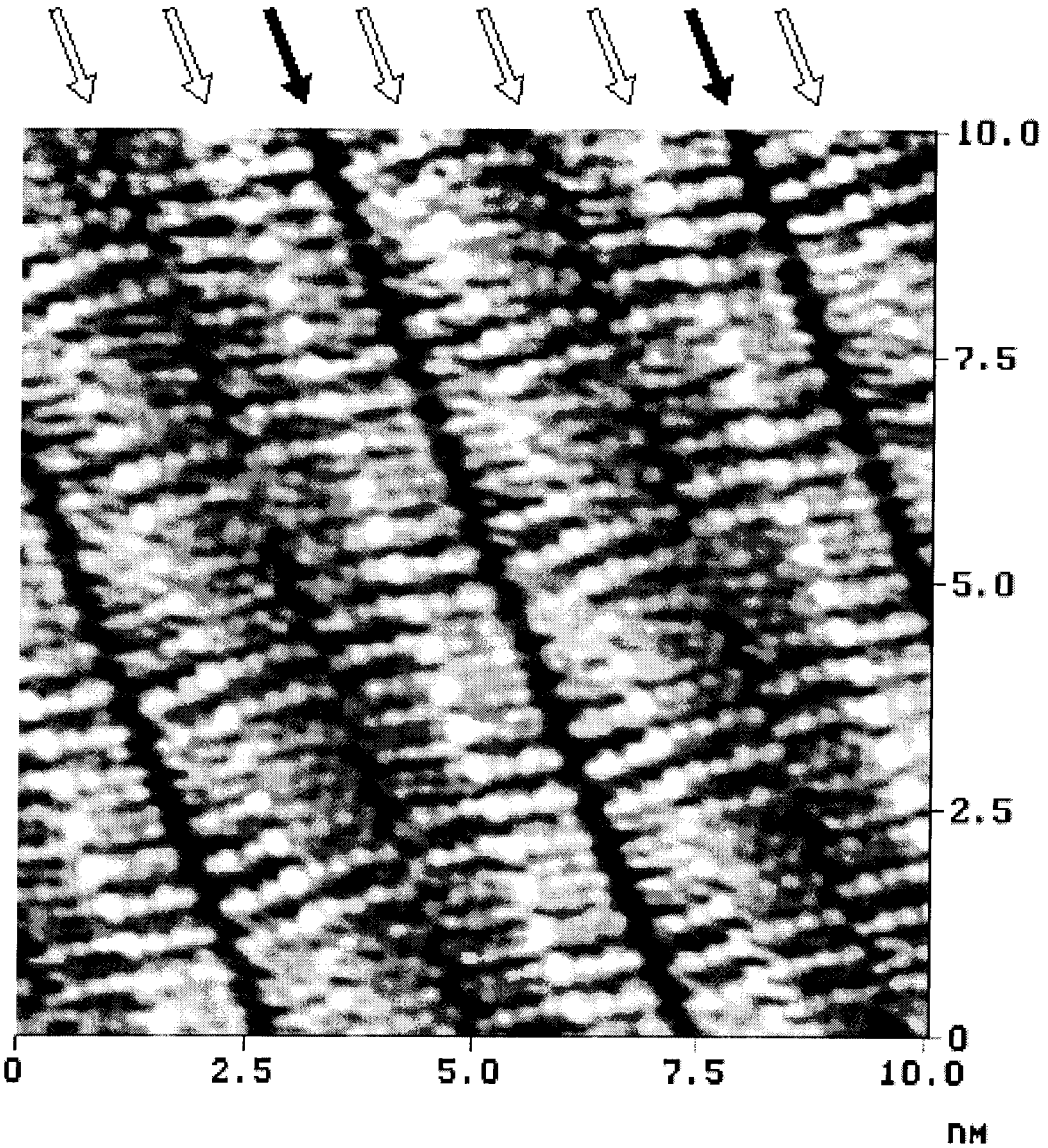

(b)

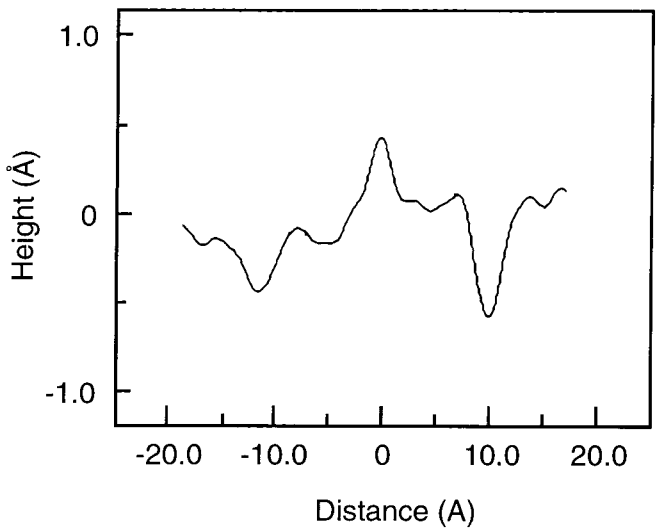

Figure 18. (a) STM image of $H_3C(CH_2)_7C{\equiv}C(CH_2)_6OH$ molecules on graphite (V=-1.216 volt, I=650 pA, line direction=right, frame direction=up). Using the dark trough associated with the terminal hydroxyl groups as a reference (black arrows), the terminal methyl end of the molecule can be identified (gray arrows), and the bright region located slightly offset from the center of the molecules is assigned to the carbon-carbon triple bond (white arrows). (b) Averaged line scan along the length of the molecules; note the asymmetric location of the peak assigned to the triple bond relative to the location of the trough assigned to the -OH group.

like the double bond, the triple bond is bright at both positive and negative bias. This observation is in accord with a previous STM image of an alkyne on graphite.[28] The average length of the molecules is 21.6±0.3 Å, which compares well with the expected length of 21.5 Å obtained from molecular modeling of the all trans- conformation of the molecule. The hydroxyl groups are easily identifiable as a trough of length 4.1±0.1 Å and depth 0.49±0.05 Å. The bright feature that is attributed to the triple bond correlates well with its location in the molecule; the feature appears 10.0 Å from the -OH end of the molecule and 11.6 Å from the methyl-terminated end (Figure 18 a,b). For comparison, molecular modeling of an all trans- alkane conformation with an internal C-C triple bond indicates that the center of the triple bond should be 10.0 Å from the -OH end of the molecule and 11.5 Å from the methyl terminated end of the molecule. In addition, the alkyl chains of the molecule are expected to have a kink about the linear C-C triple bond that should be observed experimentally if the carbon-carbon skeleton through the alkyl chains and the triple bond were oriented parallel to the plane of the HOPG surface. The predicted angle of the alkyl chain to the C-C triple bond of 146° compares well with the measured angle of 147° in the STM image. Furthermore, the offset between the two alkyl chains is predicted to be 1.43 Å, and the experimentally measured offset is 1.46±0.05 Å.

Finally, a nitrile was observed in the STM image of 1-hydroxy-12-dodecanenitrile, $HO(CH_2)_{12}C{\equiv}N$ (Figure 19). The average length of the molecules is 18.3±0.3 Å, which compares well with the expected length of 18.2 Å obtained from molecular modeling of the all trans- conformation of the molecule. Both ends of the molecule are dark, leading to the conclusion that the nitrile is dark relative to the methylenes at both positive and negative bias. The -OH groups are identifiable as the troughs of length 4.0±0.1 Å and depth 0.91±0.05 Å under negative bias, and of length 3.9±0.1 Å and depth 0.60±0.05 Å under positive bias. In either bias, the nitrile functionality is readily identified by its different length relative to the -OH functionality. The topographic features of the nitrile and other functionalities are summarized in Table 4.

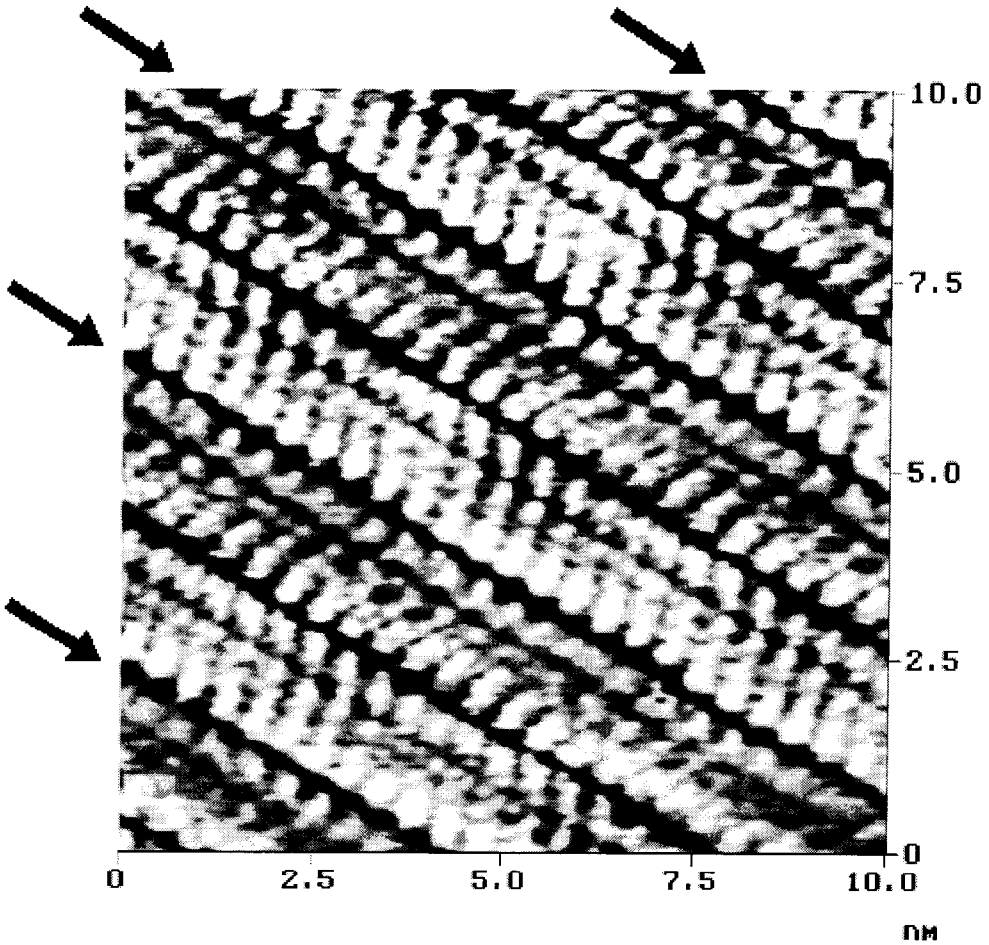

Figure 19. STM image of $HO(CH_2)_{12}C{\equiv}N$ molecules on graphite (V=-1.421 volt, I=650 pA, line direction=left, frame direction=down). Dark troughs are present on both ends of the molecule, indicating that the nitrile functionality is dark relative to the methylene groups.

Table 4

Molecule	Bias	Functional Group Features	
		length (Å)	height (Å)
$C_{16}H_{33}HC{=}CHC_{17}H_{35}$	(+)	8.3 ± 0.1	0.48 ± 0.05
$C_{16}H_{33}HC{=}CHC_{17}H_{35}$	(-)	8.4 ± 0.1	0.56 ± 0.05
$H_3C(CH_2)_7CC(CH_2)_6OH$	(+)	4.3 ± 0.1	0.60 ± 0.05
$H_3C(CH_2)_7CC(CH_2)_6OH$	(-)	3.5 ± 0.1	0.45 ± 0.05
$HO(CH_2)_{12}CN$	(+)	3.3 ± 0.1	-0.36 ± 0.05
$HO(CH_2)_{12}CN$	(-)	3.7 ± 0.1	-0.91 ± 0.05

IV. Discussion

1. Reproducibility of the Images and Assignment of the Peaks to Features of the Molecular Overlayer

Prior workers have noted the difficulty in associating the features of an individual, selected STM image with those of a specific molecule deposited onto a surface.[2(f-h), 3, 5] For instance, images of DNA on graphite have been questioned because of their lack of reproducibility as well as the fact that isolated regions of graphite (presumably near step edges and/or faults) have been observed to produce similar images under certain conditions.[4] In addition, Moiré patterns that produce periodic structures in STM images have been reported for simple, uncoated graphite surfaces under certain tip/sample bias conditions.[24, 25] Before interpretation of the data obtained herein, we therefore must first address the issue of whether the data can reliably be associated with the molecules of concern.

Several aspects of the present system lend confidence to the assignment of the features in the images to the molecules of interest. First, since the sample preparation methods yielded well-packed monolayers of the desired molecules (as confirmed by several independent physical methods),[7-11, 21] the STM images depicted in this study are not isolated, selected photographs that were observed only in one special spot of one sample, but instead are characteristic of the images that can be obtained on any representative region of the graphite/alkane assembly.

A second feature that lends confidence to the association of these images with the molecular properties of interest is the systematic variation of the images in response to variation in the nature of the functional groups in the molecular overlayer. Over a dozen different functionalities were introduced into the molecules investigated in this work, and in each case these changes produced distinctive features in the STM images. The functionalities were positioned at the ends, centers, or in non-symmetric positions of the alkane chains, and the images of each system reflected the positions of the functional groups to within the experimental error of the measurement. Also, the lengths of the lamellae in the STM data assigned to the molecules in the overlayer changed in accord with the changes in the chemical composition of the overlayer, and the unit cell dimensions of the overlayer determined from the STM data agreed closely with those determined from low angle X-ray diffraction measurements.[21] This type of systematic study not only lends confidence to the association of the image features to the molecules of interest but also allows a reliable comparison between the STM behavior of the various functional groups relative to the behavior of the methylene units in the alkane overlayers.

A third issue of possible concern is whether the data arose from some type of Moiré pattern, and instead of reflecting the molecular features in the overlayer actually are associated with the atomic positions of the graphite lattice. The distances and angles of the spots observed in the various high resolution images of alkanes and alkanols do not all correspond to an integral graphite lattice spacing, but do closely correspond to the

expected bond distances and bond angles for hydrocarbon chains. Thus, for all of the reasons given above, we feel confident that the imaged features represent modulations in the tip/sample tunneling probability that are associated with the specific properties of the molecular overlayers under investigation.

2. Topography and Orientation of the Alkane and Alkanol Overlayers on Graphite Surfaces

The topography of the overlayer needs to be defined and identified so that the influence of electronic and topographic factors on the STM images can be evaluated individually. Prior studies of alkane overlayers on graphite led to controversy because the STM images have been variously assigned either to reflect the positions of the carbon atoms in the graphite substrate or to reflect the positions of the atoms in the molecular overlayers.[12-20, 25] The available experimental data does not allow reliable differentiation between these two possibilities, due to the similarity of the distances between adjacent carbons in a graphite STM image (2.46 Å) relative to the distances between adjacent hydrogen atoms in a trans- alkane chain (2.52 Å between adjacent methylene hydrogens and 2.56 Å between next-nearest methylene hydrogens).[24] If the STM images reflect the properties of the alkane overlayer, extended Hückel calculations have suggested that the hydrogen atoms on the methylene chains should dominate the observed STM spot pattern.[25] The STM data presented herein clearly indicate that the bright spots in the STM images of such systems are dominated by the features of the molecular overlayer, and that the positions of the methylene hydrogens dominate the experimental images. These observations are in accord with the prior assignment of bright STM spots in the alkyl chain region of liquid crystals on graphite to the positions of the hydrogen atoms in the methylene chain portion of the molecules.[2b] The data presented herein also indicate that the alkanes and alkanols imaged at high resolution had their carbon-carbon skeletons oriented parallel to the graphite surface plane.

The orientations deduced from the high resolution STM data are also supported by the molecular packing arrangements evident in the lower resolution STM images, i.e., those in Figures 1a-d. The most sterically favored packing for alkanes having their carbon-carbon skeleton oriented perpendicular to the graphite surface is obtained with the hydrogen atoms on adjacent alkane chains staggered by one-half of the distance between hydrogen atoms on next nearest methylene units in the alkane chain (Figure 20a), i.e., by approximately 1.28 Å. With an intermolecular spacing of 4.5 Å, this type of packing would produce a value of the angle θ in Figure 20 of 16°. In contrast, the STM data of Figure 1d reveal that θ=0° for $C_{35}H_{72}$ overlayers on graphite. This value of θ is consistent with the carbon-carbon skeleton of $C_{35}H_{72}$ being oriented parallel to the graphite surface plane, because a sterically favored packing in this molecular orientation exhibits registry perpendicular to the molecular axis between methylene units that are structurally equivalent but are located on adjacent alkane chains (Figure 20b). Thus, the packing arrangements observed for the alkanes in the lower resolution STM images support the orientational assignments deduced from the higher resolution STM images of Figure 3.

For alkanes absorbed on graphite, a rapid reorientation process has been proposed in which the carbon-carbon skeletons in an entire domain can change from being oriented parallel to the graphite surface plane to being oriented perpendicular to the graphite surface plane in the time elapsed between single STM image scans (but apparently the reorientation process has not been observed during the collection of an individual STM image).[25] As discussed above, such a process would require a sterically unfavorable packing arrangement, with significant methylene-methylene repulsions between adjacent alkane chains, if a lamellar packing angle of θ≈0° were present in both orientations. We have only observed θ≈0°, and also have only have observed high resolution STM spot patterns that are consistent with a parallel orientation of the carbon-carbon skeleton with respect to the graphite surface, for the alkane overlayers imaged

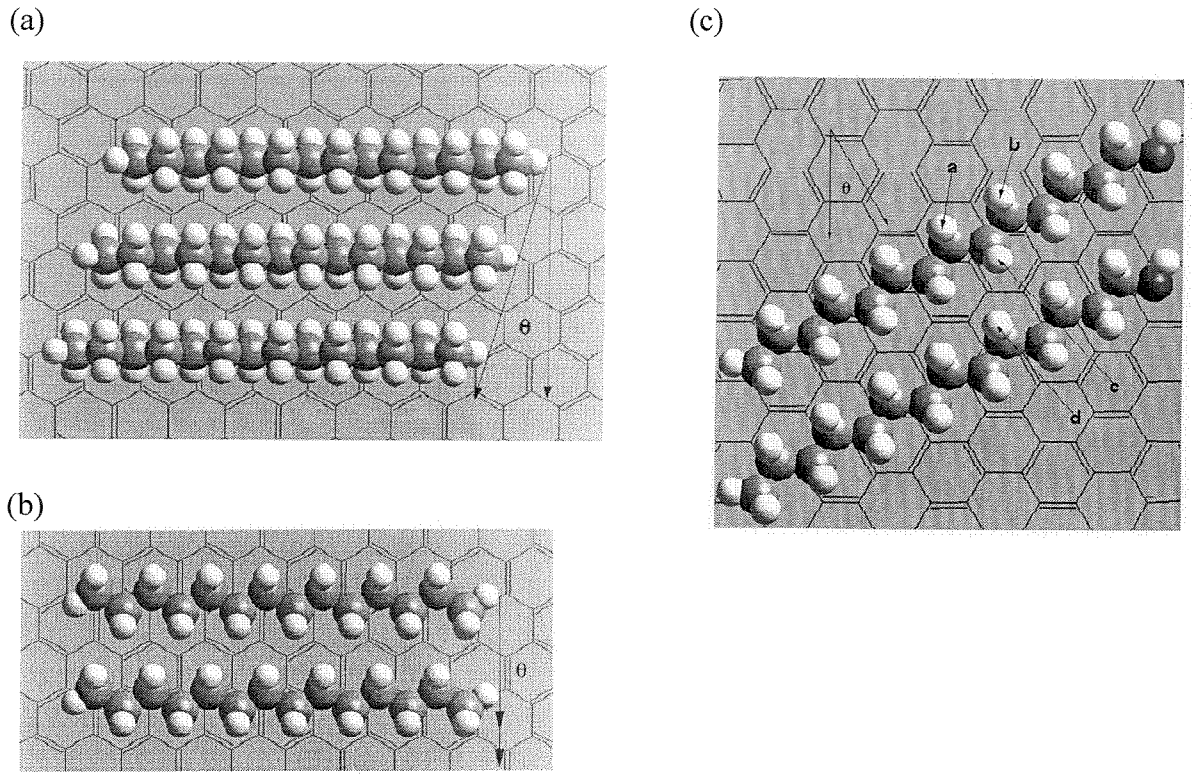

Figure 20. Schematic diagram of sterically favored packing arrangements of alkane and alkanol overlayers on graphite. (a) Alkanes oriented with their carbon-carbon skeletons perpendicular to the plane of the graphite surface. Structurally equivalent methylene units are offset in adjacent molecules, and produce $\theta=16^{\circ}$ for an offset of 1.28 Å and an intermolecular spacing of 4.5 Å. (b) Alkanes oriented with their carbon-carbon skeletons parallel to the plane to of the graphite surface. To minimize repulsions between methylene groups, adjacent molecules are expected to be in translational registry, with $\theta=0^{\circ}$, as shown. (c) Alkanols oriented with their carbon-carbon skeletons parallel to the graphite surface plane. An angle $\theta=26^{\circ}$ is produced in this packing arrangement, with the packing angle presumably driven by hydrogen bonding interactions of the terminal -OH groups (whose orientation and individual packing is only indicated schematically and cannot be assigned from the STM data available at present).

during the course of this study. The predominant form of these alkane overlayers, as well as of the alkanol overlayers, therefore appears to be the one in which the carbon-carbon skeleton lies parallel to the graphite surface plane.[34]

It was also possible to identify the orientation of most of the other molecules imaged in our studies. A value of $\theta \approx 24\text{-}26^\circ$ was observed for the molecular packing of alkanols and of substituted alkanols (Figures 1a-c, 4a, 5a, 10, 11, 13, 19). Note that although prior work has suggested that $C_{30}H_{61}OH$ lamella on graphite are aligned parallel to the graphite lattice planes, due to observation of a lamellar packing angle, θ, of approximately 30°, [20] measurements of θ from the STM data of C_{10}-C_{14} alkanols examined in this work and from low angle X-ray diffraction data on related systems[21] show that $\theta = 24\text{-}26^\circ$. This smaller angle indicates that the lamellae of these alkanol overlayers are not aligned with the underlying graphite lattice planes. Based on the steric packing arguments presented above, this angle indicates that the carbon-carbon skeleton of these molecules lies in a plane parallel to the graphite surface plane. In support of this conclusion, all of the substituted alcohols, except for the fluorinated species $CF_3(CF_2)_3(CH_2)_{10}OH$ and $CF_3(CH_2)_{11}OH$, produced sufficiently high-resolution STM images that the characteristic spot pattern displayed by the alkanols, indicating an orientation of the carbon-carbon skeleton parallel to the graphite surface plane, could be observed. In addition, the alkyne 7-hexadecyn-1-ol clearly has its carbon-carbon skeleton oriented parallel to the graphite surface plane, because a kink is observed between the molecular segments that lie on opposite sides of the carbon-carbon triple bond (Figure 18a). This observation further verifies the orientational assignments deduced from the high-resolution STM spot patterns of the other functionalized alkanols. These packing preferences indicate that the hydrogen bonding interactions between the terminal -OH groups dominate the intermolecular interactions of alkanol overlayers and induce a strong preference for the carbon-carbon skeleton of alkanols to be oriented parallel to the graphite surface plane.

3. Judging the Relative Importance of Topographic and Electronic Factors in Determining the STM Image Contrast Of Functional Groups in Alkane/Alkanol Overlayers

The detailed analysis of the lengths, angles, and vertical contrast features of high resolution STM images of a variety of molecular overlayers presented herein has allowed assignment of the locations of various functional groups relative to the "reference" methylene or -OH units in such systems. Although a prior analysis, based on lower resolution STM images of $C_{30}H_{61}OH$ on graphite, has concluded that -OH groups can not be distinguished from the methylene regions of alkanol overlayers,[20] the data of Figures 1, 2, 4, 5 and 6 clearly show that the position of the -OH group can be accurately located from the STM images of such systems. In addition, alkyl bromide, alkyl iodide, trifluoromethyl, and most of the other groups investigated in this study could be clearly distinguished both from the methylene units in the alkyl chain and from terminal -OH groups. In fact, for the 12 functional groups investigated in this work, only -Cl and -OH functionalities were too similar to resolve from each other (i.e., were too similar to assign their relative locations if they were incorporated concurrently into an alkane/alkanol overlayer).

Given the ability to locate the apparent positions of the various functional groups, it is of interest to evaluate the factors that control their relative vertical image contrast. A recent theoretical study has concluded that the orbital mixing of insulating compounds into the energy levels of the substrate is responsible for producing the STM images of insulating overlayers.[25] The experimental data presented herein support this interpretation, but the data also underscore the significant variations in STM image contrast that can occur for different functional groups present in the molecular overlayer. One study has recently suggested that the STM tunneling contrast of halides in alkyl halide monolayers on graphite surfaces might be related to the atomic polarizability of the halide group.[20b] This hypothesis is not consistent with the functional group contrast

observed in this work in which the polarizable -OH, bromide, or chloride functionalities are dark relative to the methylene chains of alkanols but the iodide group is bright relative to these same methylene chain units.[35] As discussed in more detail below, the relationship between STM contrast and atomic polarizability also does not readily provide insight into the observed bias dependence of various functional groups in the STM images.

The data of Figures 1-19 imply that both topographic and electronic coupling factors are important in determining the STM image contrast. Clearly, since the images of the methylene units were dominated by the positions of the H atoms in the alkyl chain (Figures 2,3), topography plays a dominant role in defining the image contrast of these regions of the molecular features. However, topography alone is not sufficient to explain the STM contrast of the functional groups. For example, based on topography alone, the $-CF_3$ groups in the molecules $CF_3(CF_2)_3(CH_2)_{10}OH$ and $CF_3(CH_2)_{11}OH$ should appear bright, because the C-F bonds are longer than the C-H bonds in the parent alkanes and thus produce functionality that projects topographically closer to the tip than does the unsubstituted methyl group. However, the tunneling probability over these functional groups must be low relative to the methylene groups since they appear dark in the STM image. Additionally, based on size alone, the amine functionality should be dark since it is small relative to a methylene group, but it appears bright in the STM image.

We assign these differences to variations in the local electronic coupling of the various functional groups between the STM tip and sample relative to the electronic tip-sample coupling over the methylene units in the alkane section of these overlayers. Unfortunately, since all graphite and graphite-coated samples under ambient pressure conditions reported to date display an anomalously weak dependence of the tunneling current as the tip is retracted from the substrate, a quantitative interpretation of the STM image contrast mechanism of these samples is not possible at the present time. Despite this complication, it is possible to develop a qualitatively useful formalism for

understanding the image contrast features that have been revealed during the present study. Using a McConnell superexchange formalism,[36] the electronic coupling between the tip and sample should increase as either the HOMO energy or LUMO energy of the substituted alkane approaches the Fermi level of the graphite substrate. At sufficiently large electronic coupling values, the functional group image should become bright in its STM contrast even if topographic effects alone would cause the tip to approach the sample.

A simple method for estimating the electronic coupling, and thus for predicting the image contrast of a given functional group in the STM images presented herein, would involve consideration of the ionization potentials of the various molecules of interest. When the coupling is dominated by the HOMO, functional groups with lower ionization potentials (IP) than the corresponding alkane should appear bright in the STM image, while functional groups with higher ionization potentials should appear dark. The IP values not only affect the energy denominator in the expression for the electronic coupling term, but lower IP values generally correlate with more a diffuse orbital structure of the functional groups of concern, which will enhance the wavefunction overlap term between the tip and the sample and thereby increase the value of the numerator in the electronic coupling expression.

This HOMO-IP model correlates remarkably well with the STM image contrast behavior observed in this work. Table 5 lists the ionization potentials of various substituted alkanes and related molecules of interest. In this framework, the disulfide and sulfide functionalities are predicted to exhibit a larger electronic coupling term than the methylene groups, and this expectation is in agreement with the observed STM images (Figures 14 and 15). The IP-STM contrast correlation predicts that if topographic effects are not predominant, an amine should be bright because of a large HOMO-derived electronic coupling term. This prediction is also in accord with the experimental STM data obtained in this work for dioctadecylamine, $(C_{18}H_{37})_2NH$ (Figure 16). Similar

correlations are apparent between the image contrast and the ionization potentials for the alkyl chlorides, alkyl iodides, and fluoroalkyl functionalities studied in this work (Table 5 and Figures 8, 9, 11, and 12).

On the basis of the electronic coupling term estimated from the ionization potential of *trans*-2-butene (Table 5), a carbon-carbon double bond is expected to be bright, and the STM image of 17-pentatriacontene shows this to be the case at both positive and negative bias (Figure 17). A carbon-carbon triple bond should also appear bright, and this prediction is in accord with the STM data of 7-hexadecyn-1-ol overlayers (Figure 17). The ionization potential of a nitrile, however, is so large that its HOMO should be further from the Fermi level of the graphite than the HOMO of the corresponding alkane. Thus, as long as topography does not overwhelm the electronic coupling effect, the nitrile should be dark in STM image contrast despite the presence of a pi orbital system. This prediction is consistent with the observed behavior of the nitrile functionality in the STM image of 1-hydroxy-12-dodecanenitrile (Figure 19).[37]

Table 5

Molecule	Ionization Potential (eV)[32]
n-$(C_3H_7)_2NH$	7.8
Bu-S-S-Bu	8.5
H_3C-S-CH_3	8.7
$H_3CCH{=}CHCH_3$	9.1
n-C_4H_9I	9.2
$H_3CC\int CCH_3$	9.9
n-C_4H_9Br	10.2
n-C_4H_{10}	10.6
n-C_4H_9Cl	10.7
n-C_3H_7F	11.3
n-$C_3H_7C\int N$	11.7

The alkyl bromide appears to be an exception to the predictions of the HOMO-IP electronic coupling model. The alkyl bromide is slightly larger than, and also has a slightly lower ionization potential than, the corresponding unsubstituted alkane. Nevertheless, the alkyl bromide functionality appears dark in the STM images (Figure 10). Detailed electronic structure calculations, described in the accompanying manuscript, indicate a prominent role for the unoccupied orbitals of the alkane and alkyl bromide in dominating the electronic coupling between the tip and the sample. This more detailed model differs from the HOMO-IP approach in that it places more weight on specific electronic coupling effects that can arise from the contribution of the very energetic, but highly diffuse, LUMOs of the various substituted alkanes to the highly specific tunneling matrix element that is directed along the direction defined by the tip-sample gap. Since this direction is most heavily probed in the STM experiment, the orbital diffuseness becomes much more important in defining the overall electronic coupling matrix element in the STM image than it is in an intramolecular electron transfer experiment between a donor at one end of an alkyl chain and an acceptor at the other end of an alkyl chain. Further evidence for such differences are evident from the dominance of the carbon-carbon sigma bonding framework in determining electronic couplings in intramolecular electron transfer reactions relative to the dominance of the C-H bond positions in the STM images of alkanes. Thus, although the HOMO-IP approach seems to work remarkably well in predicting most of the STM image contrast behavior observed to date, the exact weighting of the HOMO and LUMO contributions to the tunneling matrix element in the general STM experiment will require additional elucidation both experimentally and theoretically.

4. Metrics of Various Functional Groups in STM Images

Although some functional groups produced STM features with dimensions that were in good accord with those expected from molecular modeling, other functional groups, such as amines and, most notably, disulfides, appeared to be much wider than might be expected. These large apparent length metrics cannot be consistently attributed

solely to a lack of resolution in the STM data, since other portions of these images showed features that indicated significantly higher spatial resolution during the experiment.

At least three factors can contribute to this effect. First, the presence of a functional group can influence the local electronic coupling at neighboring methylene atoms in the substituted alkane, thereby creating the observed increased region of apparent functional group influence in the STM image. Another contributing factor is that the local molecular topography of the overlayer is often distorted around the functional group, resulting in a modification of the STM image over such distorted structural features. A semiquantitative estimate of these electronic and topographic effects has been obtained from *ab initio* electronic structure calculations that are described in the accompanying manuscript. These calculations yield remarkably close agreement between the computed and observed STM images for most of the molecules investigated herein. Finally, an additional factor to be considered is that the observed current profile is actually the result of a two-dimensional problem, in which the tip-sample current is free to traverse any spatial path that provides the best electronic coupling between the tip and the sample at a given position in the scan. The dominant pathway when the tip is adjacent, but not directly over, a functional group with a high electronic coupling term might involve through-space interactions to the functional group (in a direction predominantly parallel to the surface plane) as opposed to the more spatially direct, but poorer electronic coupling path directly through the functional group and normal to the surface. This effect may play a role under the ambient pressure conditions under which the current study has been performed, since it is well-documented that the tip-sample tunneling current under such conditions shows an anomalously small distance decay exponent.[38] Without still higher resolution images, and perhaps low temperatures to freeze out any molecular motion and to eliminate the anomalous distance dependence of

the tunneling current, we are unable to evaluate the relative importance of this factor in a quantitative fashion.

5. Symmetry Properties of the STM Image Contrast of Molecular Overlayers on Graphite

In addition to the theoretical expectations discussed above that address the relative contributions of topographic and electronic effects in determining the STM image contrast, it is also of interest to understand the dependence of the STM images on the tip/sample bias voltage. A striking feature of the data for all functional groups investigated herein is the insensitivity of the image contrast to the tip/sample voltage polarity.[39] The density of states in the graphite substrate is nearly independent of polarity at low bias voltages.[40] However, the molecular overlayer is not expected, in general, to possess a symmetrical distribution with respect to the Fermi level of the graphite of the energy levels or of the individual tip/sample electronic coupling matrix elements of the system. Despite this expected asymmetry, the functional group contrast observed in the images of these overlayers (c.f. Figures 1-19) was independent of the bias polarity. It is commonly assumed that tunneling into the surface should reflect the electronic coupling contours of the LUMO of the adsorbate and tunneling out of the surface should reflect the contours of the HOMO of the adsorbate.[2(g), 19] In this scenario, an asymmetry of the image contrast should generally be expected for functional groups having different locations of their HOMO and LUMO energies relative to the Fermi level of the substrate. We note, however, that this assumption strongly depends on the actual form of the potential distribution between the tip and the sample. We treat the general case below and then discuss the limiting situations as they apply to our experimental data in order to develop a fundamental understanding of the observed symmetry in image contrast with respect to bias polarity.

At a given bias voltage and location over the substrate, the tunneling current is a function of the density and occupancy of the electronic states in the tip, the density and

occupancy of the electronic states in the substrate, and the quantum mechanical matrix elements that couple the electronic states in tip and substrate. One expression that can be used to evaluate the STM current, based on the Fermi Golden rule approach to the calculation of the electronic coupling between an electron donor and an electron acceptor, is:[41]

$$i = \frac{2\pi e}{\hbar} \iint d^3\mathbf{k}_m d^3\mathbf{k}_t \left| H_{mt}(\mathbf{k}_m, \mathbf{k}_t) \right|^2 \left[f(\varepsilon_t) - f(\varepsilon_m) \right] \delta\left(\varepsilon_t - \varepsilon_m - ev\right) \qquad (1)$$

In this equation, the **k**'s refer to the orbitals in the substrate (M) and in the tip (T), and H_{mt} represents the electronic coupling matrix elements between these states at each energy and at each point in space. The occupancies of the orbitals at an energy ε (measured in excess of the respective Fermi levels of the tip and the substrate) are given by $f(\varepsilon_t)$ and $f(\varepsilon_m)$ (the Fermi-Dirac distribution functions $\left[1 + \exp(\varepsilon/k_B T)\right]^{-1}$ in the tip and substrate, respectively). The delta function in the expression of Eq. (1) insures that tunneling occurs only between states of the same energy in the tip and the substrate, and also accounts for the relative energy difference between the tip and substrate that is induced by applying a bias voltage, v, across the tip-sample gap. The bias voltage can be expressed as $v = \phi_t - \phi_m - \left(\phi_t^e - \phi_m^e\right)$, where the ϕ's denote electrostatic potentials and the e superscript denotes the value at zero current.

For a vacuum gap, the matrix elements H_{mt} are given by the well-known quantum mechanical expression for electron tunneling through a vacuum.[42] For the passage of the current across an adsorbed monolayer B, the matrix elements H_{mt} must instead describe the tip/sample coupling that arises from the presence of the orbitals in the molecular overlayer. In a superexchange formalism to calculate this coupling, the H_{mt} can be expressed as:[43]

$$H_{mt}(\mathbf{k}_m, \mathbf{k}_t) = \sum_{\beta} H_{m\beta} \; H_{\beta t} / \left(E_m - E_\beta\right) \qquad (2)$$

where $H_{m\beta}(\mathbf{k}_m)$ denotes the matrix element coupling orbital $\mathbf{k}_m$ in M to an orbital β of the molecular overlayer and $H_{\beta t}(\mathbf{k}_t)$ denotes the matrix element coupling β to the orbital $\mathbf{k}_t$ in T. The energy denominator is given by $E_m - E_\beta$, where E_m and E_β are the energies of the orbitals in M and B, with $E_m = \bar{\mu}_m + \varepsilon_m$, $\bar{\mu}_m$ being the electrochemical potential (Fermi level) of M, $\bar{\mu}_m = \mu_m^0 - e\phi_m$. (Similarly, below, $\bar{\mu}_t = \mu_t^0 - e\phi_t$ and we note that the delta function constraint in Eq. (1) can be shown to be equivalent to $\bar{\mu}_m + \varepsilon_m = \bar{\mu}_t + \varepsilon_t$.) The expression of Eq. (2) thus arises from a simple perturbation theory approach to evaluating the electronic coupling between the tip and substrate states due to the presence of the orbitals of the intervening overlayer.

Of primary concern is the symmetry of *i* with respect to the value of the tip-substrate bias, v. When the bias is changed, the relation of the M and T energy levels is changed. This effect is manifested in Eq. (1) through the constraint imposed by the delta function, which insures an isoenergetic tunneling of electrons through the tip-substrate gap. In addition, the energy denominator $E_m - E_\beta$ in Eq. (2), which determines the electronic coupling terms H_{mt} at a given tip-sample bias voltage, is a function of bias voltage. Following the recent work of Marcus,[43] the mean potential of the bridge levels β can be approximated to be $1/2(\phi_m + \phi_t)$. In other words, the molecular overlayer experiences a potential drop that is ≈1/2 of the total potential dropped between the tip and the substrate. In this case one can show that[43]

$$E_m - E_\beta = \frac{1}{2}\left(\mu_m^0 + \mu_t^0 + \varepsilon_m + \varepsilon_t\right) - E_\beta^0 \qquad (3)$$

where E_β^0 is the value of E_β at zero potential.

Using Eq. 3 to address quantitatively the bias dependence of the image contrast implies replacement of v with -v in Eq. (1). A change in sign of v to -v is equivalent to interchanging ε_m and e_t according to the delta function in Eq. (1). This interchange changes the sign of the term in square brackets in Eq. (1), but clearly [Eq. (3)] leaves

E_m - E_β unaffected. Thus, we have

$$i(v) = -i(-v) \quad (4)$$

if the $H_{m\beta}H_{\beta t}$ is independent of, or only weakly dependent on, v.

Based on the discussion above, in the regime of linear I-V behavior wherein the molecule experiences an equivalent potential drop regardless of whether the tip or the sample is biased away from equilibrium, the electronic coupling is the sum of the coupling matrix elements through the HOMO and LUMO, regardless of the bias condition. This summation over all available coupling orbitals necessarily produces a symmetry with respect to bias, and provides a natural explanation for the observation of symmetry in image contrast that was observed experimentally for all systems studied.

An alternative possibility is that the adsorbate is in strong electrical contact with the sample, and that the applied bias predominantly affects the potential across the adsorbate/tip region but not between the sample and the adsorbate. In this case, a large enough bias perturbation would produce a differential electronic coupling to the LUMO with the tip negative of the Fermi level and to the HOMO with the tip biased positive relative to the Fermi level of the substrate. This situation would, however, require a fortuitously symmetric (or nearly so) positioning of the HOMO and LUMO levels relative to the Fermi level of the graphite substrate and would also require nearly equal orbital diffuseness in the HOMO and LUMO for all of the functional groups investigated in this study. As described in the accompanying manuscript, theoretical calculations do not support the occurrence of this unlikely set of coincidences for any of the molecules studied in this work. Variation of the Fermi level of the substrate over a sufficiently wide range of energy while maintaining all of the other desirable properties of the graphite/alkane-alkanol overlayer system would thus be of interest to probe this effect further. Such experiments might be possible through the use of substrates such as H-terminated Si or on TaS_2, and such systems are being investigated experimentally at present.

V. Conclusions

In conclusion, we have shown that it is possible to distinguish between the topographic locations of various functional groups based on their image contrast and apparent geometric properties using STM data obtained at room temperature and atmospheric pressure. Such studies are made possible by the investigation of ordered overlayers of molecular systems, which can be reproducibly imaged and varied chemically in a systematic fashion. An analysis of high resolution STM images of alkanes and alkanols reveals that topographic factors dominate the image contrast of such systems and also indicates that the molecules in these overlayers are oriented with their carbon-carbon skeleton parallel to the graphite surface. Additionally, the bright spots in these molecular images are predominantly determined by the positions of the hydrogen atoms on the methylene units of the alkyl chains. The STM contrast of the various functional groups investigated in this work was not only a function of topography but also was influenced by the local electronic coupling. For molecules in which electronic effects overwhelmed topographic effects in dominating the image contrast, electronic coupling between both the HOMO and LUMO must be considered at low and moderate bias in an STM image, leading to an explanation of the observed functional group image contrast as well as an explanation of the bias symmetry of several representative functional groups.

VI. Acknowledgments

We acknowledge the NSF, grants CHE-9202583 (NSL), CHE-95-22179 (WAG), and ASC-92-17368 (WAG) for partial support of this work. C.C. acknowledges the NIH for a training grant, and we also acknowledge helpful discussions with Dr. J. Miller of Argonne National Laboratories regarding orbital coupling issues.

VII. References

(1) Binnig, G.; Rohrer, H. *Angew. Chem.* **1987**, *99*, 622; *Angew. Chem. Int. Ed. Engl.* **1987**, *26*, 606.

(2) For STM of organic materials, see: (a) Frommer, J. *Angew. Chem. Int. Ed. Engl.* **1992**, *31*, 1298. (b) Smith, D.; Hörber, J.; Binnig, G.; Nejoh, H. *Nature* **1990**, *344*, 641. Foster, J.; Frommer, J. *Nature* **1988**, *333*, 542. (c) Smith, D; Hörber, J.; Gerber, C.; Binnig, G. *Science* **1989**, *245*, 43. (d) Ludwig, C.; Gompf, B.; Glatz, W.; Petersen, J.; Eisenmenger, W. *Z. Phys. B.* **1992**, *86*, 397. (e) Smith, D.; Heckl, W. *Nature* **1990**, *346* 616. (f) Ohtani, H.; Wilson, R.; Chiang, S.; Mate, C. *Phys. Rev. Lett.* **1988**, *60*, 2398. (g) Lippel, P.; Wilson, R.; Miller, M.; Wöll, C.; Chiang, S. *Phys. Rev. Lett.* **1989**, *62*, 171. (h) Hallmark, V.; Chiang, S.; Brown, J.; Wöll, C. *Phys. Rev. Lett.* **1991**, *66*, 48. (i) Kim, Y.; Bard, A. *Langmuir* **1992**, *8*, 1096. (j) Smith, D.; Bryant, A.; Quate, C.; Rabe, J.; Gerber, C.; Swalen, J. *Proc. Natl. Acad. Sci. USA* **1987**, *84*, 969. (k) McMaster, T.; Carr, H.; Miles, M.; Cairns, P.; Morris, V. *Macromolecules* **1991**, *24*, 1428. (l) Yang, R.; Naoi, K.; Evans, D.; Smyrl, W.; Hendrickson, W. *Langmuir* **1991**, *7*, 556. (m) Wilson, R.; Meijer, G.; Bethune, D.; Johnson, R.; Chambliss, D.; de Vries, M.; Hunziker, H.; Wendt, H. *Nature* **1990**, *348*, 621. (n) Li, Y.; Chander, M.; Patrin, J.; Weaver, J.; Chibante, L.; Smalley, R. *Science* **1991**, *253*, 429. (o) Allen, M.; Ballooch, M.; Subbiah, S.; Tench, R.; Siekhaus, W.; Balhorn, R. *Scanning Microsc.* **1991**, *5*, 625. (p) Youngquist, M.; Driscoll, R.; Coley, T.; Goddard, W.; Baldeschwieler, J.; *J.Vac. Sci. Technol. B* **1991**, *9*, 1304. (q) Lu, X.; Hipps, K.W.; Wang, X.D.; Mazur, U.; *J. Am. Chem. Soc.*, **1996**, *118*, 7197.

(3) For example, see: Driscoll, R. J.; Youngquist, M. G.; Baldeschwieler, J. D. *Nature* **1990**, *346*, 294.

(4) (a) Clemmer, C.; Beebe, T. *Science* **1991**, *251*, 640. (b) Chang, H.; Bard, A. *Langmuir* **1991**, *7*, 1143.

(5) Kim, Y.; Long, E. C.; Barton, J. K.; Lieber, C. M. *Langmuir* **1992**, *8*, 496.

(6) (a) Patrick, D. L.; Cee, V. J.; Beebe, T. *Science* **1994**, *265*, 231.

(b) Patrick, D. L.; Cee, V. J.; Beebe, T. P. *J. Phys. Chem.*, **1996**, *100*, 8478.

(7) Groszek, A. J. *Nature* **1962**, *196,* 531.

(8) Findenegg, G. H.; Lippard, M. *Carbon* **1987**, *25*, 119.

(9) Parfitt, G. D.; Willis, E. *J. Phys. Chem.* **1964**, *68*, 1780.

(10) Groszek, A. J. *Proc. Roy. Soc. London Ser. A* **1970**, *314*, 473.

(11) Findenegg, G. H *J. Chem. Soc. Faraday Trans.* **1973**, *69*, 1069.

(12) Rabe, J. P.; Buchholz, S. *Science* **1991**, *253*, 424.

(13) Cincotti, S.; Rabe, J. P. *Appl. Phys. Lett.* **1993**, *62*, 3531.

(14) McGonigal, G. C.; Bernhardt, R. H.; Thomson, D. J. *Appl. Phys. Lett.* **1990**, *57*, 28.

(15) McGonigal, G. C.; Bernhardt, R. H.; Yeo, Y.; Thomson, D. J. *J. Vac. Sci. Technol. B* **1991**, *9*, 401.

(16) Buchholz, S.; Rabe, J. P. *Angew. Chem. Int. Ed. Engl.* **1992**, *31*, 189.

(17) Yeo, Y. H.; McGonigal, G. C.; Thomson, D. J. *Langmuir* **1993**, *9*, 649.

(18) Buchholz, S.; Rabe, J. P. *J. Vac. Sci. Technol. B* **1991**, *2*, 1126.

(19) Rabe, J. P.; Buchholz, S.; Askadskaya, L. *Synth. Met.* **1993**, *54*, 349.

(20) (a) Venkataraman, B.; Flynn, G. W.; Wilbur, J. L.; Folkers, J. P.; Whitesides, G. M. *J. Phys. Chem.* **1995**, *99*, 8684. (b) Cyr, D. M.; Venkataraman, B.; Flynn, G. W.; Black, A.; Whitesides, G. M. *J. Phys. Chem.* **1996**, *100*, 13747. (c) Cyr, D. M.; Venkataraman, B.; Flynn, G. W. *Chem. Mater.* **1996**, *8*, 1600.

(21) Morishige, K.; Takami, Y.; Yokota, Y. *Phys. Rev. B* **1993**, *48*, 8277.

(22) (a) Larsson, U.; Carlson, R.; Leroy, J. *Acta Chem. Scand.* **1993**, *47*, 380.

(b) Bennett, G. M.; Gudgeon, H. *J. Chem. Soc.* (London) **1938**, 1679.

(23) *CRC Handbook of Chemistry and Physics*, Weast, R. C.; Lide, D. R.; Astle, M. J.; Beyer, W. H., ed.; CRC Press: Boca Raton, 1989.

(24) Vollhardt, P. C.; *Organic Chemistry*; W. H. Freeman: New York, 1987; pp 58-59.

(25) Liang, W.; Whangbo, M. H.; Wawkuschewski, A.; Cantow, H. J.; Magonov, S. N. *Adv. Mater.* **1993**, *5*, 817.

(26) Kuwabara, M.; Clarke, D. R.; Smith, D. A. *Appl. Phys. Lett.* **1990**, *56*, 2396.

(27) Xhie, J.; Sattler, K.; Ge, M.; Venkateswaran, N. *Phys. Rev. B* **1993**, *47*, 15835.

(28) Rabe, J. P.; Buchholz, S.; Askadskaya, L. *Synth. Met.* **1993**, *54*, 349.

(29) Wawkuschewski, A.; Cantow, H. J.; Magonov, S. N.; Möller, M.; Liang, W.; Whangbo, M. H. *Adv. Mater.* **1993**, *5*, 821.

(30) Pomerantz, M.; Aviram, A.; McCorkle, R. A.; Li, L.; Schrott, A. G. *Science* **1992**, *255*, 1115.

(31) Niki, K., personal communication.

(32) Mizutani, W.; Shigeno, M.; Ono, M.; Kajimura, K. *Appl. Phys. Lett.* **1990**, *56*, 1974.

(33) Okumura, A.; Miuamura, K.; Gohshi, Y. *Jpn. J. Appl. Phys.* **1992**, *31*, 3452.

(34) We note that the image which was interpreted as evidence for the alkane reorientation process was obtained under conditions of significant thermal drift in order to produce the rectangular spot pattern for the methylene units in the alkyl chain. In addition, a recent neutron diffraction study has concluded that vapor-deposited $C_{32}D_{66}$ overlayers are adsorbed on graphite with their carbon-carbon skeletons oriented parallel to the graphite surface plane, in accord with our STM images: Herwig, K.W.; Matthies, B.; Taub, H.. *Phys. Rev. Lett.* **1995**, *75*, 3154.

(35) Note that the image contrast observed in this work for alkanol and substituted alkanol overlayers on graphite is in good agreement with STM images reported recently for substituted alkane overlayers on graphite. This earlier study

concluded that -OH and -Cl functionalities could not be observed by STM, [20] and thus these groups were ordered as similar in STM image contrast to the methyl and methylene functionalities of substituted alkane overlayers. This ordering seems to require modification in view of the STM data presented in this work. Data for an alkyl bromide ($C_{22}H_{45}Br$) overlayer indicated that the bromide group was typically dark in STM image contrast relative to the methylene chains of this overlayer,[20] in agreement with the STM data for overlayers of $Br(CH_2)_{12}OH$ displayed in Figure 10. When the $C_{22}H_{45}Br$ films were imaged continuously for a significant time period, the Br groups were reported to change contrast to bright.[20] Such changes in image contrast have not been observed in our work, presumably because the substituted alkanols used herein are more constrained in their orientational preferences than are the substituted alkanes. This difference is reasonable because of the presence of the hydrogen bonding network between the -OH groups in the alkanol overlayer. As described in more detail in the accompanying manuscript, a change in STM contrast from dark to bright would be expected if the Br group were to move from a trans- position to a gauche- position relative to the carbon-carbon skeleton of an alkane chain. Such a process might explain the image contrast changes observed for the alkyl bromide after significant observation time under the STM tip.[20]

(36) McConnell, H. M. *J. Chem. Phys.* **1961**, *35*, 508.

(37) STM data for a nitrile group in an overlayer of the liquid crystal 4'-*n*-alkyl-4-biphenyl has been obtained previously.[2 (a,b,c,e), 6a] Smith et al reported that the nitrogen atom of the nitrile appeared to be brighter than the carbon atom of the nitrile.[2b] Inspection of the published images of the liquid crystals appears to indicate that it would be extremely difficult to identify atomically-localized regions of the nitrile group based on the STM data available to date.

(38) (a) Binnig, G.; Rohrer, C.; Gerber, C.; Weibel, E. *Appl. Phys. Lett.* **1982**, *40*, 178. (b) Gimzewski, J. K.; Möller, R. *Phys. Rev. B* **1987**, *36*, 1284. (c) Gimzewski, J. K.; Möller, R.; Pohl, D. W.; Schlittler, R. R. *Surf. Sci.* **1987**, *189*, 15. (d) Mamin, H.J.; Ganz, E.; Abraham, D. W.; Thomson, R. E.; Clarke, J. *Phys. Rev. B* **1986**, *34*, 9015.

(39) Preliminary results of the STM images of stearone, $(C_{17}H_{35})_2CO$, indicate that this symmetry with bias may not always be observed. At negative sample bias, a bright feature associated with the carbonyl functionality is observed to have a length of 9.0 Å and height of 0.22 Å. At positive bias, however, a dark feature associated with the carbonyl functionality is observed to have a length of 8.5 Å and a depth of 0.25 Å. The STM image contrast of this molecule, and related ketones, is under further investigation in order to ascertain the origin of this effect.

(40) *Metals: Phonon States, Electron States and Fermi Surfaces*, Hellwege, K.H.; Olsen, J. L., ed.; Springer-Verlag: Berlin, 1981.

(41) Hui, O.-Y..; Kallebring, B.; Marcus, R. A. *J. Chem. Phys.* **1993**, *98*, 7565.

(42) Hansma, P. K.; Tersoff, J. *J. Appl. Phys.* **1987**, *61*, R21.

(43) Marcus, R. A. *J. Chem. Soc. Faraday Trans.* **1996**, *92*, 3905.

electronic and geometric effects. Thus, to fully exploit this imaging technique, it is important to understand how different aspects of the adsorbate and the experimental conditions blend together to create the observed images.

In order to study and explain such phenomena for a large number of molecules, this chapter describes a theoretical model that has been developed to simulate the STM process. The method is accurate enough to be useful and reliable, it is simple enough to provide a facile method for interpretation of the available STM results, and it is cheap enough to be applicable to the systems of interests--small functionalized alkanes on HOPG--with affordable computational effort, e.g., a few hours on an HP9000 workstation.

In order to attain this goal, we have developed an alternative to expensive quantum mechanics computations that include explicitly the wave functions of the tip and/or the graphite. Our approach is to (1) use a force field (FF) to optimize the geometry of the adsorbed molecules on graphite, (2) determine the shapes and the energies of the molecular orbitals using Hartree-Fock (HF) computations for the isolated molecule, and (3) then simulate the STM image using a simple perturbative approach, which adds negligible cost with respect to steps 1 and 2.

Several theories have already been developed to predict and explain STM images of both surfaces and adsorbates. Tersoff and Hamman[6] used the transfer Hamiltonian approach first introduced by Bardeen.[7] Their conclusion is that the observed current is proportional to the local density of states (LDOS) at the Fermi energy of the sample, at the position of the tip. Adsorbates are observed through the change they induce in the LDOS of the support. Lang[8] replaced the support and the tip with the jellium model and used a metal atom to mimic the tip. This procedure was used to predict the images of adsorbed atoms using the transfer Hamiltonian approach in the low bias limit. Doyen and co-workers[9] have used semiempirical techniques to study the exact tunneling current, evaluating the interactions between the tip and the support explicitly and without the

assumptions of the transfer Hamiltonian. More recently Hallmark, Chiang, and co-workers[10] have used extended Hückel calculations to predict images of aromatic molecules adsorbed on a metal substrate, and Sautet[11] used electron scattering techniques for the same purpose. Liang *et al.*[2] have also used the extended Hückel method to investigate the STM images of alkanes on graphite. Fisher and Blöchl[12] instead have performed *ab initio* density functional theory studies to simulate the STM imaging of adsorbed benzene molecules on graphite and MoS_2. Hui, Marcus, and Källebring[13] have developed a model for STM imaging of adsorbed molecules that includes the effect of *d* orbitals on the tip.

The models based on the transfer Hamiltonian have proven effective in predicting images of conducting surfaces in the low bias limit. Tersoff-Hamman theory has been used to interpret atomic resolution STM images of insulating molecules on a metallic substrate, and these studies have indicated that the molecular features of the images are determined by the most protruded atoms of the adsorbed molecules.[2,5] In addition, this work indicated that the insulating molecules were detected because their orbitals mix slightly into the Fermi level of the metallic substrate and because they are close to the tip.[2,5] When adsorbed insulating molecules are sampled with higher biases, this approach requires that the periodic molecular structure, as well as the supporting graphite, be included in the simulation.[2,12] As a result, significant effort is spent computing the band structure of the graphite every time a new molecule is studied. The method then becomes as complex as other approaches that can lead, in principle, to an exact prediction but are not based on the transfer Hamiltonian approximation. The result is that most methods that include the detailed wave functions of the graphite and the tip give excellent results but require extensive computations.

The goal of our work was to develop a theoretical approach that could aid in the interpretation of the experimental images obtained for alkanes and alkanols on graphite, in which the overlayer only is observed at high tip/sample biases.[1-3] Of course, the states of the graphite and of the tip are the initial and final states for tunneling processes for all of

these molecular overlayers on a graphite surface. However, the primary goal of this theoretical study was to gain insight into the relative contributions of topographic and electronic factors in determining the STM contrast of different functional groups in the molecular overlayer. Since the experimental images for the different overlayers were obtained at a relatively constant tip/sample bias, the theoretical treatment focused on describing the changes in STM contrast for the various different molecules. To achieve this goal, a simple model was built that ignores the shape of the graphite states and that considers the coupling, or perturbation, between molecular states and a simplified version of graphitic states. In the high bias limit, such a model is expected to produce, at a fraction of the cost, the same results as a more complete treatment that explicitly includes the graphite orbitals. Of course, in the low bias limit, and for intermediate bias situations, this model will not be computationally useful nor physically appropriate. Our approach does, however, allow simulations of STM images on reasonably big systems with a good description of the molecular states involved mediating the tunneling process.

In section II we present the theoretical model and the approximations used to implement it. Section III then describes the predictions of the model and compares model and experiment for a number of molecules for which the experimental images have been obtained.

II. Theoretical Model

We are interested in determining how the electric current between a tip and a graphite support is modulated by one molecule adsorbed on the graphite. In the cases of concern, the molecules are physisorbed onto the graphite via van der Waals interactions. These interactions are small compared to the intramolecular forces, since van der Waals forces are typically on the order of 1 kcal/mol per pair of atoms, while bond energies are on the order of 100 kcal/mol per bond. Thus, the shape of the molecular wave function for the adsorbed molecule is not expected to change significantly relative to that of the unadsorbed molecule. Also, the interaction between the tip and the molecule must be

small; otherwise the molecule would be displaced by the tip, and it could not be observed in the experimental STM image. The orbital energies, on the other hand, are expected to be affected by the presence of two conductors in close proximity to the molecule. According to classical electrostatics, the presence of the conductors results in a shift of the ionization potentials and electron affinities of the molecule, as described in section II.E.

II.A. Formalism

We will use the symbol $|t\rangle$ to describe the wave function of the tip. $|t\rangle$ belongs to a continuum of states with energies E_t and with a density of states $\rho_t(E_t)$. E_t^f indicates the Fermi energy of the tip. Similarly, $|g\rangle$ indicates the wave function of the graphite support, with E_g, $\rho_g(E_g)$, and E_g^f defined as the corresponding energy, density of states, and Fermi energy, respectively. Also, the adsorbed molecule is described by its molecular orbitals $|k\rangle$ (and occasionally $|l\rangle$) having orbital energies $E_k(E_l)$.

When a potential E_b, equivalent to a bias $-E_b$, is applied to the graphite support, electrons may flow from the more negative to the more positive side of the tunnel gap. When $E_g^f + E_b > E_t^f$, the electrons will flow from the states with energy $E_g \in (E_t^f, E_g^f + E_b)$ on the graphite to the states with energy $E_t \in (E_t^f, E_g^f + E_b)$ on the tip. The reverse is true when $E_g^f + E_b < E_t^f$. Throughout the chapter, the energy band into which the electrons are transferred under such a bias is denoted as the conduction region.

II.B. Coupling Potential

The perturbative potential, V, is the effective potential experienced by an electron in the region of space occupied by the molecule. Within the independent particle approximation, this potential is due to the Coulomb attraction of the nuclei, the average Coulomb repulsion from the molecular electrons, and the exchange interaction (from the Pauli principle).

V is exactly the potential used to solve the Hartree-Fock equation for the isolated

molecule, so it acts on the molecular orbitals k as described in eq 1:

$$V^{HF}\,|k\rangle = (H^{HF} - T)\,|k\rangle = (E_k - T)\,|k\rangle \qquad (1)$$

where E_k is the orbital energy from the HF computation, T is the kinetic energy operator and H^{HF} is the Hartree-Fock Hamiltonian.

We are interested in tunneling conditions corresponding to the experimental observations, for which the molecules dominate the STM image contrast. This observation indicates that the direct coupling between the tip and the graphite is much smaller than the coupling through the molecular states. Thus it is legitimate to neglect the direct coupling of tip and graphite and to consider only the coupling through the molecular orbitals. This is equivalent to assuming that the unperturbed states of both tip and graphite overlap with the molecular wave function but not with each other. We also assume that there is no coupling between different states on the tip or on the graphite.

In this case, evaluation of all the relevant matrix elements for the coupling potential is readily performed:

$\langle t\|V\|g\rangle = 0$	assumed	
$\langle t\|V\|k\rangle = E_k S_{tk} - T_{tk}$	from eq 1	
$\langle g\|V\|k\rangle = E_k S_{gk} - T_{gk}$	from eq 1	
$\langle k\|V\|k'\rangle = 0$	because the Mos are HF solutions	
$\langle t\|V\|t'\rangle \approx 0$	assumed	
$\langle g\|V\|g'\rangle \approx 0$	assumed	(2)

where S and T are the overlap and kinetic energy matrices, respectively.

II.C. Perturbation Theory: Nondegenerate Case

The tunneling probability will be evaluated through the use of time-independent perturbation theory.[14] When the perturbation is off, the tip, molecule, and graphite do not interact. Thus, the unperturbed eigenstates are the functions $|t\rangle$ and $|g\rangle$ for the tip and

the graphite along with the molecular orbitals $|k\rangle$ for the molecule. In the presence of the perturbation, the tip wave function is corrected by the first-order term of (3),

$$|t^{(1)}\rangle = \sum_k \frac{V_{kt}}{(E_t - E_k)}|k\rangle \tag{3}$$

and by the second-order term of (4),

$$|t^{(2)}\rangle = \sum_k \frac{V_{gk}V_{kt}}{(E_t - E_k)(E_t - E_g)}|g\rangle - \frac{1}{2}\sum_k \frac{|V_{kt}|^2}{(E_t - E_k)^2}|t^{(0)}\rangle \tag{4}$$

The first correction due to the function $|g\rangle$ appears in the second-order term. It is as if the functions $|t\rangle$ and $|g\rangle$ were coupled to first-order by the effective element:

$$v_{tg} = \sum_k \frac{V_{gk}V_{kt}}{(E_t - E_k)} \tag{5}$$

To first-order, this matrix element will be responsible for the tunneling current.

According to the Fermi golden rule, the number of transitions per unit time $d\omega_{gt}$ between an initial state $|t\rangle$ and all final states $|g\rangle$ with energy between E_g and $E_g + dE_g$ is[14]

$$\mathrm{d}\omega_{gt} = \frac{2\pi}{\hbar}|v_{tg}|^2 \delta(E_t - E_g)\, \rho_g(E_t)\, \mathrm{d}E_g \tag{6}$$

The total current is then

$$I_{gt} = \frac{2\pi}{\hbar}\int \rho_t(E_t)\, \mathrm{d}E_t \int \rho_g(E_g)\, \mathrm{d}E_g \left|\sum_k \frac{V_{gk}V_{kt}}{(E_t - E_k)}\right|^2 \delta(E_t - E_g) \tag{7}$$

$$= \frac{2\pi}{\hbar}\int \left|\sum_k \frac{V_{gk}V_{kt}}{(E - E_k)}\right|^2 \rho_t(E)\, \rho_g(E)\, \mathrm{d}E \tag{8}$$

where all integrals are over the conduction region. A more detailed description of the bias dependence is given in Appendix A.

This approach provides an alternate method, relative to the traditional transfer Hamiltonian formalism,[6,7] for obtaining an expression for the tunneling current under our conditions. In the transfer Hamiltonian formalism,[6] the graphite wave function includes explicitly the contributions from the molecular states.[2] Its coupling with the tip is due, in the high bias limit, mainly to these contributions. In our approach, the same physical picture is described, but within the framework of a perturbation theory formalism. The results are thus consistent with the transfer Hamiltonian theory and help to gain insight into the STM process of concern in the experimental data by focusing on the properties due to molecular states.

It should be noted that the common assumption that all of the STM current flows to or from states near the graphite Fermi level[2] does not hold in the high bias regime. The current involves all the states in the conduction region; hence an integration over energy in this region is required. This integration was performed for all of the molecular overlayers investigated during the course of this study.

II.D. Perturbation Theory: General Case

The above theory holds only for the case when all the energy differences in the denominators are large with respect to the coupling elements in the numerators. A more general treatment is described in this section. The molecular spectrum can be considered as a continuum with the following distribution:

$$S(E) = \sum_k V_{gk} V_{kt} \delta^{(\epsilon)}(E - E_k) \tag{9}$$

where $\delta^{(\epsilon)}(x)$ is such that

$$\lim_{\epsilon \to 0} \delta^{(\epsilon)}(x) = \delta(x) \tag{10}$$

and ε is a small quantity with the physical meaning of uncertainty in the energy. For instance, $\delta^{(\varepsilon)}(x)$ can be taken to be a square function centered at $x = 0$ of width ε and height $1/\varepsilon$.

It is now necessary to estimate the order of magnitude of ε. Whenever one of the orbitals falls in the conduction region, it is expected to be responsible for most of the observed current. A typical current used in STM imaging is 650 $pA = 9.8 \times 10^{-8}$ au, so on average one electron leaves the orbital to contribute to the current every $1/9.8 \times 10^{-8} \approx 1 \times 10^{-7}$ au of time. If we further assume that the orbital is doubly occupied half of the time, then each electron spends about 5×10^{-6} au of time in the orbital; that is, the state with the electron in the orbital has an average lifetime of 5×10^{-6} au, which implies an uncertainty in its energy of $\hbar/5 \times 10^{-6} = 2 \times 10^{-7}$ hartrees. Thus, a very rough order-of-magnitude estimate gives $\varepsilon \approx 2 \times 10^{-7}$ and yields $\delta^{(\varepsilon)}(0) \approx 5 \times 10^{-6}$ au.

The number of transitions per unit time is then[14]

$$d\omega_{gt} = \frac{2\pi}{\hbar}\left|\int \frac{S(E)}{(E_t - E + i0)}dE\right|^2 \delta(E_t - E_g)\,\rho_g(E_t)\,dE_g \tag{11}$$

where the notation $i0$ indicates that in evaluating the integral, one must take the principal value plus half the contribution from the residue on the integration path:

$$\int \frac{S(E)}{(E_t - E + i0)}dE = \mathscr{P}\int \frac{S(E)}{(E_t - E)}dE + i\pi S(E_t) \tag{12}$$

Since ε is small, the integral can be computed easily. When all orbitals are not degenerate with the tip, this expression becomes the same as the one found for the nondegenerate case. When one of the orbitals, for example $|l\rangle$, is degenerate with the tip, its contribution to the principal value of the integral vanishes, so the integral becomes

$$\int \frac{S(E)}{(E_t - E + i0)} dE = \sum_{k \neq l} \frac{V_{gk} V_{kt}}{E_t - E_k} + i\pi V_{gl} V_{lt} \delta^{(\epsilon)}(0) \tag{13}$$

The number of transitions per unit time due to the degenerate orbital is then

$$d\omega_{gt} = \frac{2\pi}{\hbar} \pi^2 |V_{gl} V_{lt}|^2 [\delta^{(\epsilon)}(0)]^2 \, \delta(E_t - E_g) \, \rho_g(E_t) \, dE_g \tag{14}$$

The actual formula for the current is therefore

$$I \propto \int_{CR} \rho_t(E) \, \rho_g(E) \left| \sum_{k \notin CR} \frac{V_{gk} V_{kt}}{(E - E_k)} + i\pi \sum_{k \in CR} V_{gk} V_{kt} \delta^{(\epsilon)}(E - E_k) \right|^2 dE \tag{15}$$

where CR indicates the conduction region. Expanding the absolute value yields the desired expression:

$$I \propto \int_{CR} \rho_t(E) \, \rho_g(E) \left\{ \left[\sum_{k \notin CR} \frac{V_{gk} V_{kt}}{(E - E_k)} \right]^2 + [\pi \sum_{k \in CR} V_{gk} V_{kt} \delta^{(\epsilon)}(E - E_k)]^2 \right\} dE \tag{16}$$

where again the bias dependence (described explicitly in Appendix A) is included implicitly into the energy terms of (16).

II.E. Practical Implementation

Several other approximations were made in order to simplify the practical implementation of this approach. These are described below.

First, the tip wave function was replaced by a single 2*s* oxygen orbital (using the STO-3G basis).[15] This orbital is similar in size to one lobe of a platinum d_z2 orbital, which would be the dominant orbital in computing the tip sample wave function overlap properties in a more complete quantum mechanical representation of the tip.

Second, the graphite wave function was replaced by an array of *2p* carbon orbitals (STO-3G basis) that were centered onto a grid of points. The coupling between the graphite and each MO was obtained by summing the absolute contributions from each lobe on the grid. Tests with various grid spacings gave essentially identical results. This choice of graphite basis set is one of several possible methods to implement practically our algorithm. As long as the wave function decay with distance is reasonable and coupling is allowed to occur to all of the graphite states, the result is expected to depend little on the actual form of the graphite wave function, especially when the features of interest are the relative functional group contrasts of the various molecular STM images under high bias conditions.

The grid used in the simulation was deliberately chosen to be more dense than the carbons on the real graphite surface in order to avoid accidental couplings that might arise due to the position of the grid.

Third, since the continuum and the discrete states cannot be easily normalized using the same criteria, the unnormalized states were used for the continuum part. As a consequence, all coupling elements are only known up to a proportionality constant. Thus, the actual current cannot be estimated at each tip position, but only the ratio between currents at different points is obtained.

This is not a practical drawback at the present time since only the relative tunneling probabilities are of primary interest in modeling the observed image contrast.

This approach does have the disadvantage that it requires tuning the tip-molecule distance based on the experimental images rather than on the intensity of the current. This approximation is a limitation to the method that could, in principle, be removed by explicitly taking into account the proper normalization of the continuum states. We prefer to keep the model as simple as possible and thus have not pursued such refinements at the present time.

Fourth, the orbital energies of the MOs used in (16) were shifted to account for the presence of two conductors in close proximity to the molecule. This required an estimate of the Coulomb term acting on the molecular state. Within the HF framework, the energy of an occupied orbital has the physical meaning of an ionization potential: $E_{occ} = -IP = E_{molecule} - E_{cation}$. The presence of the conductors has little effect on $E_{molecule}$, but it stabilizes the cation; therefore E_{occ} becomes less negative, and the ionization potential decreases. Another way to view this effect is the following: in vacuum, the IP is the energy needed to move one electron from the molecule to infinity, whereas in the presence of the conductors, the electron must be moved only from the molecule to the conductor; therefore the IP decreases.

The stabilization effect can be computed with the method of image charges. Let the charge on the molecule be localized at its center of mass. The center of mass is estimated to be roughly halfway between the tip and the graphite, which, for this purpose, are taken to be two semi-infinite conductors terminated by two parallel planes.

Let R be the distance between the two planes and $R/2$ the distance between each plane and the localized charge. In order for the potential to be zero on the surfaces of the conductors, a first pair of negative charges can be placed at a distance $R/2$ into each conductor. Each one of these charges will have positive images at a distance $3R/2$ into the opposite conductor, and so on, to infinity, as depicted in Figure 1.

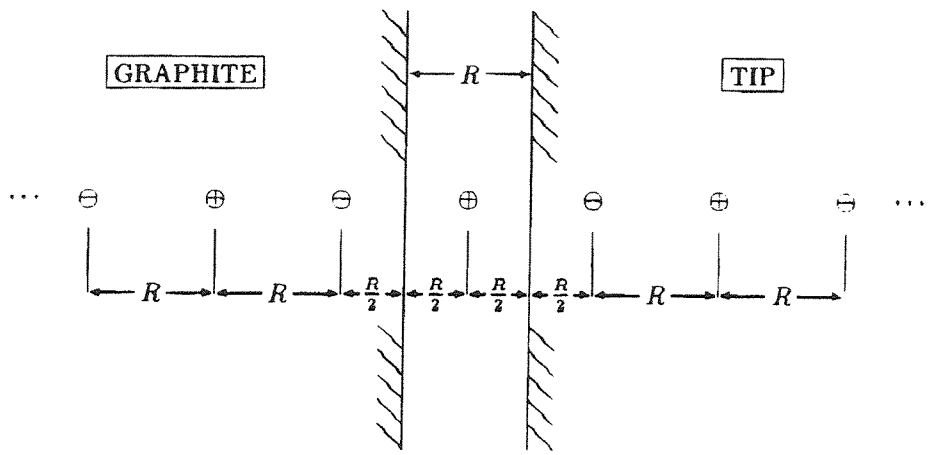

Figure 1. Charge distribution used to estimate the effect of the conductors on the orbital energies of the adsorbed molecule with the method of image charges. The molecular ion is replaced by a point charge halfway between the tip and the graphite, seen as semi-infinite conductors. R is the tip-graphite distance.

The electrostatic stabilization of the original charge due to this series of images is (in au)

$$\Delta E = 2\left\{-\frac{1}{R}+\frac{1}{2R}-\frac{1}{3R}+\ldots\right\} = \frac{2}{R}\sum_{n=1}^{\infty}\frac{(-1)^n}{n} = -\frac{2\log(2)}{R} \tag{17}$$

Thus, the occupied orbital energies used in the computation of the current are shifted by adding 2 log(2)/R, where R is the distance between the tip and the graphite.

The HF virtual orbitals, on the other hand, describe the energy required to add an electron to the molecule and thus have the physical meaning of electron affinities: $E_{\text{virt}} = E_{\text{anion}} - E_{\text{molecule}}$. In this case, the anion is stabilized by the presence of the two conductors, but the molecule is not, so the virtual orbital energies must be corrected by subtracting the quantity 2 log(2)/R. This treatment is not rigorous, as we do not account for the different shapes and polarizabilities of different orbitals. However, it is very simple, and it gives a reasonable estimate of this Coulombic correction term.

The different behavior of occupied and virtual orbitals is a consequence of the definition of orbital energy arising from the HF treatment. All HF orbital energies include the interactions of an electron in the orbital with the nuclei and with all the other electrons in the system. For a molecule containing N electrons, for instance, the energy of an occupied orbital includes interactions with the remaining (N – 1) electrons while the energy of a virtual orbital includes interactions with all N electrons. Occupied orbital energies, therefore, describe the removal and virtual orbital energies describe the addition of one electron with respect to the state for which the orbitals were optimized.

Fifth, orbitals that fall in the conduction region must be treated separately. During the flow of current their occupations and their orbital energies are not easily defined. A simple approximation is to assume that these orbitals fall in the middle of the conduction region. Notice also that orbitals that are occupied in the isolated molecule, but that fall

above the conduction region, are not well-described and hence should be treated as conduction orbitals.

Sixth, it is necessary to estimate the potential distribution when a bias is applied across the tip-sample gap. When the tip, molecule, and graphite are brought together, the Fermi levels of the three components tend to become equal at the interface.[16] The rigorous description of this effect is rather complicated, requiring sophisticated computational techniques that would considerably increase the cost of the simulation. For the situation of interest, the Fermi energies of the metal tip and of the graphite were assumed to be equal to each other. Additionally, as derived previously, the bias was assumed to be distributed in the tip-sample gap such that the molecule experiences half of the bias potential.[1,17]

To account for the effects of the initial charge equilibration on the energies of the molecular orbitals, all orbital energies were considered to be shifted from their values in vacuum by an amount λ. This quantity represents the difference between the computed HF orbital energies, rescaled to account for the presence of the conductors, and the real orbital energies of the adsorbed molecules during the STM imaging experiment.

λ includes contributions from two very different phenomena. One contribution to λ arises from the inability of HF calculations to reliably predict ionization potentials. This contribution can be evaluated by comparison of the HOMO energy obtained from the HF calculation to a reliable value for the ionization potential of the molecule, obtained either from experimental data or from high-level calculations. For a number of small molecules, the energies of both the molecules and the corresponding cations were computed at the HF and MP2 level, and the resulting ionization potentials, as well as the experimental ones whenever available, are displayed in Table 1. Although the HOMO energy obtained from the HF calculation tends to overestimate the true ionization potential by about 1 eV, the error changes considerably for different molecules. The correction for this effect was estimated for every class of molecules, and this correction

TABLE 1: Ionization Potentials (eV)

Molecule	IP[a] (Koopmans')	IP[b] (HF)	IP[c] (MP2)	IP[d] (exptl)
$CH_3(CH_2)_4CH_3$	11.57	10.12	10.44	(10.22)[e]
$CH_3(CH_2)_3OH$	11.87	9.24	10.56	10.37-10.44
$CH_3(CH_2)_3F$	12.53	11.10	11.30	*f*
$CH_3(CH_2)_3Cl$	11.42	9.96	10.60	10.84
$CH_3(CH_2)_3Br$	10.55	9.38	9.75	(10.15)[e]
$CH_3(CH_2)_3I$	9.62	8.66	8.99	9.5
$CH_3(CH_2)_3CN$	11.92	10.48	12.05	*f*
$C_2H_5CF_3$	14.02	12.85	12.72	*f*
$C_2H_5COC_2H_5$	11.14	7.97	9.55	9.52
$C_2H_5NHC_2H_5$	9.87	7.37	8.54	8.63-8.68
$C_2H_5NH_2$	10.47	8.19	9.33	9.47-9.50
$C_2H_5OC_2H_5$	11.32	8.46	9.85	9.59-9.70
$C_2H_5SC_2H_5$	9.00	7.44	8.23	7.45-8.44
C_2H_5SH	9.60	8.21	8.94	(9.15)[e]
$C_2H_5SSC_2H_5$	9.13	8.06	8.15	8.70-8.85
CH_3COOH	11.90	8.78	10.35	(10.66)[e]
$C_2H_5CCC_2H_5$	9.37	7.90	9.14	(9.32)[e]
$C_2H_5CHCHC_2H_5$	8.74	7.35	8.69	9.14

[a] Estimated based on Koopmans' theorem (HF orbital energy) with 6-31G** basis set. [b] Estimate obtained by comparing the total HF/6- 31G** energies of the molecule and the cation. [c] Estimate obtained by comparing the total MP2/6-31G** energies of the molecule and the cation. [d] Experimental value from ref 24. [e] Adiabatic ionization potential. [f] Data not available.

was included in the value of λ for each different molecule. For consistency, the value chosen for the correction was taken as the difference between the HF HOMO energy and the ionization potential that was computed at the MP2 level.

The other contribution to λ arises from a need to account for possible energetic differences between the energy levels of molecules adsorbed onto graphite and those in vacuum. It is likely that the reference energy for a molecule (the chemical potential of the electrons in the molecule) changes from its value in vacuum when the molecule instead is adsorbed on graphite, surrounded by solvent, and approached by the tip. For the substituted alkane chains under similar tunneling conditions (i.e., similar bias and tunneling current), this component of λ was chosen to best reproduce in general the entire set of observed images and then was not varied for calculations on individual systems.

Seventh, the density of states for the tip $\rho_t(E)$ was assumed to be a constant in the conduction region. The density of states for the graphite $\rho_g(E)$ was assumed to be a parabola having a vertex at the initial value of the graphite Fermi level,[18] $\rho_g(E) \propto (E - E_f)^2$.

Adopting these approximations, the STM current is then

$$I \propto \int_{CR}(E_f - E)^2\left[\sum_{k\in CR}\frac{V_{gk}V_{kt}}{(E - E_k)}\right]^2 dE + \int_{CR}(E_f - E)^2[\pi \sum_{k\in CR} V_{gk}V_{kt}\delta^{(\epsilon)}(E - E_k)]^2\, dE \qquad (18)$$

where again the bias dependence is implicitly contained in the energy terms of (18). The first of these integrals is computed numerically (e.g., using Simpson's rule), and the second one uses the estimates of E_k described above and the value of $\delta^{(\epsilon)}(E - E_k)$ obtained in section II.D.

II.F. General Procedure

For every chemical species, one molecule was laid onto a rigid graphite slab and the molecular geometry was optimized using the DreidingII FF[19] with charges estimated

using charge equilibration.[20] Two more molecules were then added, parallel to the first one and sandwiching it, at a distance of about 4.5 Å. The molecular geometry was then reoptimized. The distance of 4.5 Å was chosen because it is close to the one observed experimentally, both in STM images 1 and in low-angle X-ray diffraction experiments of alkane and alkanol overlayers on HOPG.[21]

The central molecule was then isolated without changing its geometry. All alkyl chains were truncated four carbons away from any functional group, and the cleaved bonds were saturated with hydrogens. The resulting molecules were then checked for symmetry elements. The molecules that were found to be symmetric (with a tolerance of 0.04 Å) were symmetrized in order to speed up the Hartree-Fock computation. A standard HF computation was then performed on the resulting molecules using the 6-31G** basis set.[22] The choice of the basis set was motivated by the desire for reasonably accurate orbital energies.

To simulate an STM scan, a grid of 26×26 points was positioned to correspond to the graphite surface in the FF computation. All of the coupling elements with the graphite were then computed placing one carbon 2p orbital at each grid point. The tip was positioned on a grid of 51×51 points that was positioned parallel to, and at a fixed distance from, the plane of the graphite grid. For each position of the tip, the coupling elements were computed and the tunneling current was estimated assuming a bias of -1eV. The resulting data were then used to produce three-dimensional plots or contour diagrams of the current. This approach simulates a constant height STM image and was used to calibrate the tip-graphite distance and to establish the value of the parameter λ. For each molecule, a constant current simulation was also performed, in which the tip was allowed to move in a direction perpendicular to the graphite in order to adjust the current to a fixed value. The tip displacement was then plotted with respect to an arbitrary plane that was parallel to the graphite surface. These simulations are 3-4 times more computationally expensive than the constant height simulations, but resemble more

closely the experimental STM technique. Qualitative agreement was observed between the computed constant height and constant current images for all the cases studied in this work.

In order to facilitate interpretation of the results in terms of electronic and geometric effects, the overlap between the tip wave function and the occupied molecular orbitals was also evaluated. The resulting images have no experimental equivalent, but represent what the STM image would look like if only the geometry of the molecule were mapped while all electronic effects were ignored. The comparison of these images with the results of the complete simulations will point out whether topographic or electronic effects are primarily responsible for the features that are observed in the experimental and computed STM images.

The tip-molecule distance that was used for the constant height simulations and the current used in the constant current simulations were each chosen to reproduce as closely as possible the features that were observed experimentally. A tip-molecule distance of 7 au ($\approx$ 3.7 Å) was selected for the constant height simulations. At this distance, the maximal current observed for the alkane molecules is close to 0.001 arbitrary units (only relative current densities are computed in the present model), and this value was used for the constant current simulations. For much shorter distances, the resulting images seem to be determined mainly by the topology of the molecule, while at much longer distances the computed resolution decreased below that observed experimentally.

In all constant current plots, the tip was not allowed to get too close to the graphite, so these plots produce features that appear to be bumps on a flat surface. In previous simulations reported in the literature,[2] STM images have been related to the local density of states at a distance of 0.5 Å from the adsorbed molecule. We believe such distances are unrealistically small to describe actual STM measurements. In our work, the distance corresponding to the flat surface was set to be 14.5 bohrs for molecules oriented with their carbon-carbon skeletons parallel to the graphite surface plane and 15 bohrs for

molecules having their carbon-carbon skeletons oriented perpendicular to the plane of the graphite surface. These values correspond to a tip-molecule distance of about 2.9 Å.

The value of the parameter λ was chosen to best reproduce the experimental images. While the value of λ has little or no effect on most molecules, it plays a fundamental role for the molecules having their highest occupied molecular orbitals (HOMOs) close to the conduction region. After correcting for the difference between the HOMO orbital energy and the MP2 ionization potential, as reported in Table 1, the second contribution to λ was estimated by the value needed to bring the HOMO of the amines into the conduction region and to leave the HOMO of the alkyl bromide at lower energy. This condition is satisfied for any correction between 1.3 and 1.8 eV, assuming a tip- molecule distance of 7 au. We arbitrarily selected a correction of 1.5 eV. This value was fixed for all the simulations, on the basis that it should be approximately equal for all the molecules of concern.

III. Results

The orientation of the carbon-carbon skeletons of the alkyl chains relative to the graphite surface plane must be carefully considered in order to accurately model the STM images that have been observed experimentally. In the discussion that follows, the term flat will be used to indicate adsorption orientations in which the carbon-carbon skeleton of the alkane chain lies parallel to the plane containing the graphite surface, while the term vertical will be used to indicate the situation in which the carbon-carbon skeleton is oriented perpendicular to the graphite surface plane. Also, since the tip is assumed to be above the graphite, down and up will be used to describe atomic positions that are located toward the graphite and toward the tip, respectively.

III.A. Alkanes

To investigate the geometry and packing of adsorbed alkanes, the molecule $CH_3(CH_2)_{33}CH_3$ was considered, since it is the alkane that was imaged experimentally with the STM.[1] According to the results from the FF study, a single *trans*-

$CH_3(CH_2)_{33}CH_3$ molecule adsorbs on graphite in the flat orientation, with the vertical orientation being less stable by 8 kcal/mol. The adsorption energy (from the gas phase) for $CH_3(CH_2)_{33}CH_3$ was computed to be on the order of 70 kcal/ mol. In these computations, only the all *trans*-conformation was considered. This was justified because conformations with *gauche*-bonds were likely to be significantly less favorable energetically and because the experimental STM[1] and X-ray diffraction[21] data strongly suggest that the alkanes are adsorbed in an *all-trans*-conformation onto the graphite surface.

When three *trans*- $CH_3(CH_2)_{33}CH_3$ molecules are adsorbed from the gas phase, each pairwise interaction between neighboring molecules was computed to further stabilize the system by about 23 and 56 kcal/mol in the flat and the vertical orientations, respectively. Consequently, for a three-molecule overlayer model, the vertical orientation is computed to be more stable by an energy difference of 25 kcal/mol. The experimental images indicate that the molecules are generally adsorbed in the flat orientation.[1,2] Although the vertical orientation is computed to be more stable, if the monolayer is built by adding one molecule at a time and by letting it migrate on the graphite surface, it is conceivable that the system would be trapped into the flat orientation. Migration of a single $CH_3(CH_2)_{33}CH_3$ molecule on the graphite surface was computed to have a barrier of 1-2 kcal/mol. However, the barrier to flip one $CH_3(CH_2)_{33}CH_3$ molecule into the vertical orientation is estimated to be around 18 kcal/mol, making this process unlikely at room temperature. This proposed nucleation process is similar to one that has been recently observed in an STM study of the growth dynamics of self-assembled thiol monolayers on gold.[23] An alternative possibility that was not explored in the present calculations is that since the adsorption occurs from solution, differential solvation plays a significant role in determining the energetically favored orientation of the molecules in the graphite overlayer.

Instead of carrying out more extensive simulations to include both dynamical effects and solvation effects, both orientations of the alkane were investigated in order to evaluate which produced computed STM images that more closely matched the experimental data. The images for $CH_3(CH_2)_7CH_3$ in the vertical orientation are reported in Figure 2A. The constant current image of Figure 2A clearly does not match the high-resolution STM image observed experimentally for alkanes on HOPG.[1] The constant height and the constant current images show spots corresponding to the hydrogens closest to the tip, leading to a rectangular pattern that is predominantly due to the geometry of the molecule, similar to the conclusions of a previous extended Hückel level analysis of this system.[2] Our calculations produced an average distance between maxima in the constant current mode of 2.59 Å in the direction along the backbone and an average distance of 1.57 Å between nearest neighbors.

The STM images predicted for the flat molecule $CH_3(CH_2)_6CH_3$ at a bias of -1 eV are reported in Figure 2B. The constant current and constant height images of the alkane in this orientation were similar to each other, and both displayed patterns that closely match the pattern produced by the geometric locations of the hydrogens that were closest to the tip. This effect can be seen more clearly by comparison of the image in Figure 2B to the overlap plot of Figure 2C. This comparison indicates that the molecular topography alone is sufficient to explain the qualitative aspects of the computed STM image of this system.

The images of Figure 2B are in excellent agreement with the experimental images obtained for alkanes on graphite.[1] In the constant current simulation, the average distance between subsequent spots along the alkane chain is 2.61 Å and the average distance between spots along the direction of the molecule is 2.56 Å, whereas the experimental data are 2.35 Å between spots along the chain and 2.54 Å between spots along the direction of the molecule. The positions of the spots observed experimentally are not in

(A) Vertical $CH_3(CH_2)_7CH_3$ at $-1.0\ eV$ Constant current

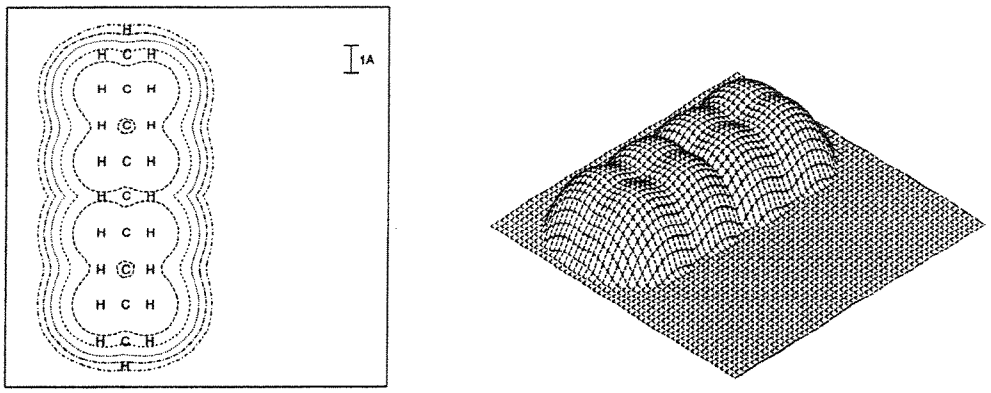

(B) Flat $CH_3(CH_2)_6CH_3$ at $-1.0\ eV$ Constant current

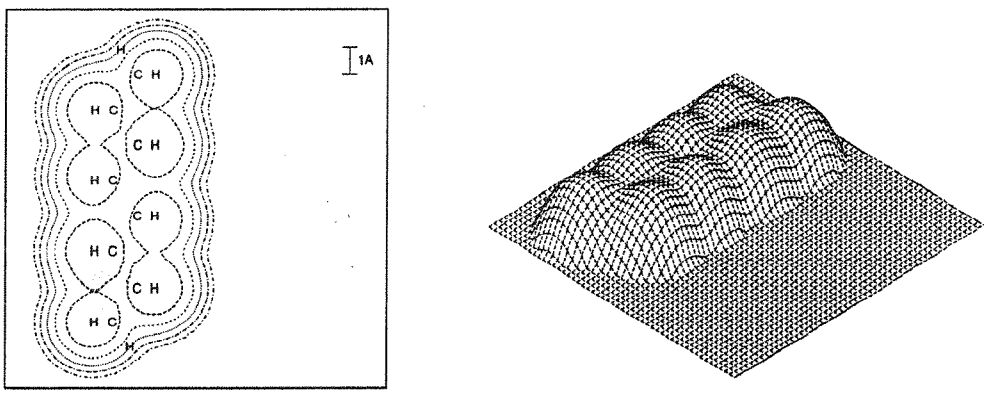

(C) Flat $CH_3(CH_2)_6CH_3$ at $-1.0\ eV$ Overlap Only

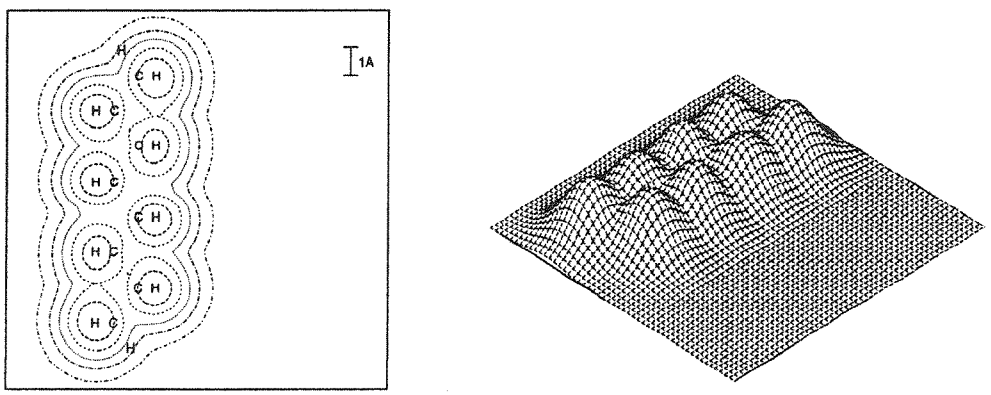

Figure 2. Computed STM images of an alkane molecule adsorbed onto the graphite surface. The contour levels are at 1/6, 2/6, 3/6, 4/6, and 5/6 of the maximum peak of each plot; the same spacing criteria for contour levels is used for all the contour plots of the paper. 3-D plots are shown to the right of the contour plots. The bias is -1 eV in all panels of Figures 2-16 unless otherwise noted. In A, the vertical orientation is assumed, while B and C depict results for the flat orientation. (A) Constant current simulation; the plot represents the tip displacement perpendicular to the graphite surface. The maximum displacement is 1.71 au. (B) Constant current simulation in the flat orientation. The maximum displacement is 1.47 au. (C) Simulation of only the overlap of the tip with the occupied MOs at each tip position (see text for details). The maximum current is 0.050 arbitrary units.

exact agreement with those in the simulation presumably due to the approximations contained in both the model and the computation.

It is also of interest to examine the relative contribution of the occupied and unoccupied orbitals to the overall tunneling current. Since the occupied orbitals of the alkane are very stable, the computations indicate that the current is determined mainly by the virtual orbitals. A simple interpretation of this behavior is that the tunneling electrons behave as low-energy electrons elastically scattered by the adsorbed molecules. Because the same coupling is present in both biases, the images are predicted to be symmetric with bias voltage,[1,17] in accord with experimental observations.[1]

III.B. Alkanols

Since the experimental STM images show that alkanols lay flat on HOPG,[1] only the flat adsorption orientation was considered computationally for these systems. The molecular geometry of the adsorbed alkanol was computed for the molecule $CH_3(CH_2)_{11}OH$, and the *ab initio* computation of the STM image was carried out on the molecule $CH_3(CH_2)_3OH$.

Three conformations were investigated for the flat orientation of $CH_3(CH_2)_{11}OH$ on graphite. For one adsorbed molecule, the most stable conformation was the one with the OH group *trans* to the alkyl chain. This conformation was computed to have an adsorption energy of 26.3 kcal/mol from the gas phase. The two *gauche*-conformers, in which the OH group was either pointing toward the graphite (OH down) or toward the tip, denoted as OH up, were less stable by 3.4 and 3.0 kcal/mol, respectively. For three $CH_3(CH_2)_{11}OH$ molecules adsorbed on graphite, the *trans*-conformer was again the most energetically favored in the computations, while the *gauche*-conformers were 3.2 and 3.1 kcal/mol higher in energy, respectively.

Figure 3A displays the computed STM images for the most energetically favorable *trans*-conformer of $CH_3(CH_2)_3OH$ at a bias of -1 eV in the flat orientation. The simulation shows that the alcohol is dark with respect to the alkyl chain, in accord with

$CH_3(CH_2)_3OH$ Constant current

(A) Flat

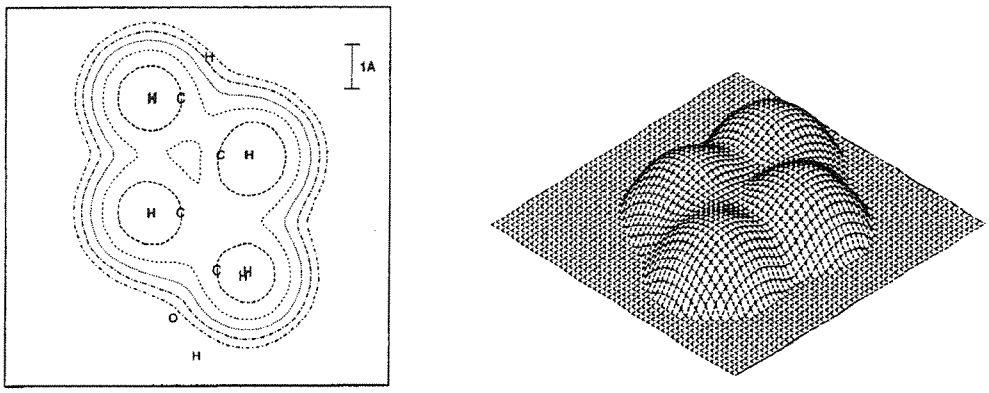

(B) $-OH$ down

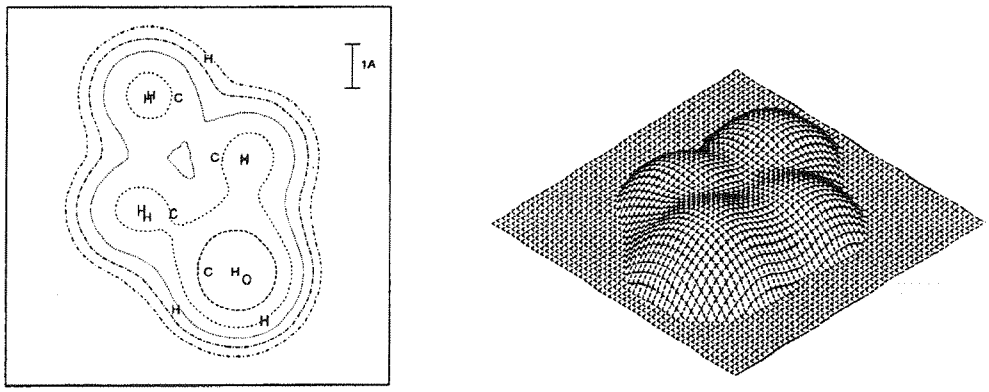

(C) $-OH$ up

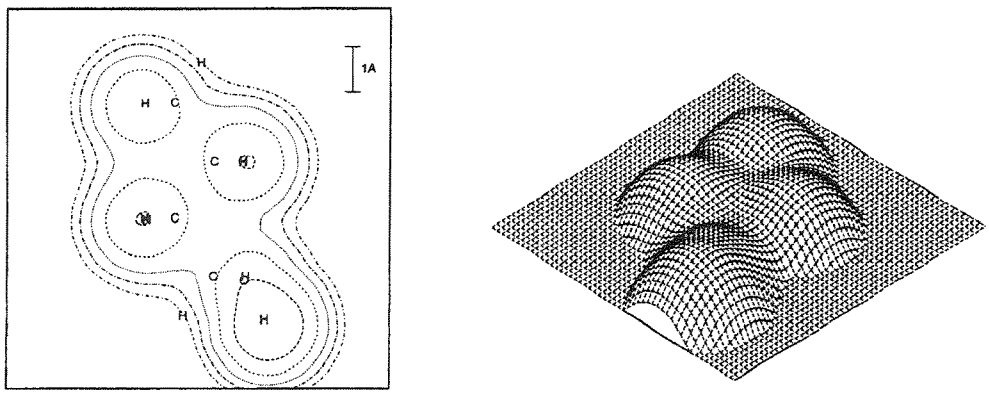

Figure 3. Computed constant current STM images of an alcohol molecule laid flat on the graphite surface. (A) The OH group is *trans* to the alkyl chain. The maximum value of the plot is 1.00 au. (B) The OH group is *gauche* to the alkyl chain and it points toward the graphite. (C) The OH group is *gauche* to the alkyl chain and it points away from the graphite. The maximum values of the plots in B and C are 1.32 and 1.12 au, respectively.

experiment. Additionally, the image of the chain is dominated by the spots corresponding to the hydrogen atoms closest to the tip, as in the case of unsubstituted alkanes.

The average distance between spots is 2.63 Å along the direction of the molecule and 2.62 Å between nearest neighbors. The average angle between spots imaged on the alkyl chain is 60.2°. The experimental values for $CH_3(CH_2)_{13}OH$ are 2.57 Å, 2.36 Å, and 61°, respectively.[1] The difference between these computed values and the ones obtained for the unsubstituted alkane can be attributed to the fact that the alkyl chain used in the computational modeling of the alkanol overlayer is shorter and hence is less representative of the real system. Again the virtual orbitals were primarily responsible for the contrast between the OH group and the hydrogens in the methylene chain.

The *gauche*-conformers of the alkanol produced significantly different computed STM images. The OH group in the computed STM plot for both *gauche*-isomers is brighter than the spots in the alkyl chain, although the computations indicate that the oxygen atom is not observed directly by the STM for either conformation of the alkanol. For the OH down conformation, the α hydrogen is forced up toward the tip and becomes bright due to a topographic effect (Figure 3B). For the OH up conformation, the hydrogen atom of the OH group is close to the tip and is thus computed to be imaged as a bright spot (Figure 3C). Since the *gauche*-conformations produce computed images that do not agree with experimental observation, but the computed STM image of the *trans*-conformation does agree with the data, it is therefore reasonable to conclude that the more energetically favored *trans*-conformer was in fact being imaged experimentally.[1]

III.C. Halogenated Alkanols

For these molecules, only the flat orientation was considered. This was justified by the observation that the experimental images of halogenated alkanols show the same packing as that displayed by unsubstituted alkanols,[1] for which the high-resolution STM images clearly revealed a flat orientation.[1] The parameters of the adsorbed molecules were

determined for $X(CH_2)_{12}OH$, where X = F, Cl, Br, and I, whereas the *ab initio* STM image computations were performed on the smaller molecules $X(CH_2)_3CH_3$.

Figure 4 depicts the images computed for these adsorbates at a bias of -1 eV. These images display the results obtained for the most energetically stable conformation, in which the halide was in a *trans*-conformation relative to the alkyl chain. The images show that the functional groups F, Cl, and Br appear dark in the STM images relative to the alkyl chain, while I is much brighter than any other part of the iodoalkanol. These predictions are in excellent agreement with the experimental observations.[1]

In the case of $(CH_3)(CH_2)_3I$, the two highest occupied molecular orbitals (HOMOs) fall in the conduction region. The molecule then becomes a conductor, and most of the current goes through the lone pairs on the iodine.

In the case of $(CH_3)(CH_2)_3X$, with X = F, Cl, and Br, both the occupied and virtual orbitals are far in energy from the conduction region. As the virtual orbitals reach farther out from the molecule than the occupied orbitals, they couple better with the tip and with the graphite. Consequently, the virtual orbitals are computed to be responsible for most of the current. These halogens cannot transmit current and thus appear dark in the STM image contrast, because they have no low-energy virtual orbital available. To illustrate these effects, Figure 5 compares the constant current images obtained from the entire STM image computation to those computed for the alkyl bromide and alkyl iodide adsorbates when only the occupied or the virtual orbitals are considered. When only the occupied orbitals are considered, both Br and I are bright, even though I is much brighter.

Computations were also performed for two other conformations of the alkyl bromide, both of which had the Br in a *gauche*- position relative to the alkyl chain. In one conformation, the Br group was pointing toward the graphite (Br down), and in the other conformation the Br was pointing away from the graphite (Br up).

For a single adsorbed molecule, the adsorption energy (from the gas phase) of the *trans*-Br conformation was 28.9 kcal/mol, whereas the *gauche*-conformers were found to

(A) $CH_3(CH_2)_3F$

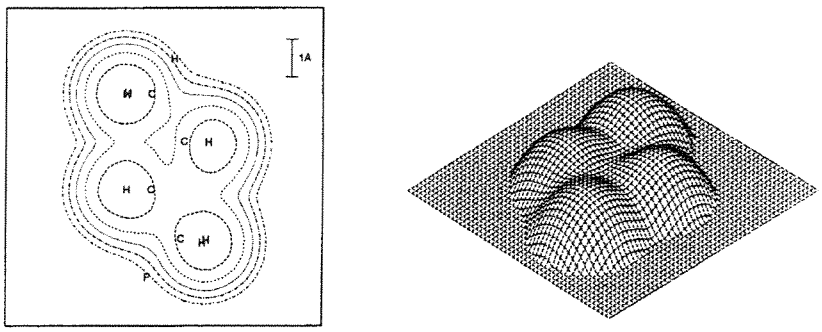

(B) $CH_3(CH_2)_3Cl$

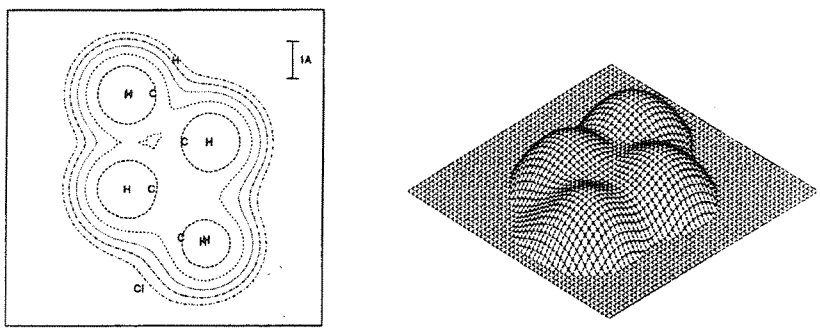

(C) $CH_3(CH_2)_3Br$

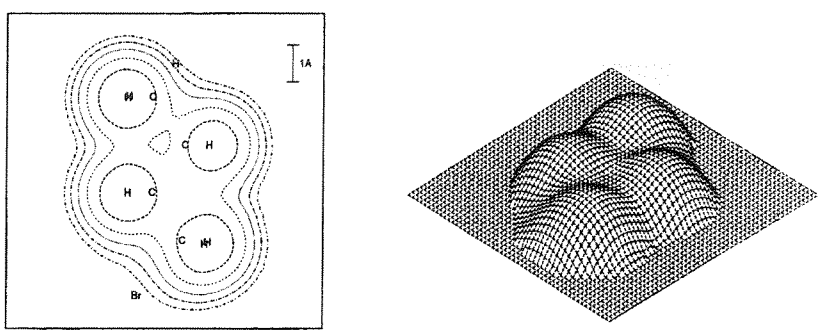

(D) $CH_3(CH_2)_3I$

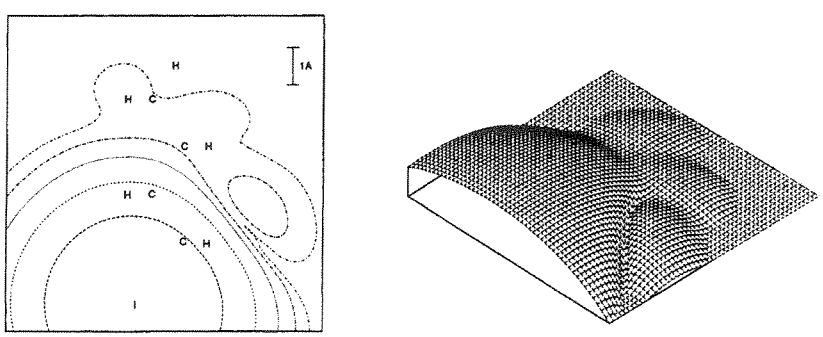

Figure 4. Computed constant current STM images of halobutanes laid flat on graphite: (A) fluorobutane; (B) chlorobutane; (C) bromobutane; (D) iodobutane. The maximum values for the plots are 0.99, 0.99, 0.98, and 5.16 au, respectively.

Bromo-butane – all orbitals

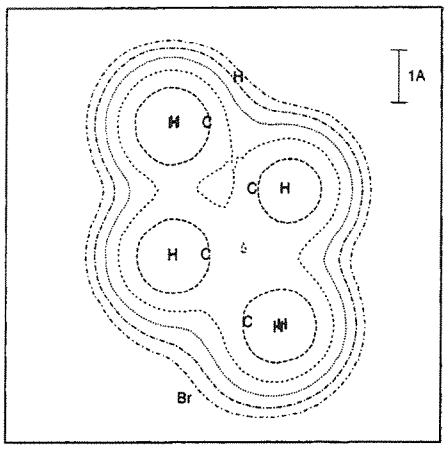

Iodo-butane – all orbitals

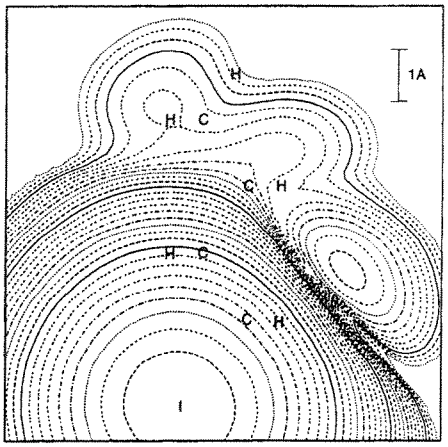

Bromo-butane – occupied orbitals

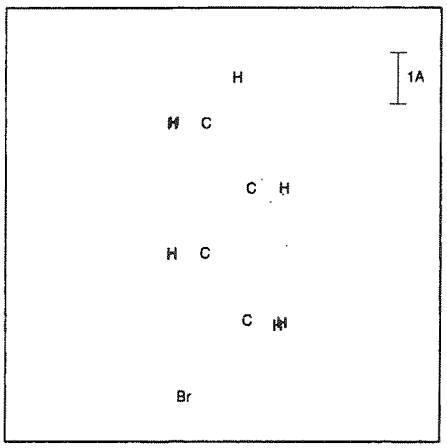

Iodo-butane – occupied orbitals

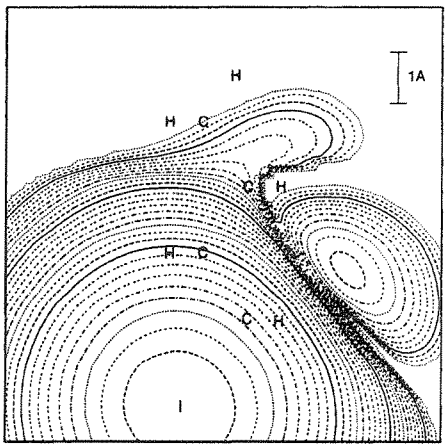

Bromo-butane – virtual orbitals

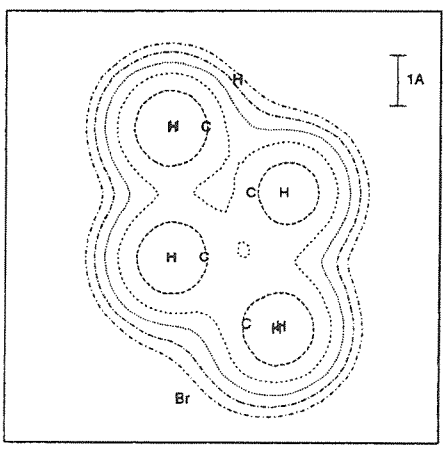

Iodo-butane – virtual orbitals

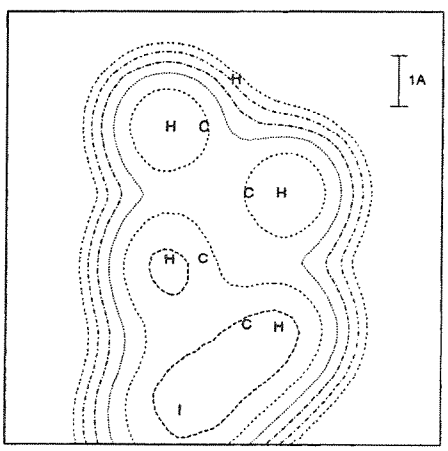

Figure 5. Computed STM images of bromo- and iodobutane in the constant current mode. The top two plots represent the total current transmitted. The contributions to the current due to the occupied (center) and the virtual (bottom) orbitals alone are reported to show the similarity between the two molecules. To illustrate the differences between the two molecules, the same contour levels and reference distance were used in all plots. Each contour line represents a tip displacement of 1/6 au. The zero corresponds to a tip-graphite distance of 14.5 au (i.e., a tip-molecule distance of about 2.9 Å), and only positive displacements are computed. In the bromine, the total current is dominated by the virtual orbitals, while in the iodine it is dominated by the occupied orbitals.

be less stable by 3.6 kcal/mol (Br down) and 3.5 kcal/mol (Br up). For three adsorbed molecules, the *gauche*-conformers were less stable than the *trans* by 11.9 kcal/mol (Br down) and 13.7 kcal/mol (Br up).

STM simulations were performed on both of these *gauche*-conformations. As displayed in Figure 6, changing the conformation from a *trans*-to a *gauche*-alkyl halide is predicted to effect a large and diagnostic change in the STM image. Although the Br is dark relative to the alkyl chain in a *trans*-conformation, it is predicted to be bright in both *gauche*-conformations. With the Br down, the Br pushes up one of the hydrogen atoms on the α carbon, and this topographic effect causes the α hydrogen atom to become bright in an STM image (Figure 6A). With the Br up, the Br atom itself is bright (Figure 6B). Neither of these predictions correspond to the experimental data on the alkanol bromide, which are instead in accord with the computational prediction that the more energetically stable *trans*-conformation is being imaged in the STM experiment. The prediction that a bromide group would change from dark to bright in an STM image if its conformation changed from *trans* to *gauche* is consistent with the image-contrast reversal that has been recently reported for bromide groups after sustained imaging of alkyl bromide overlayers on graphite substrates.[3]

III.D. Fluorinated Alkanols

Figures 7 and 8 depict the STM images that were computed for the CF_3 and C_3F_7 functional groups. Both of these molecules were considered in the flat adsorption orientation. As observed experimentally, both of these functional groups appear darker than the alkyl chain.

In these molecules, some fluorine atoms are closer to the tip than any other atom in the alkyl chain. Despite this topographic effect that should cause the flourine atoms to be bright in the STM contrast, they are dark both theoretically and experimentally. This electronic effect results from the fact that the occupied orbitals describing the wave function in the fluorine region are computed to be very strongly bound, while the virtual

(A) $CH_3(CH_2)_3Br$ *Br* down

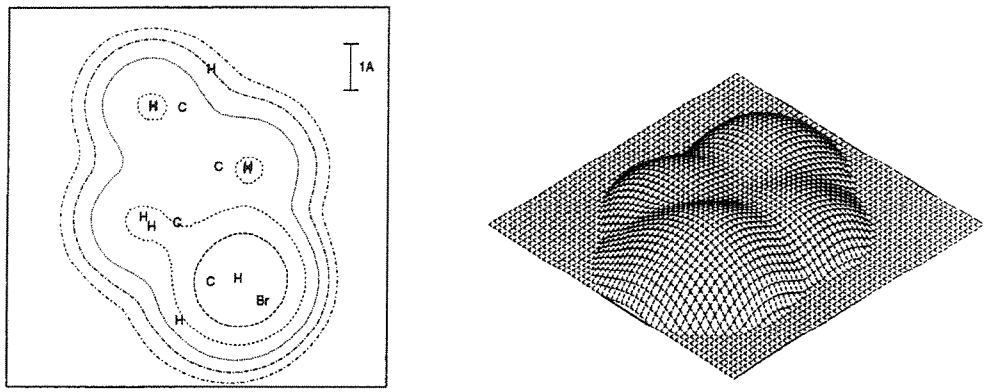

(B) $CH_3(CH_2)_3Br$ *Br* up

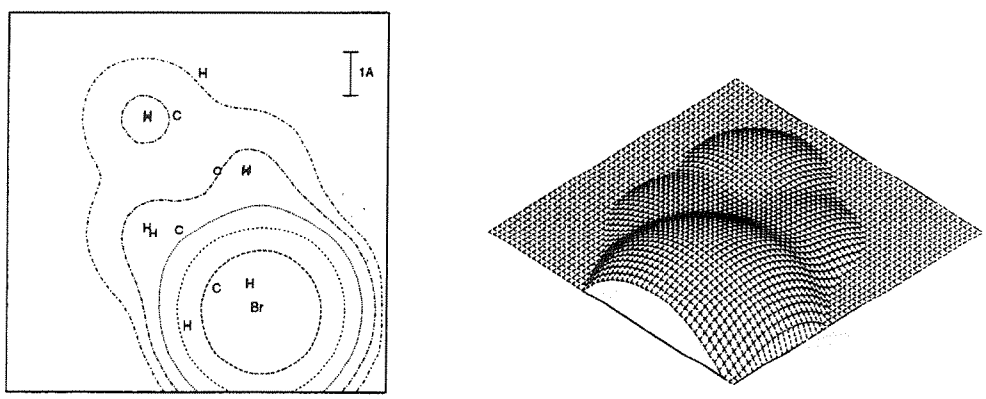

Figure 6. Computed constant current STM images of bromobutane on graphite. (A) The Br is *gauche* to the alkyl chain and points toward the graphite. (B) The Br is *gauche* to the alkyl chain and points away from the graphite. The maximum values in the plots are 1.91 and 2.95 au, respectively.

Flat $CH_3(CH_2)_3CF_3$ at $-1.0\ eV$

(A) Constant current

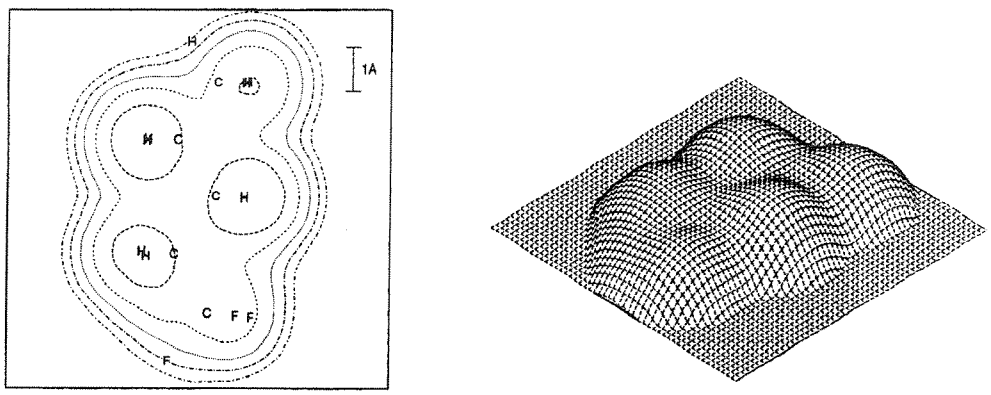

(B) Constant height

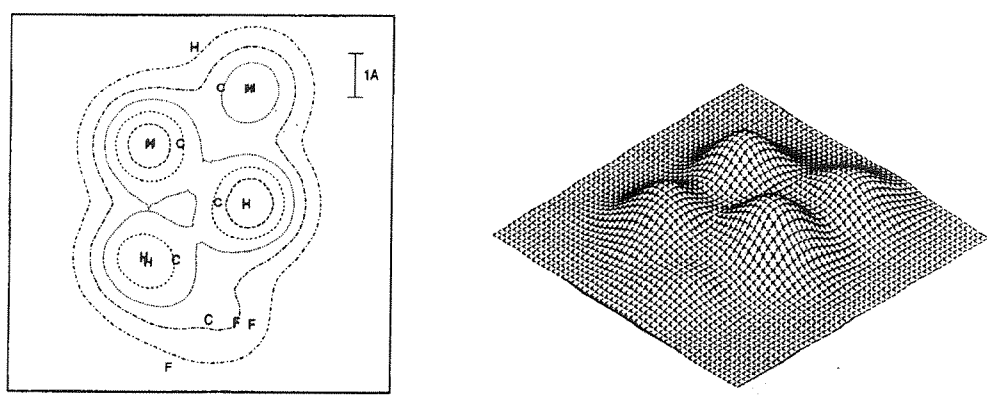

(C) Constant height – Overlap only

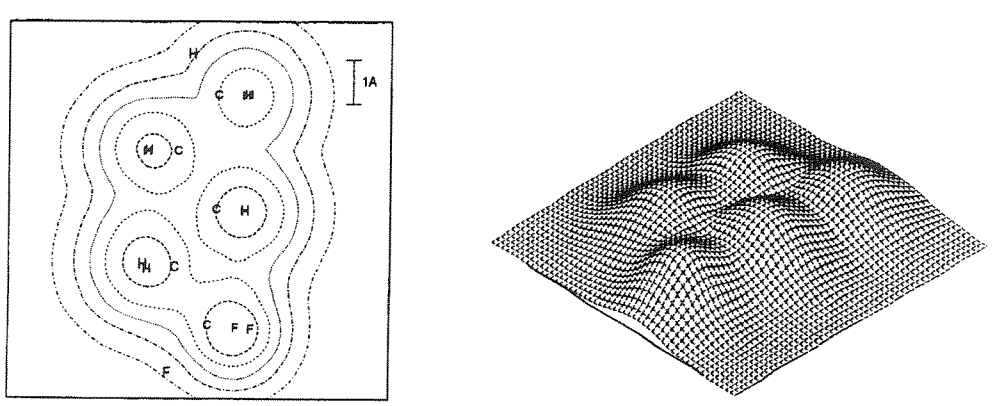

Figure 7. Computed constant current STM images of $CH_3(CH_2)_3CF_3$ laid flat on the graphite surface. The maximum values for the three plots are (A) 1.12 au; (B) 0.00038 arbitrary units; and (C) 0.054 arbitrary units.

Flat $CH_3(CH_2)_3(CF_2)_2CF_3$ at $-1.0\ eV$

(A) Constant current

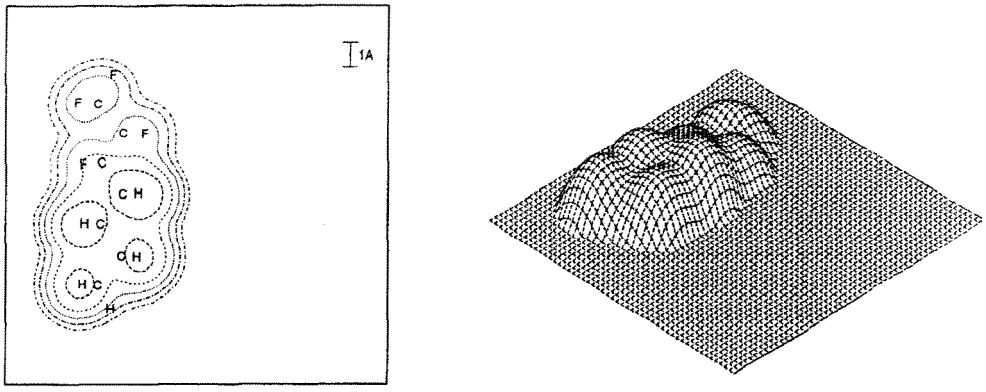

(B) Constant height

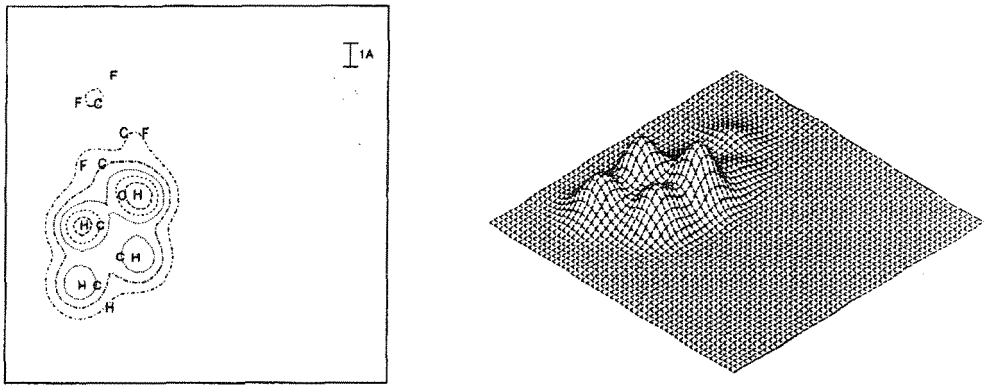

(C) Constant height – Overlap only

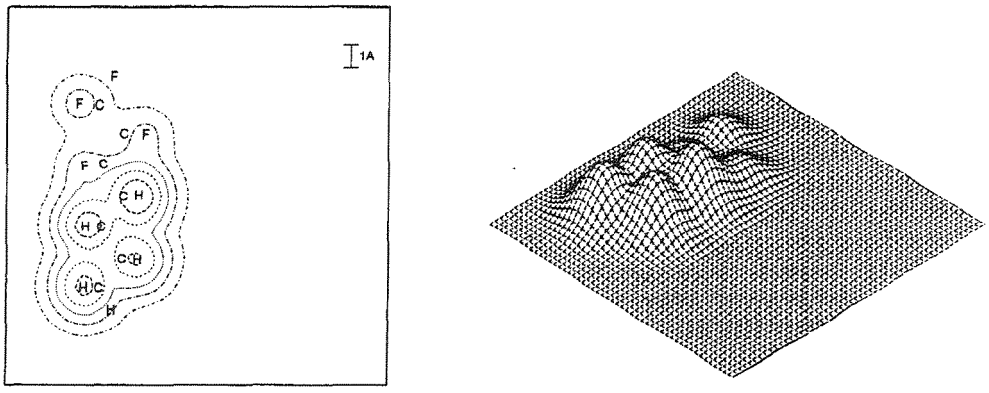

Figure 8. Computed constant current STM images of $CH_3(CH_2)_3(CF_2)_3CF_3$ laid flat on the graphite surface. The maximum values for the three plots are (A) 1.55 au; (B) 0.0011 arbitrary units; and (C) 0.097 arbitrary units.

orbitals are very far above the vacuum level. Hence, the current due to these orbitals is very small, despite a good overlap with the tip wave function, and these functional groups thus appear to be dark in STM contrast.

III.E. Ethers

The adsorption orientation on a graphite surface was determined for the long chain ether $CH_3(CH_2)_{15}O(CH_2)_{15}CH_3$. According to FF simulations, a single molecule prefers to be adsorbed in the flat orientation, and the vertical orientations are computed to be less stable by 9.3 and 9.5 kcal/ mol when the oxygen is pointing down and up, respectively. When the molecules are packed with a density close to the experimental one, the vertical orientation with oxygen pointing up is computed to be the most stable, followed by the vertical orientation with oxygen pointing down (1 kcal/mol) and the flat (8.2 kcal/mol) orientation. STM images for all three possibilities were therefore simulated.

Figure 9 reports the results obtained for a bias of -1 eV for the molecule $CH_3(CH_2)_3O(CH_2)_3CH_3$. In the vertical orientation with the oxygen down (Figure 9A), the ether is bright, due to the hydrogens on the α carbons. This image is thus not in agreement with experiment.

In the flat orientation (Figure 9B), the ether is dark and it appears similar to a missing hydrogen in the alkyl chain. In the vertical orientation with the oxygen pointing up (Figure 9C), the ether is also dark. In this orientation, the dark area is bounded by the spots corresponding to the hydrogens on the β carbons with respect to the oxygen.

Since by itself the observed STM contrast does not distinguish between the flat and O up orientations, it would be useful to obtain independent support for the orientational assignment suggested above. Such support can be obtained by inspection of the molecular packing arrangement of the ether overlayer. As discussed in the previous chapter, the characteristic angle θ is expected to be 0° for the sterically favored packing arrangement in the flat orientation (cf. Figure 20b in the previous article) and is expected to be 16° for the sterically favored packing in the vertical orientation (cf. Figure 20a in

$CH_3(CH_2)_3O(CH_2)_3CH_3$

(A) Vertical, O down

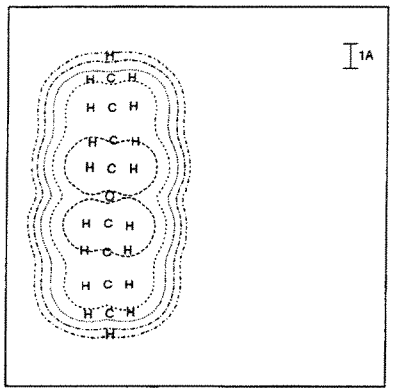

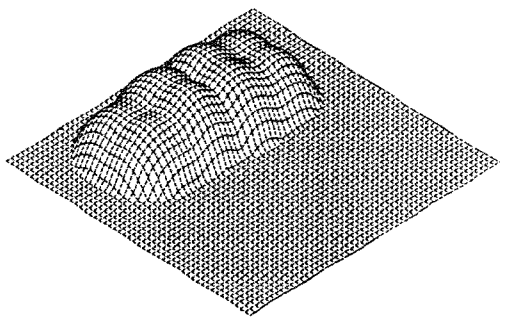

(B) Flat

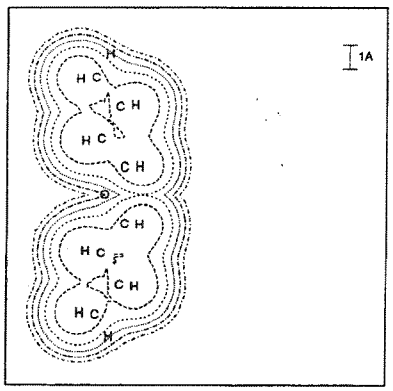

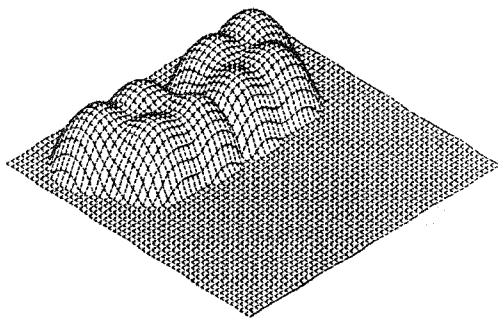

(C) Vertical, O up

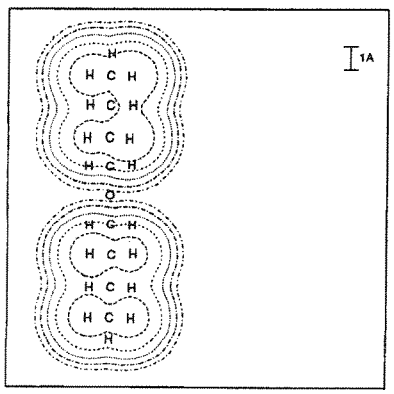

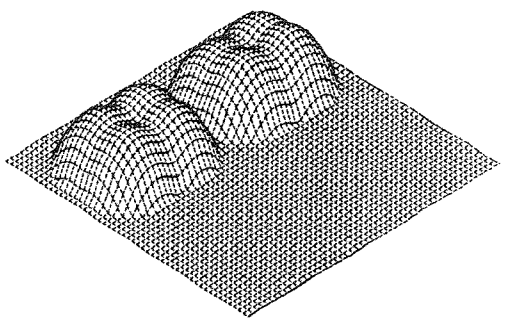

Figure 9. Computed constant current STM images of $CH_3(CH_2)_3O(CH_2)_3CH_3$ on graphite: (A) vertical orientation with the oxygen atom pointing down; (B) flat orientation; (C) vertical orientation with the oxygen atom pointing up. The maximum values for the three plots are 2.12, 1.51, and 1.76 au, respectively.

the previous chapter). The option for producing $\theta = 26°$ arises from the flat orientation with an offset of adjacent molecules by the distance of one methylene unit. The experimental observation of $\theta = 26°$ for the ether packing arrangement in the experimental STM images[1] therefore provides additional support for the suggestion that the ether is adsorbed in the flat orientation on the graphite surface.

III.F. Thioethers and Thiols

The FF simulation predicts one molecule of $CH_3(CH_2)_{13}S(CH_2)_{13}CH_3$ to be most stable when adsorbed in the flat orientation, and the vertical orientations are predicted to be higher in energy by 7.8 (S down) and 8.8 (S up) kcal/mol. When more molecules are packed at the density observed experimentally, the vertical orientation with the sulfur pointing down becomes the most stable. The other vertical orientation is higher in energy by 6.9 kcal/mol, and the flat orientation is higher in energy by 9.2 kcal/mol. Since these orientations were close in energy, STM images were computed for molecules in all three adsorption orientations.

Figure 10 presents the STM images predicted for the molecule $CH_3(CH_2)_3S(CH_2)_3CH_3$ in each of the three orientations. In all three orientations the alkyl chains define a linear intramolecular axis, so inspection of the molecular shape alone does not allow identification of the orientation that is being observed experimentally in the STM image unless the position of the sulfur relative to the alkyl chain can be accurately resolved. In all three orientations, the sulfur appears much brighter than any other portion of the molecule. The lone pair orbitals on the sulfur atom are in the conduction region and are responsible for most of the tunneling current. Under these conditions, the actual size of the bright spot is expected to depend strongly on the dimensions and the shape of the tip. However, for the constant experimental conditions assumed in the simulations, the size of the bright spot is different for the three orientations, being larger in the vertical orientation having the sulfur pointed toward the graphite. The bright spot in the various computed constant current STM images is

$CH_3(CH_2)_3S(CH_2)_3CH_3$

(A) Vertical, S down

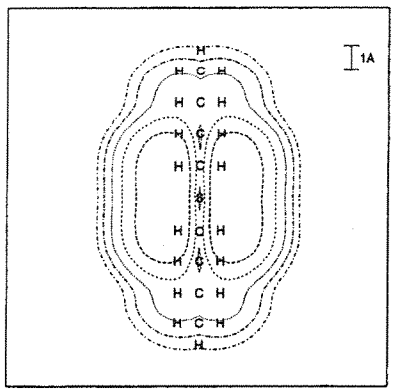

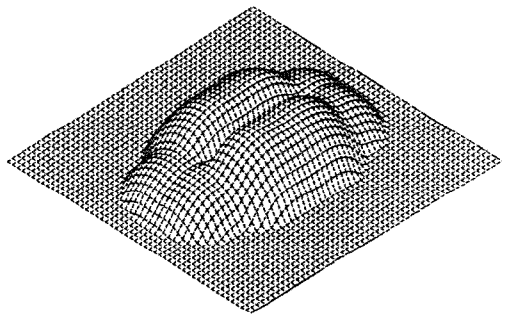

(B) Flat

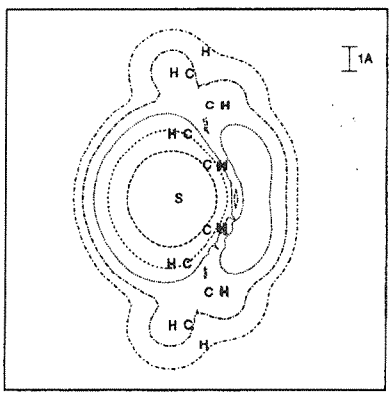

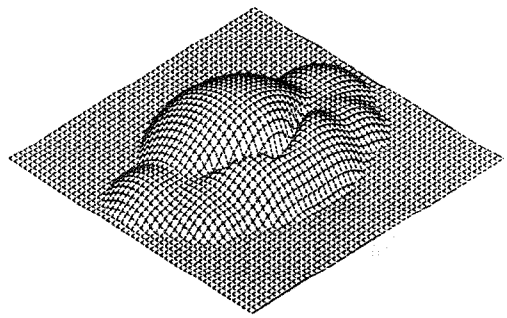

(C) Vertical, S up

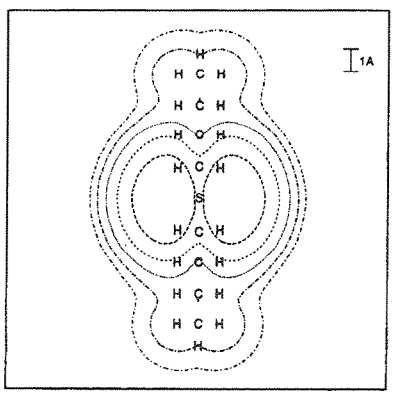

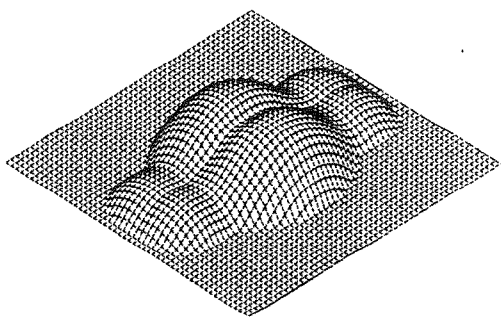

Figure 10. Computed constant current STM images of $CH_3(CH_2)_3S(CH_2)_3CH_3$ on graphite: (A) vertical orientation, with the sulfur atom pointing down; (B) flat orientation; (C) vertical orientation with the sulfur atom pointing up. The maximum values for the three plots are 3.17, 4.26, and 3.74 au, respectively.

approximately 10 Å (S down), 8.2 Å (flat), or 5.4 Å (S up), as compared to the experimentally observed value of 6.5-6.7 Å.[1] This comparison is very instructive, indicating that the large apparent width of the thioether functionality observed in the experimental images[1] can be naturally explained by the electronic structure of this molecule.

Because alkanethiols have also been recently imaged using STM, the images of alkanethiol overlayers were also modeled theoretically in this study. Only the flat adsorption geometry was considered for the molecule $CH_3(CH_2)_7SH$, and the STM simulation was conducted on the molecule $CH_3(CH_2)_3SH$. As displayed in Figure 11, the thiol group is overwhelmingly brighter than the rest of the molecule. This prediction is in good agreement with experimental results.[3] The brightness is due to the sulfur nonbonding electrons which enter the conduction region, making the thiol a conductor for the same reason that the S functionality is bright in the STM image of the thioether.

$CH_3(CH_2)_3SH$

(A) Flat

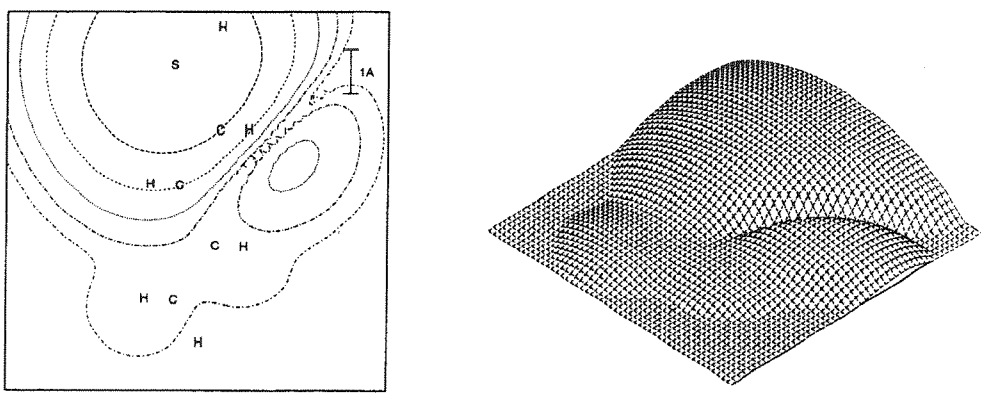

Figure 11. Computed constant current STM images of $CH_3(CH_2)_3SH$ laid flat on graphite. The maximum value for the plot is 4.30 au.

III.G. Disulfide

The molecule used to study the adsorption orientation is $CH_3(CH_2)_{15}SS(CH_2)_{15}CH_3$. Once again, for a single molecule, the flat adsorption orientation was computed to be favored, being lower in energy by 10.4 kcal/mol, while the vertical orientation is more stable by 7.9 kcal/mol for densely packed systems. Also, for this system, the lowest energy conformation of the vertical orientation of $CH_3(CH_2)_{15}SS(CH_2)_{15}CH_3$ had the carbon-carbon skeletons of both alkyl chains oriented perpendicular to the graphite surface plane. This adsorbate geometry is significantly different than the lowest energy molecular conformation for the disulfide in the gas phase, in which the carbon-carbon skeletons of the alkyl chains are mutually perpendicular. The STM predictions for the computed lowest energy flat and vertical orientations are reported for negative bias in Figure 12.

The computed images reveal that the disulfide functionality is much brighter than the rest of the molecule in either orientation. As discussed above for the iodoalkanol, the bright spot is due to the lone pair electrons on the sulfur, which become conducting electrons and thereby facilitate electronic coupling between the tip and the graphite. The apparent width of the disulfide functionality in the computed STM images is 9.4- 11.3 Å, which is in good agreement with the experimentally observed value of 11.6- 12.6 Å. As is the case for the thioether, this agreement indicates that the very large width of the disulfide functional group in the experimental STM image has a very plausible physical explanation in terms of the electronic structure of the disulfide moiety.

III.H. Primary and Secondary Amines

Both primary and secondary amines have been imaged recently using STM. We first discuss the theoretical results for the secondary amine and then extend these findings to a primary amine.

For the secondary amine, four possible adsorption orientations must be considered: two flat and two vertical, with the amine hydrogen pointing either toward the

$CH_3(CH_2)_3SS(CH_2)_3CH_3$

(A) Flat

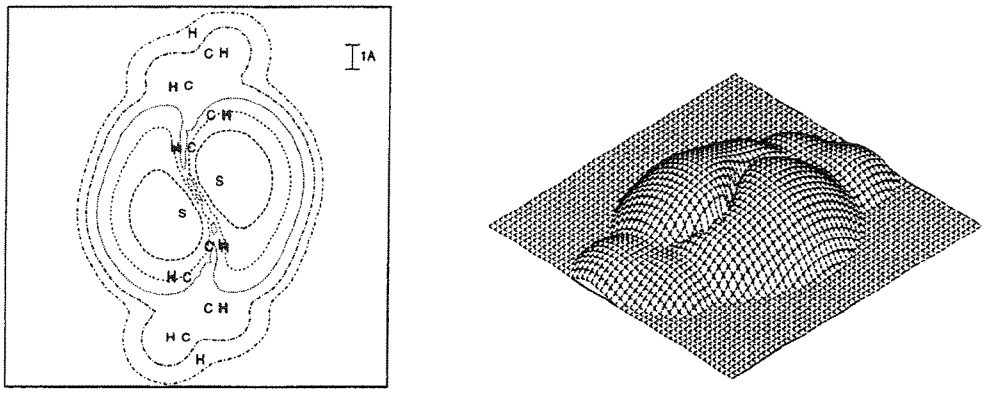

(B) Vertical

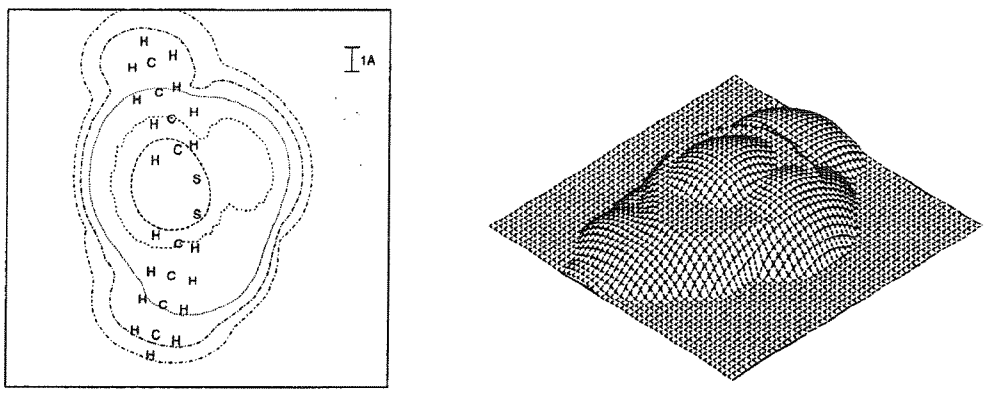

Figure 12. Computed constant current STM images of $CH_3(CH_2)_3SS(CH_2)_3CH_3$ on graphite: (A) flat orientation; (B) vertical orientation. The maximum values of the plots are 4.10 and 4.57 au, respectively.

graphite or away from the graphite. FF simulations on the molecule $CH_3(CH_2)_{17}NH(CH_2)_{17}CH_3$ predict isolated molecules to be more stable by 9.9 kcal/mol in the flat orientations and packed molecules to be more stable by 10.4 kcal/mol in the vertical orientations. Nevertheless, STM images were computed for all four orientations (Figure 13).

When the molecule is flat, the amine is predicted to be brighter than the rest of the molecule (Figures 13A,B). The brightness is localized on the hydrogen atoms which are close to the nitrogen and point toward the tip. The predicted brightness is due to the fact that the HOMO, which is localized on the amine, is in the conduction region, making the molecule a conductor.

When the molecule is vertical, the amine is only slightly brighter than the alkane chain when the NH group is pointing up (Figure 13C), and it is bright when the NH is pointing down (Figure 13D). The prediction is in qualitative agreement with the experimental image for three of the four possible orientations,[1] and further assignment cannot be made with the resolution of the STM data available at present.

To describe the properties of primary amines, the adsorption geometry of the molecule $CH_3(CH_2)_7NH_2$ was studied when the alkyl chain is flat. Three conformations were considered, in which the lone pair of the amine group was either flat (*trans* to the alkyl chain), pointing up, or pointing down. All three conformations are found to lie within 0.5 kcal/mol of each other and were investigated theoretically.

The STM simulation was carried out on the molecule $CH_3(CH_2)_3NH_2$, and the results are reported in Figure 14. For all three conformations, the amine appears to be bright, with the main spot centered on the α hydrogens. This result is in qualitative agreement with the experimental images reported in the literature for a primary amine,[3] although the exact position of the bright spot could not be determined from the STM data on this system. The computations indicate that the low ionization potential of the amine brings the HOMO of the adsorbate into the conduction region. The HOMO has

$CH_3(CH_2)_3NHCH_3(CH_2)_3$

(A) Flat, NH up

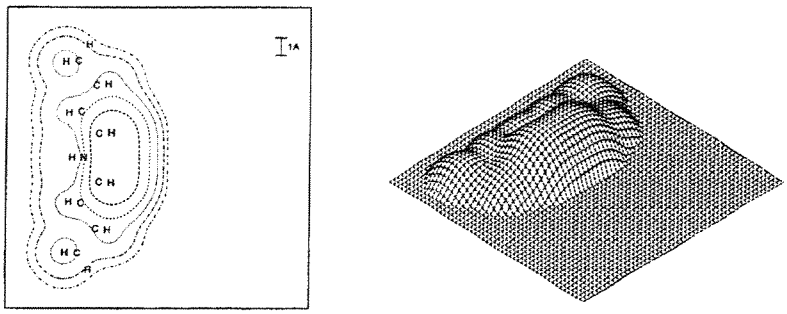

(B) Flat, NH down

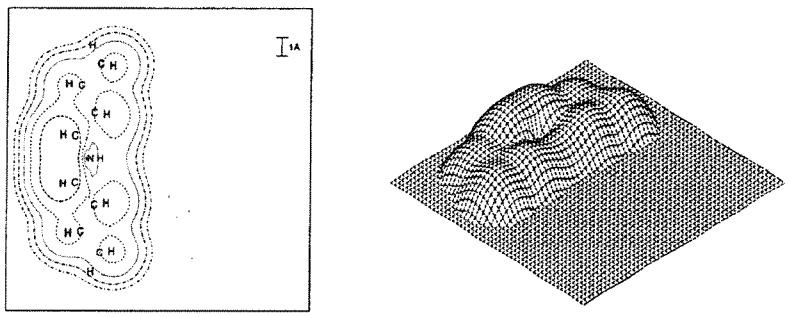

(C) Vertical, NH up

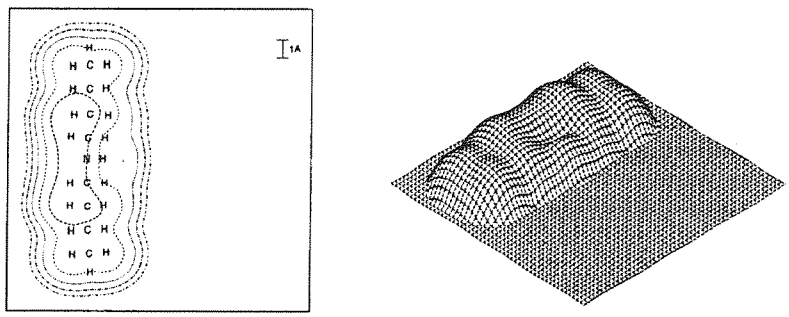

(D) Vertical, NH down

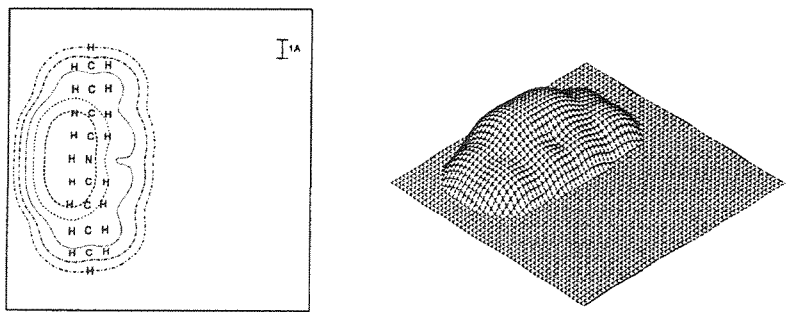

Figure 13. Computed constant current STM images of $CH_3(CH_2)_3NH(CH_2)_3CH_3$ on graphite: (A) flat orientation with the NH group pointing up; (B) flat orientation with the NH group pointing down; (C) vertical orientation with the NH group pointing up; (D) vertical orientation with the NH group pointing down. The maximum values for the plots are 2.71, 2.16, 2.26, and 3.00 au, respectively.

$CH_3(CH_2)_3NH_2$ Flat

(A) Lone pair flat

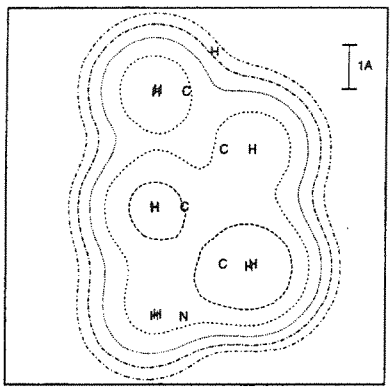

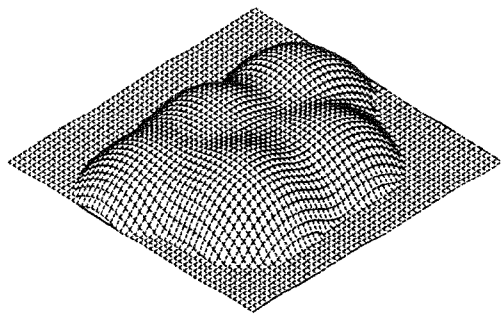

(B) Lone pair up

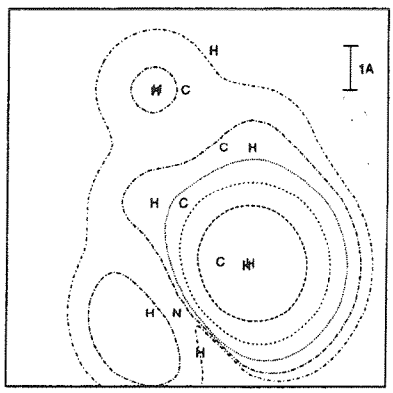

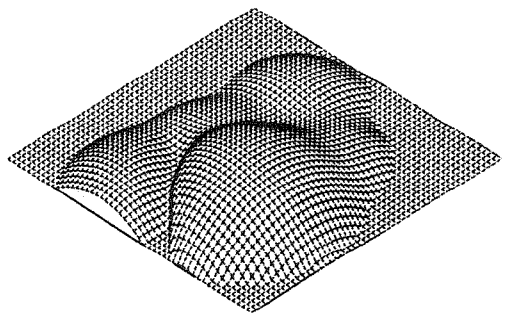

(C) Lone pair down

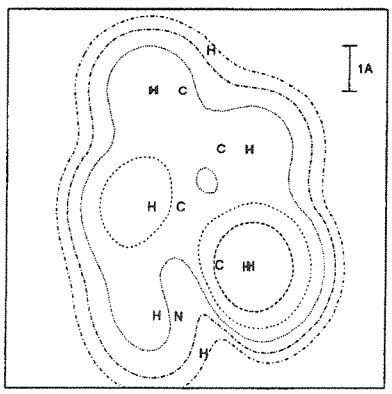

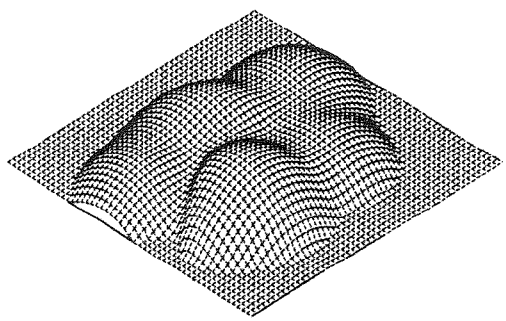

Figure 14. Computed constant current STM images of $CH_3(CH_2)_3NH_2$ adsorbed flat on graphite: (A) amine lone pair flat; (B) amine lone pair pointing up; (C) amine lone pair pointing down. The maximum values for the three plots are 1.39, 2.49, and 1.74 au, respectively.

significant contributions from the R hydrogens, which have a good coupling with the tip and the graphite and appear therefore bright in the simulation.

III.I. Alkene

FF minimizations on the adsorbed molecule $CH_3(CH_2)_{15}CHCH(CH_2)_{16}CH_3$ predict that isolated molecules should adsorb in the flat orientation, with the vertical orientation being more energetic by 9.1 kcal/mol. Packed molecules on the graphite surface are more stable by 11.8 kcal/mol in the vertical orientation, with the double-bond region strongly distorted toward a flat orientation and the rest of the molecule oriented vertically. We considered both orientations for the STM simulation.

The images obtained for *trans*-5-decene are reported in Figure 15. Both orientations exhibit a bright spot located close to the double bond, in agreement with the experimental results.[1] The high conductivity of this functionality in the STM experiment is due to the HOMO being located in the conduction region. In the flat orientation, the bright spot is centered on top of the double bond, essentially imaging the π system of the molecule (Figure 15A). In contrast to this electronic effect, in the vertical orientation the bright spot is dominated by topographical considerations and arises from the location of one of the hydrogen atoms pointing up from the molecule toward the tip (Figure 15B). Better resolution would be needed to distinguish between these possibilities experimentally.

Interestingly, the packing arrangement displayed by the *trans*-pentatriacontene produced an angle θ of 0° in the experimental STM images.[1] In this case, the possibility of significant intermolecular forces between the double bonds in the overlayer must be considered. Thus, for this system, the observed packing angle does not uniquely identify the orientation of the carbon- carbon skeleton, but it can be taken to indicate that the double bonds are in translational registry in the overlayer, as would be expected for significant π-π interactions between adsorbed molecules.

$$CH_3(CH_2)_3HC = CH(CH_2)_3CH_3$$

(A) Flat

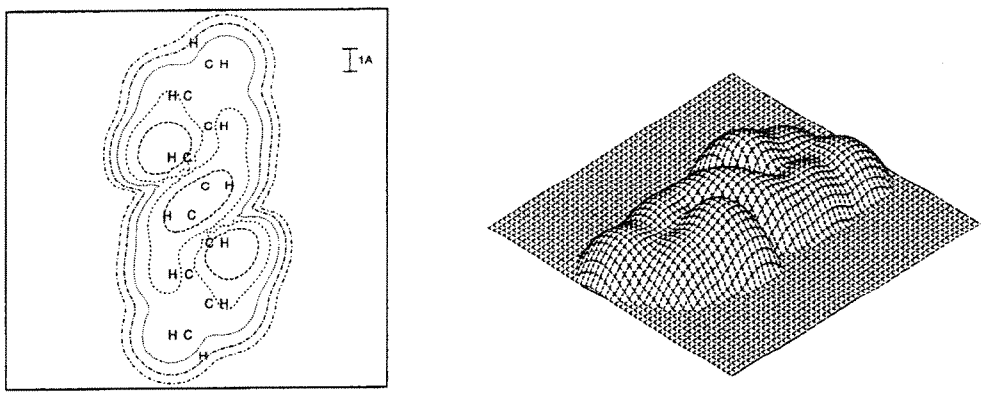

(B) Vertical

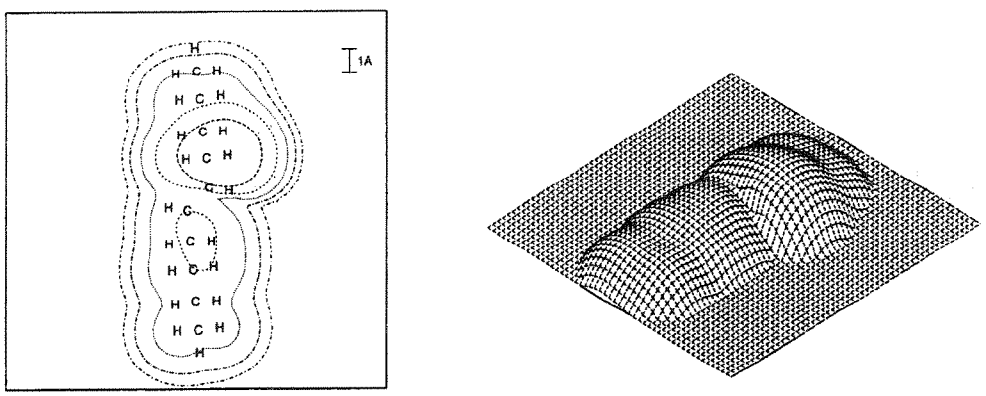

Figure 15. Computed constant current STM images of $CH_3(CH_2)CHCH(CH_2)_3CH_3$ on graphite: (A) flat orientation; (B) vertical orientation. The maximum values for the plots are 2.38 and 3.52 au, respectively.

III.J. Alkyne

The molecule studied experimentally is 7-hexadecyn-1-ol.[1] Since alkanols prefer to lie flat on the graphite,[1] only the flat orientation was investigated computationally.

The predicted image for 5-decyne, at a bias of -1 eV, is reported in Figure 16. In this image, the triple bond and the surrounding hydrogens appear to be brighter than the rest of the molecule, in agreement with experimental data on 7-hexa-decyn- 1-ol 1 as well as on 10,12-octadecadiynoic acid.[4] The simulated width of the bright spot around the triple bond was 6.4 Å, vs. the experimental observation of 3.5-4.3 Å.[1] Additionally, the flat orientation is expected to produce a kink around the triple bond due to the geometry of the molecule, and this feature is observed in the experimental STM images of the alkyne overlayers.[1]

$$CH_3(CH_2)_3C \equiv C(CH_2)_3CH_3$$

(A) Flat

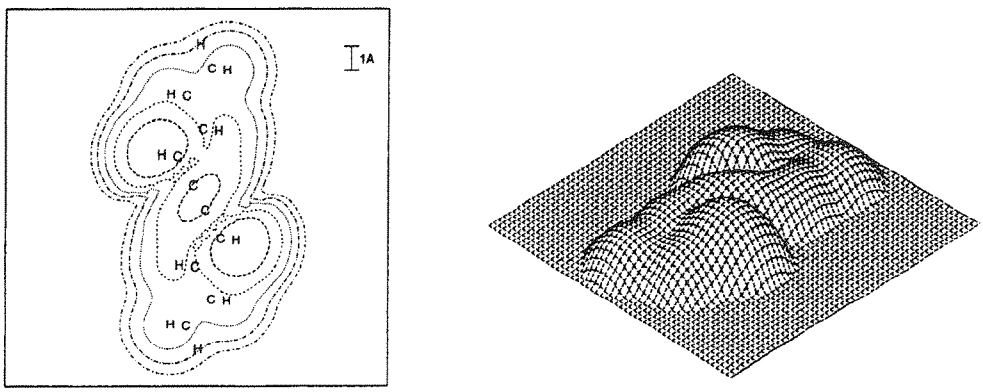

Figure 16. Computed constant current STM images of $CH_3(CH_2)_3CC(CH_2)CH_3$ laid flat on graphite. The maximum value for the plot is 2.58 au.

III.K. Nitrile

Figure 17 depicts the predicted STM image of a nitrile. This functionality also has a π system, like the alkenes and alkynes discussed above, yet it appears dark in the experimental STM image.[1] This behavior is reproduced in the computed STM images. The nitrile HOMO is much lower in energy than that of the alkyl chain; additionally, in the energetically favored *trans*-conformation, the nitrile group is farther from the tip than are the methylene hydrogens in the alkyl chain. Thus, both electronic and geometric considerations would predict the group to be dark, in accord with the experimental STM data for nitrile-containing alkyl overlayers on graphite.[1]

$CH_3(CH_2)_3CN$

(A) Flat

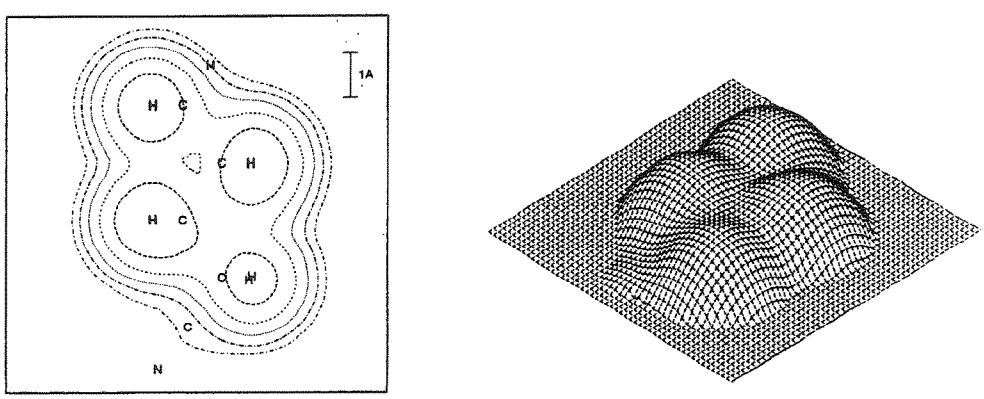

Figure 17. Computed constant current STM images of $CH_3(CH_2)_3CN$ laid flat on graphite. The maximum value of the plot is 1.09 au.

III.L. Acid Dimer

Prior work has described STM images of carboxylic acids on graphite.[2,4] To investigate this system theoretically, the dimer $[CH_3(CH_2)_7COOH]_2$ was studied to determine the adsorption geometry. Only the adsorption of one dimer was studied in the flat configuration.

The STM simulation was then performed on the smaller dimer $[CH_3(CH_2)_3COOH]_2$, and the results are reported in Figure 18. The acid region appears to be dark, in good agreement with the experimental results.[2] This occurs because, similar to the nitrile group, the π system of the acid group is very stable. The HOMO remains far from the conduction energy, and the image is dominated by the alkyl hydrogens, which are closer to the tip.

$(CH_3(CH_2)_3COOH)_2$

(A) Flat

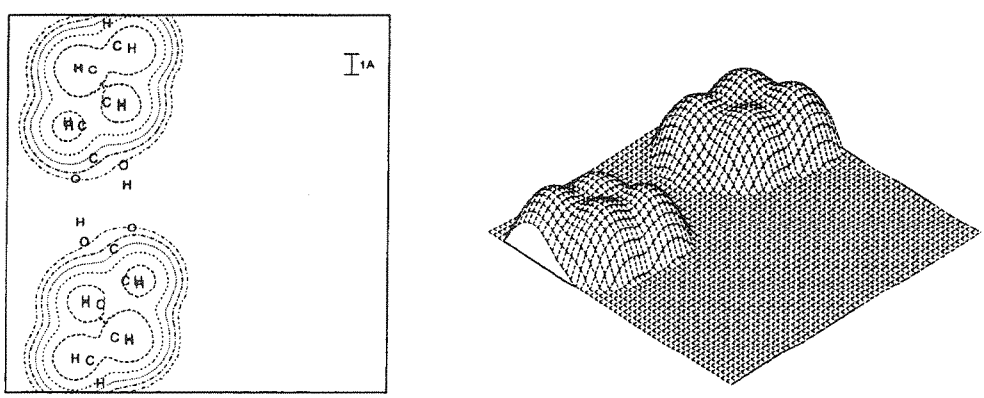

Figure 18. Computed constant current STM images of $[CH_3(CH_2)_3COOH]_2$ laid flat on graphite. The maximum value for the plot is 1.72 au.

III.M. Ketone

FF simulations on the molecule $CH_3(CH_2)_{16}CO(CH_2)_{16}CH_3$ indicate that the flat orientation is expected to be most stable for a singly adsorbed molecule, while the vertical orientations with CO pointing down and up are 12.4 and 9.0 kcal/mol more energetic, respectively. For packing densities close to those observed experimentally, the vertical orientation with CO pointing up is most stable, the vertical orientation with CO pointing down is less stable by 8.5 kcal/mol, and the flat geometry is less stable by 9.5 kcal/mol.

Figure 19 reports the computed STM images for $CH_3(CH_2)_3CO(CH_2)_3CH_3$ in each of the three orientations. The ketone region is bright in the STM image when the molecule is in the vertical orientation with the CO pointing down (Figure 19A). The brightness is predominantly topographic in origin and is due to the fact that the hydrogens closest to the CO are pushed toward the tip. In the flat orientation, the ketone is predicted to be dark (Figure 19B). The dark region extends over the hydrogens on the α carbons and, to a minor extent, to those on the β carbons with respect to the CO. In the vertical orientation with the CO pointing up, the ketone is predicted to be bright in the STM image (Figure 19C).

No conclusive experimental images are available for comparison with these computational results. Preliminary experimental data, however, gave a bright spot on the ketone for negative bias and a dark region for positive bias.[1] According to the theoretical model presented above for the effects of bias in STM experiments, based on the derivation of Marcus,[1,17] images obtained under positive and negative bias should be very similar unless the orientation or geometry of the molecule is different at the different bias polarities. Since the ketone is a polar group, it is possible that the transition from the flat to the vertical orientation with the CO pointing up is more favorable when the graphite has a negative charge (negative bias) than when the graphite has a positive charge. If this is the case, the observed images should depend on the history of the sample, with fresh samples having the molecules in the flat orientation and old samples, as well as samples

$CH_3(CH_2)_3CO(CH_2)_3CH_3$

(A) Vertical, CO down

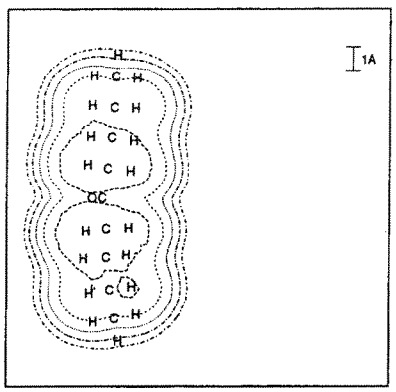

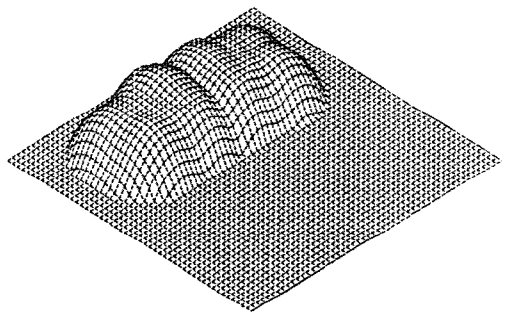

(B) Flat

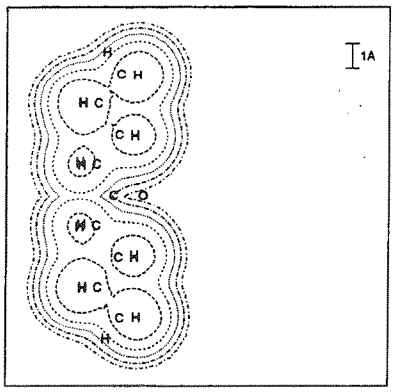

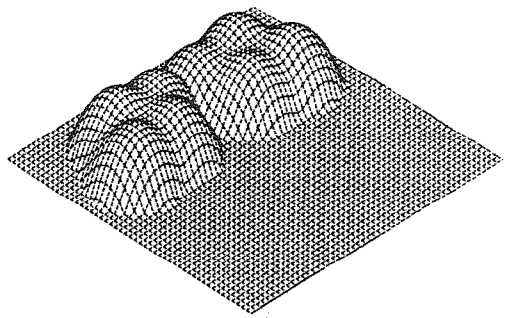

(C) Vertical, CO up

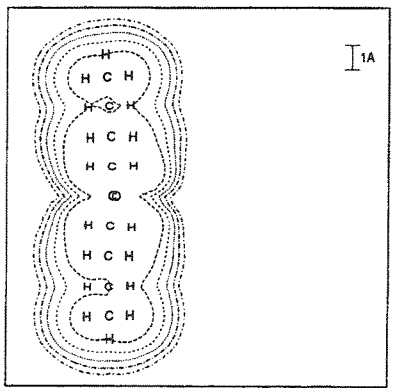

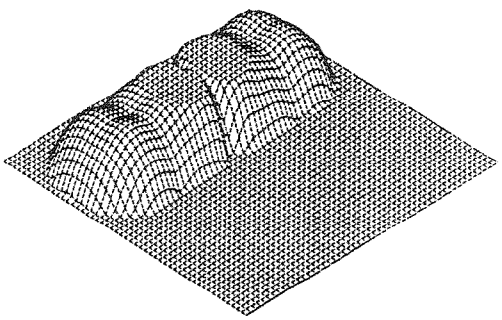

Figure 19. Computed constant current STM images of $CH_3(CH_2)_3CO(CH_2)_3CH_3$ on graphite: (A) vertical orientation with the CO pointing down toward the graphite; (B) flat orientation; (C) vertical orientation with the CO pointing up. The maximum values for the three plots are 2.23, 1.63, and 1.77 au, respectively.

already used for negative bias STM, having the molecules in the vertical orientation. These considerations are being investigated experimentally at present for ketones and for other highly polar functionalities adsorbed on graphite surfaces.

IV. Discussion

The predicted STM images reproduce the qualitative features of all of the experimental STM data reported in the accompanying chapter as well as those of other results on related systems.[1-5] These computations have provided physically reasonable explanations for the STM image contrast of all of the functional groups investigated experimentally and also allow an understanding of the widths of the various functional groups that have been observed in the experimental STM data.[1] In addition, the results explain the angles between the spots observed in the STM images of alkyl chains and in a number of cases allow assignment of the orientation of the adsorbates with respect to the graphite surface plane. The computations also allow separation of the importance of electronic and topographic effects in the STM images of many of the systems studied experimentally.

An interesting result arising from the computational model used in this work is the predicted importance of the virtual orbitals of the halogenated alkanols and of other related substituted alkanes in defining the STM image contrast. This result is different from the HOMO-dominated electronic coupling that is believed to determine electron tunneling matrix elements in intramolecular electron transfer processes between a donor and an acceptor connected to an alkane chain. The difference in importance of the occupied and virtual orbitals arises because the STM experiment is much more sensitive to the shape of the orbitals that are projected into the localized region defined by the tip-sample gap; thus, the more diffuse virtual orbitals can play a much more dominant role in defining the overall electronic coupling term in an STM experiment despite being significantly farther in energy from the Fermi level of the substrate than the occupied orbitals. Although the relative contributions of the virtual and occupied orbitals in

determining electronic coupling matrix elements in an STM image have not been definitively established experimentally, the calculations presented herein should offer a framework for future experimental studies that are designed to evaluate these effects in a systematic fashion.

The computational results have allowed classification of the functional groups into three categories, based on how their electronic structure affects the contrast in an STM image. These categories are discussed briefly below.

IV.A. Conductors

These functional groups have an ionization potential lower than a fixed value I_0. The exact value of I_0 is not known, but on the basis of the available data it is between the ionization potential of an alkyl bromide and that of an alkyl amine.[1] These groups have one (or more) orbital, in resonance with the conduction states on the tip and on the graphite, that is responsible for most of the observed current. As the STM image is essentially a map of the conducting orbitals, these groups tend to appear much brighter than the alkyl chain. For functionalized alkanes on graphite, this category of functional groups includes disulfides, thioethers, thiols, amines, alkenes, alkynes, and alkyl iodides. This functional group classification is closely related to the HOMO- IP model discussed in the previous chapter.[1]

IV.B. Dark Groups

Functional groups that are not conductors and that have low electron affinities appear dark. This is because the coupling is small through both the HOMO and LUMO. In addition, the computations indicate that most of the tunneling current in the systems evaluated in this work is described by the low lying virtual orbitals, much like a low-energy electron diffraction process. Virtual orbitals, in fact, need to be orthogonal to the occupied orbitals. Since the occupied orbitals tend to be close to the nuclei, the virtual orbitals are therefore squeezed toward the outside of the molecule and have better overlap, in general, with the tip and graphite, so they can dominate the tunneling matrix

element that is responsible for the STM process. Functional groups with electron affinities lower than that of the corresponding alkane will hence be dark in the STM image. Nonconducting functional groups in this class include *trans*-conformations of alkyl fluorides, alkyl chlorides, alkyl bromides, and alcohols, as well as ethers and trifluoromethylene units.

IV.C. Bright Groups

Functional groups with high electron affinities but that are not conductors are expected to be brighter than the alkyl chain. However, these groups are not expected to appear as bright as conductors. Since the relative energies of the virtual orbitals localized on different parts of the molecule must be compared, it is also important to consider that charge-withdrawing groups will lower the electron affinity of the alkyl chain, effectively shifting the reference intensity of neighboring groups that might be used to establish the STM image contrast of the functional group. No functional groups in this class have apparently been observed yet.

IV.D. Relative Importance of Geometric and Electronic Effects

Since the electronic coupling is determined strongly by the overlap of each orbital with the tip and the graphite, the geometry of the molecule plays a key role in determining the STM image. In fact, the theoretical STM images presented in this work reveal that the experimental STM data for most of the functionalized alkane overlayers investigated to date are dominated by topographic effects of the molecules in the overlayer. Functional groups that are close to the tip (or to the graphite) will thus tend to appear bright unless there are strong electronic effects that reduce the orbital overlap in this region of space. Fluorinated alkyls (Figure 7) provide an example of this interplay between topographic and electronic effects in determining the contrast of an STM image. A theoretical description of the image contrast of such systems therefore requires an evaluation of electronic and steric effects in a fairly detailed fashion. The conclusion that most molecules are imaged through the virtual orbitals is consistent with the observation

that at low bias the graphite is imaged while at high bias the molecules are observed. The long-range behavior of an electronic wave function in a Coulomb potential is described by[14]

$$\psi(\mathbf{r}) = f(\mathbf{r})e^{-\chi r} \quad \chi = \sqrt{2|E|} \tag{19}$$

where $f(r)$ diverges at most like a polynomial. Therefore, in general, the occupied MOs of the absorbate decay faster than the orbitals of the substrate that have energies near the graphite Fermi level. These graphite orbitals, in turn, decay faster than the virtual MOs of the absorbate overlayer. It follows that if the occupied orbitals dominate the STM images at large distances, then they should also dominate the image at smaller distances. Thus, the experimental data, which show a transition from images of graphite at small tip-sample biases to images of the overlayer at large tip-sample biases, are in accord with the behavior expected for the situation where the virtual orbitals of the molecular overlayer dominate the electronic coupling in the tip-sample gap. This result is, however, only described qualitatively at present because the graphite states were omitted in our simulation method so that the description of the STM data at high bias could be obtained in a straightforward fashion.

IV.E. Expense of the Computational Methods

The computational methods were reasonably inexpensive to perform. The computational cost of each prediction can be roughly divided as follows: 40% to optimize the adsorption geometry, 55% to run the HF computation, and 5% to run the actual STM simulation. The overall computer (CPU) time on HP9000/735 workstations is on the order of 30 min. for the small molecules and 1 h for the largest ones. Thus, this theoretical framework can be readily adopted by a variety of researchers in order to guide future experimental investigations of the mechanisms underlying the image contrast of molecules in an STM experiment. Numerous theoretical predictions have been advanced

in this chapter that will be interesting to explore experimentally, and the hope is that this set of predictions will stimulate experimental studies designed to elucidate further the factors that control these interesting atomic-resolution imaging processes.

V. Summary and Conclusions

In summary, a simple model, based on perturbation theory, was used to predict the STM images of molecules adsorbed on graphite. The geometries of the adsorbed molecules were estimated using a force field and the unperturbed molecular wave function was assumed to be the Hartree-Fock wave function for the gas-phase molecule, except for a simple shifting of the orbital energies to account for the fact that during the tunneling process the molecule is in close proximity to two conductors: the tip and the graphite.

The model contains one adjustable parameter representing the interaction between the molecules and the graphite. This parameter is expected to change very little for different molecules of the same family, and it was fixed to a value that seems to reproduce most of the experimental images.

For most of the molecules investigated in this study, topographic effects were observed to play a key role in determining the contrast observed in the experimental STM images. In fact, this correlation allows assignment of the orientation of most of the molecules with respect to the plane of the graphite surface and allows formulation of predictions regarding how the image contrast should be affected as the molecular orientation is varied. Electronic effects on the STM image contrast were revealed through an analysis of the orbital coupling properties of functional groups such as fluoromethyl and perfloromethylene units in the alkane and alkanol overlayers investigated in this work.

The theoretical predictions are mainly qualitative, but they can provide significant insight into the experimental STM images and can define further avenues of interest in the experimental investigation of STM imaging mechanisms with a minor computational cost.

Acknowledgments

The research was funded by NSF (CHE 9522179 and ASC 9217368, W.A.G.; and CHE-9634152, N.S.L.). C.C. also acknowledges the NIH for a predoctoral training grant. The facilities of the MSC are also supported by grants from DOE-BCTR, Chevron Petroleum Technology Co., Asahi Chemical, Aramco, Owens-Corning, Asahi Glass, Chevron Research Technology Co., Chevron Chemical Co., Hercules, Avery-Dennison, BP Chemical, and the Beckman Institute.

Appendix A: Bias Dependence in Formulas (8), (16), and (18)

The bias dependence in eq 8 appears in two forms: (1) the integration domain is the conduction region CR defined as

$$\mathrm{CR} = \begin{cases} \{E{:}E \in (E_f, E_f + E_b)\} & \text{for negative bias } (E_b > 0) \\ \{E{:}E \in (E_f + E_b, E_f)\} & \text{for positive bias } (E_b < 0) \end{cases}$$

where E_f is the fermi energy and $-E_b$ is the bias; (2) the scaled orbital energies E_k are

$$E_k = \epsilon_k + \frac{1}{2}E_b$$

where ε_k is the original orbital energy.

We can write eq 8 as

$$I_{gt} = \frac{2\pi}{\hbar}\int_{E_f}^{E_f+E_b}\left|\sum_k \frac{V_{gk}V_{kt}}{\left(E - E_k - \frac{1}{2}E_b\right)}\right|^2 \rho_t(E)\,\rho_g(E)\,dE$$

with the assumption that the absolute value of the integral be taken.

Including explicitly the dependence in eq 16 requires the definition of a new function $F(E)$:

$$F(E) = \begin{cases} 1 & \text{if } E \notin \mathrm{CR} \\ 0 & \text{if } E \in \mathrm{CR} \end{cases}$$

Equation 16 becomes then (again, we need to take the absolute value of the integral, but this time the relation is formally correct due to the $\propto$ symbol)

$$I \propto \int_{E_f}^{E_f+E_b} \rho_t(E)\rho_g(E)\left\{\left[\sum_k \frac{F\left(E_k+\frac{1}{2}E_b\right)V_{gk}V_{kt}}{\left(E-E_k-\frac{1}{2}E_b\right)}\right]^2 + \left[\pi\sum_k\left(1-F\left(E_k+\frac{1}{2}E_b\right)\right)V_{gk}V_{kt}\delta^{(\epsilon)}\left(E-E_k-\frac{1}{2}E_b\right)\right]^2\right\}dE$$

Finally, eq 18 becomes

$$I \propto \int_{E_f}^{E_f+E_b}(E_f-E)^2\left[\sum_k \frac{F\left(E_k+\frac{1}{2}E_b\right)V_{gk}V_{kt}}{\left(E-E_k-\frac{1}{2}E_b\right)}\right]^2 + \int_{E_f}^{E_f+E_b}(E_f-E)^2\left[\pi\sum_k\left(1-F\left(E_k+\frac{1}{2}E_b\right)\right)V_{gk}V_{kt}\delta^{(\epsilon)}\left(E-E_k-\frac{1}{2}E_b\right)\right]^2 dE$$

References and Notes

(1) Claypool, C. L.; Faglioni, F.; Goddard, W. A., III; Gray, H. B.; Lewis, N. S.; Marcus, R. A. *J. Phys. Chem. B* **1997**, *101*, 5978.

(2) Liang, W.; Whangbo, M.-H.; Wawkuschewski, A.; Cantow, H.-J.; Magonov, S. N. *Adv. Mater.* **1993**, *5*, 817. Bar, G.; Magonov, S. N.; Cantow, H.-J.; Kushch, N. D.; Yabubskii, E. B.; Liang, W.; Ren, J.; Whangbo, M.-H. *New J. Chem.* **1993**, *17*, 439.

(3) Venkataraman, B.; Flynn, G. W.; Wilbur, J. L.; Folkers, J. P.; Whitesides, G. M. *J. Phys. Chem.* **1995**, *99*, 8684. Cyr, D. M.; Venkataraman, B.; Flynn, G. W.; Black, A.; Whitesides, G. M. *J. Phys. Chem.* **1996** *100*, 13747. Cyr, D. M.; Venkataraman, B.; Flynn, G. W. *Chem. Mater.* **1996** *8*, 1600.

(4) Rabe, J. P.; Buchholz, S. *Science* **1991**, *253*, 424. Rabe, J. P.; Buchholz, S.; Askadskaya, L. *Synth. Met.* **1993**, *54*, 339.

(5) Magonov, S. N.; Whangbo, M.-H. *Surface Analysis with STM and AFM*; VCH: New York, 1996.

(6) Tersoff, J.; Hamman, D. R. *Phys. Rev. Lett.* **1983**, *50*, 1998. Tersoff, J.; Hamman, D. R. *Phys. Rev.B* **1985**, *31*, 805.

(7) Bardeen, J. *Phys. Rev. Lett.* **1961**, *6*, 57.

(8) Lang, N. D. *Phys. Rev. Lett.* **1985**, *55*, 230. Lang, N. D. *Phys. Rev. Lett.* **1986**, *56*, 1164.

(9) Doyen, G.; Drakova, D.; Kopatzki, E.; Behm, R. J. *J. Vac. Sci. Technol. A* **1988**, *6*, 327. Kopatzki, E.; Doyen, G.; Drakova, D.; Behm, R. J. *J. Microsc.* **1988**, *152*, 687.

(10) Hallmark,V. M.; Chiang, S.; Meinhardt, K. P.; Hafner, K. *Phys. Rev. Lett.* **1993**, *70*, 3740. Hallmark, V. M.; Chiang, S. *Surf. Sci.* **1995**, *329*, 255.

(11) Sautet, P.; Joachim, C. *Chem. Phys. Lett.* **1991**, *185*, 23; *Surf. Sci.* **1991**, *271*, 387. Sautet, P.; Bocquet, M. L. *Surf. Sci.* **1994**, *304*, L445.

(12) Fisher, A. J.; Blöchl, P. E. *Phys. Rev. Lett.* **1993**, *70*, 3263.

(13) Yang, H. O.; Marcus, R. A.; Källebring, B. *J. Chem. Phys.* **1994**, *100*, 7814.

(14) Landau, L. D.; Lifshits, E. M. *Quantum Mechanics*; Pergamon Press: New York, 1977.

(15) Hehre, W. J.; Stewart, R. F.; Pople, J. A. *J. Chem. Phys.* **1969**, *51*, 2657.

(16) Koryta, J.; Dvorak, J.; Kavan, L. *Principles of Electrochemistry*, John Wiley & Sons Ltd.: New York, 1993.

(17) Marcus, R. A. *J. Chem. Soc., Faraday Trans.* **1996**, *92*, 3905.

(18) Landolt-Börnstein. *Numerical Data and Functional Relationships in Science and Technology,* New Series; Springer-Verlag: Berlin, 1984; Group III, Vol. 13c. Charlier, J. C.; Gonze, X.; Michenaud, J. P. *Phys. Rev. B* **1991**, *43*, 4579.

(19) Mayo, S. L.; Olafson, B. D.; Goddard, W. A., III *J. Phys. Chem.* **1990**, *94*, 8897.

(20) Rappe′, A. K.; Goddard, W. A., III *J. Phys. Chem.* **1991**, *95*, 3358.

(21) Morishige, K.; Takami, Y.; Yokota, Y. *Phys. Rev.B* **1993**, *48*, 8277.

(22) Frisch, M. J.; Trucks, G. W.; Schlegel, H. B.; Gill, P. M. W.; Johnson, B. G.; Wong, M. W.; Foresman, J. B.; Robb, M. A.; Head-Gordon, M.; Replogle, E. S.; Gomperts, R.; Andres, J. L.; Raghavachari, K.; Binkley, J. S.; Gonzalez, C.; Martin, R. L.; Fox, D. J.; Defrees, D. J.; Baker, J.; Stewart, J. J. P.; Pople, J. A. *Gaussian 92/DFT*, Revision F.4; Gaussian, Inc.: Pittsburgh, PA, 1993. Frisch, M. J.; Trucks, G. W.; Schlegel, H. B.; Gill, P. M. W.; Johnson, B. G.; Robb, M. A.; Cheeseman, J. R.; Keith, T.; Petersson, G. A.; Montgomery, J. A.; Raghavachari, K.; Al- Laham, M. A.; Zakrzewski, V. G.; Ortiz, J. V.; Foresman, J. B.; Peng, C. Y.; Ayala, P. Y.; Chen, W.; Wong, M. W.; Andres, J. L.; Replogle, E. S.; Gomperts, R.; Martin, R. L.; Fox, D. J.; Binkley, J. S.; Defrees, D. J.; Baker, J.; Stewart, J. P.; Head-Gordon, M.; Gonzalez, C.; Pople, J. A. *Gaussian 94*, Revision B.3; Gaussian, Inc.: Pittsburgh, PA, 1995.

(23) Pairler, G. E.; Pylant, E. O. *Science* **1996**, *272*, 1145.

(24) Lias, S. G.; Levin, R. D. *Ionization Potential and Appearence Potential Measurements, 1971-1981*; U.S. Department of Commerce/National Bureau of Standards: Washington, DC, 1982.

Chapter 3

Effects of Molecular Geometry on the STM Image Contrast of Alkanes and Alkanols on Graphite

Abstract

With the continued goal to understand in a systematic fashion the factors that control the spatial image contrast in molecularly resolved STM images, several functionalized alkanes and alkyl alcohols have been synthesized and imaged by scanning tunneling microscopy (STM) methods on graphite and MoS_2 surfaces. To further distinguish between the contributions of electronic and topographic factors in the STM images of adsorbed organic molecules, a series of molecules has been prepared with internal functional groups that alter the adsorbed molecular geometries from those obtained previously,[1] and include bromo-, methyl-, hydroxyl-, and allene functionalities. The resulting STM image contrast can be understood and explained using the theoretical model proposed by Faglioni *et al.*[2]

I. Introduction

The previous chapters investigated the effects of molecular geometry and electronic structure on the STM image contrast of organic molecules adsorbed on graphite.[1] The quantum calculations[2] have indicated that the geometry and resulting topography of the adsorbed molecules play a critical role in the observed STM image contrast. For example, the STM images of unfunctionalized alkane and alkanol molecules were observed to predominately reflect the topography of the adsorbed molecules; that is, the hydrogen atoms nearest the tip were observed in the sub-molecular resolution STM images. The effect of various functionalities incorporated into these molecules was observed in the STM image contrast and understood with a simple argument used to

estimate the electronic coupling based on the ionization potential of the molecules (HOMO-IP model). More detailed quantum calculations showed that topographic factors were responsible for much of the observed image contrast; however, the experiments and calculations also revealed that the effects of electronic structure had the potential to overwhelm the effects of molecular geometry on the observed STM image contrast and *vice versa*. This chapter discusses experiments designed to test some of the theoretical predictions made from the model presented in Chapter 2 and further investigate the effects of molecular geometry on the STM image contrast. Specifically, the predictions of the theoretical model that are tested include the contrast over an alkyl chain adsorbed in the vertical as opposed to the flat orientation; the contrast for a bromine heteroatom pointing away from the graphite surface; and the contrast for an hydroxyl group pointing away from the graphite surface.

II. Experimental

Sample preparation and imaging conditions were similar to those reported previously.[1] Briefly, samples were prepared by placing a 6 μl droplet of a concentrated solution of the organic compound in phenyloctane onto a freshly cleaved graphite (HOPG, Union Carbide) or MoS_2 (gift from John Baldeschwieler, Caltech) surface. A mechanically formed Pt/Ir tip was then immersed into the liquid droplet and the imaging (Nanoscope III, Digital Instruments, Santa Barbara, CA) was performed at the liquid/graphite interface. All of the images presented were obtained at constant current in the variable height mode. Bright portions of the images displayed herein correspond to points at which the tip retracted away from the surface in order to maintain a constant current. Nearly every prepared sample yielded evidence of the adsorbed monolayer in the STM image; however, several different tips were often necessary to achieve the reported images.

The lattice spacing of graphite (2.46 Å) was used as the calibration standard for the x and y piezo dimensions. Step edges observed on an oxidized graphite surface[3] (3.35

Å) were used as a calibration standard for the z piezo dimension. Metrics were determined using Nanoscope III software, and the apparent heights of heteroatoms and groups are reported with respect to the average height of the image over the methylene portion of the adsorbed molecule. Errors in the distances quoted in this manuscript include our estimates of the measurement errors associated with determining the metrics from the images as well as the reproducibility of these metrics over various experiments. To reduce noise, after data collection the images were filtered using Nanoscope III software. The filtering was primarily performed to enhance the visual presentation of the printed images, but the filtering was performed in such a way that it did not distort any of the primary metrics evident in the original data nor did the filtering procedure introduce any new spot patterns or new topographic features into an image. Tetradecanol (Aldrich), stearone (TCI), dimethyl 10-bromoeicosane-1,20-dicarboxylic acid (Aldrich), and phenyl octane (Aldrich) are commercially available and were used as received.

Synthesis of $\mathbf{H_3C(CH_2)_{15}C{=}C{=}C(CH_2)_{15}CH_3}$. Following the literature procedure,[4] lithium diisopropylamide (LDA) was added to a solution of stearone in dry THF at 0 °C and allowed to stir for 1 h. Diethyl chlorophosphate was then added, and the solution was allowed to stir for 45 minutes at 0 °C. After cooling to -78 °C, 2.2 equivalents of LDA was added and the solution was stirred for 48 h. The mixture was quenched with water and poured onto pentane, and the aqueous layer was extracted with pentane three times. After filtering the combined extracts, the solvent was removed *in vacuo*. Purification by chromatography on silica gel (eluting with pentane) gave the desired product. ^{1}H NMR ($CDCl_3$) 0.89-0.98 (m, 6 H), 1.36 (s, 56 H), 1.97-2.09 (m, 4 H), 5.09-5.18 (m, 2 H).

Synthesis of $\mathbf{H_3CO_2C(CH_2)_9CH{=}CH(CH_2)_9CO_2CH_3}$. Methyl undecylenate (2.58 g, 13.0 mmol) was treated with $(PCy_3)_2Cl_2Ru{=}CHPh$ (108 mg, 0.132 mmol) and vigorously stirred under vacuum for 5 h. Filtration of the crude reaction mixture through silica gel eluting with 25% EtOAc in hexanes afforded 2.33 g (97 %) of dimethyl eicos-10-

ene-1,20-dicarboxalate. Further purification was achieved by recrystallization from methanol. ^{1}H NMR ($CDCl_3$): 1.27 (s, 20 H), 1.61 (t, 4 H), 1.91-1.98 (m, 4 H), 2.30 (t, 4 H), 3.66 (s, 6 H), 5.37 (t, 2 H).

Synthesis of $H_3CO_2C(CH_2)_9CHBr(CH_2)_{10}CO_2CH_3$. Dimethyl eicos-10-ene-1,20-dicarboxylate (0.415 g, 1.13 mmol) was dissolved in acetic acid (10 mL) and treated with HBr in acetic acid (4.0 mL of a 30% solution). The product was isolated by pouring the solution into water after 6 h. The resulting oil was recovered from the aqueous layer by extraction with ether/hexanes (1:1) and dried over anhydrous Na_2SO_4. Concentration afforded an oil (0.320 g) which was used crude in the next step.

Synthesis of $HO(CH_2)_9CHBr(CH_2)_{10}OH$. Dimethyl 10-bromoeicosane-1,20-dicarboxylic acid was dissolved in dry CH_2Cl_2 (20 mL) and cooled to 0 °C. To this solution was added diisobutylaluminum hydride (7.0 mL of a 1.0 M solution in THF) dropwise over 10 min. After 4.5 h, the reaction was quenched by slow addition of methanol (3.0 mL) and 10 min of stirring followed by the addition of 1 M HCl (10 mL). The solution was warmed to rt and more 1.0 M HCl (30 mL) was added. The organic layer was separated, washed with brine (50 mL) and dried over anhydrous Na_2SO_4. Removal of the solvent yielded an oil which solidified upon standing (0.314 g, 71% for 2 steps). Further purification was achieved by crystallization from CH_2Cl_2/hexanes at -6 °C to give a white powder. Anal. Calcd for $C_{20}H_{41}BrO_2$: C, 61.06; H, 10.50. Found: C, 61.51; H, 10.19.

Synthesis of $CH_3(CH_2)_{16}CHOH(CH_2)_{16}CH_3$. Following the literature procedure,[5] stearone (3.00 g, 5.92 mmol) and $LiAlH_4$ (0.339 g, 8.93 mmol) were dissolved in THF (200 mL) and stirred for 3 d. Excess reducing agent was quenched by sequential addition of water (0.30 mL), 10% NaOH solution (0.45 mL), and water (0.90 mL). The resulting salts were filtered off on a fritted funnel and the product recovered from the filtrate by evaporation (0.612 g, 20%). ^{1}H NMR ($CDCl_3$): 0.88 (t, 6 H), 1.25 (s, 60 H), 1.55 (br s, 4H), 3.58 (br s, 1 H).

Synthesis of $CH_3(CH_2)_{16}CHBr(CH_2)_{16}CH_3$. To 18-pentatriacontanol (0.403 g, 0.792 mmol) suspended in dry THF (75 mL) was added PPh_3 (1.00 g, 3.82 mmol) and Br_2(180 μL, 3.49 mmol). After 20 h, methanol (0.50 mL) was added and the solvent was removed under reduced pressure. Purification by column chromatography on silica gel with hexanes as eluent provided a colorless oil which solidified upon standing. Further purification was achieved by crystallization from CH_2Cl_2/methanol at 0 °C.

Synthesis of $CH_3(CH_2)_{16}(CCH_2)(CH_2)_{16}CH_3$. To a solution of methyl triphenylphosphonium bromide (3.67 g, 10.3 mmol) in THF (100 mL) was added butyllithium (5.60 mL of a 1.6 M solution in hexanes, 8.96 mmol). After 5 min, stearone (1.50 g, 2.96 mmol) was added and the solution was allowed to stir for 3 d. Excess reagent was quenched by addition of acetone (1.5 mL) and the solvent was removed under reduced pressure. Pure product was obtained after chromatography on silica gel eluting with hexanes followed by evaporation of the solvent (1.13 g, 76%). ^{1}H NMR ($CDCl_3$): 0.88 (t, 6 H), 1.25 (s, 60 H), 2.01 (t, 4 H), 5.45 (br s, 2 H)

Synthesis of $CH_3(CH_2)_{16}CHCH_3(CH_2)_{16}CH_3$. Following the literature procedure,[6] the alkene (0.190 g, 0.375 mmol) and 10% Pd/C (20.5 mg) were suspended in THF (50 mL) and kept under a hydrogen atmosphere for 1d. The product was recovered after filtration through silica gel eluting with hexanes and concentration of the resulting filtrate.

III. Results

1. STM Image of an Allene

Figure 1a shows an STM image of a monolayer of 17, 18-pentatriacontadiene molecules, $H_3C(CH_2)_{15}C{=}C{=}C(CH_2)_{15}CH_3$, adsorbed on highly ordered pyrolytic graphite. The individual allene molecules are clearly resolved, and the mean molecular length of 46.3 ± 0.5 Å corresponds well with the length of 45.1 Å calculated for the all-*trans*-conformation of the molecule using the standard bond length values and van der Waals radii for the terminal atoms. The pattern of bright spots within individual

(a)

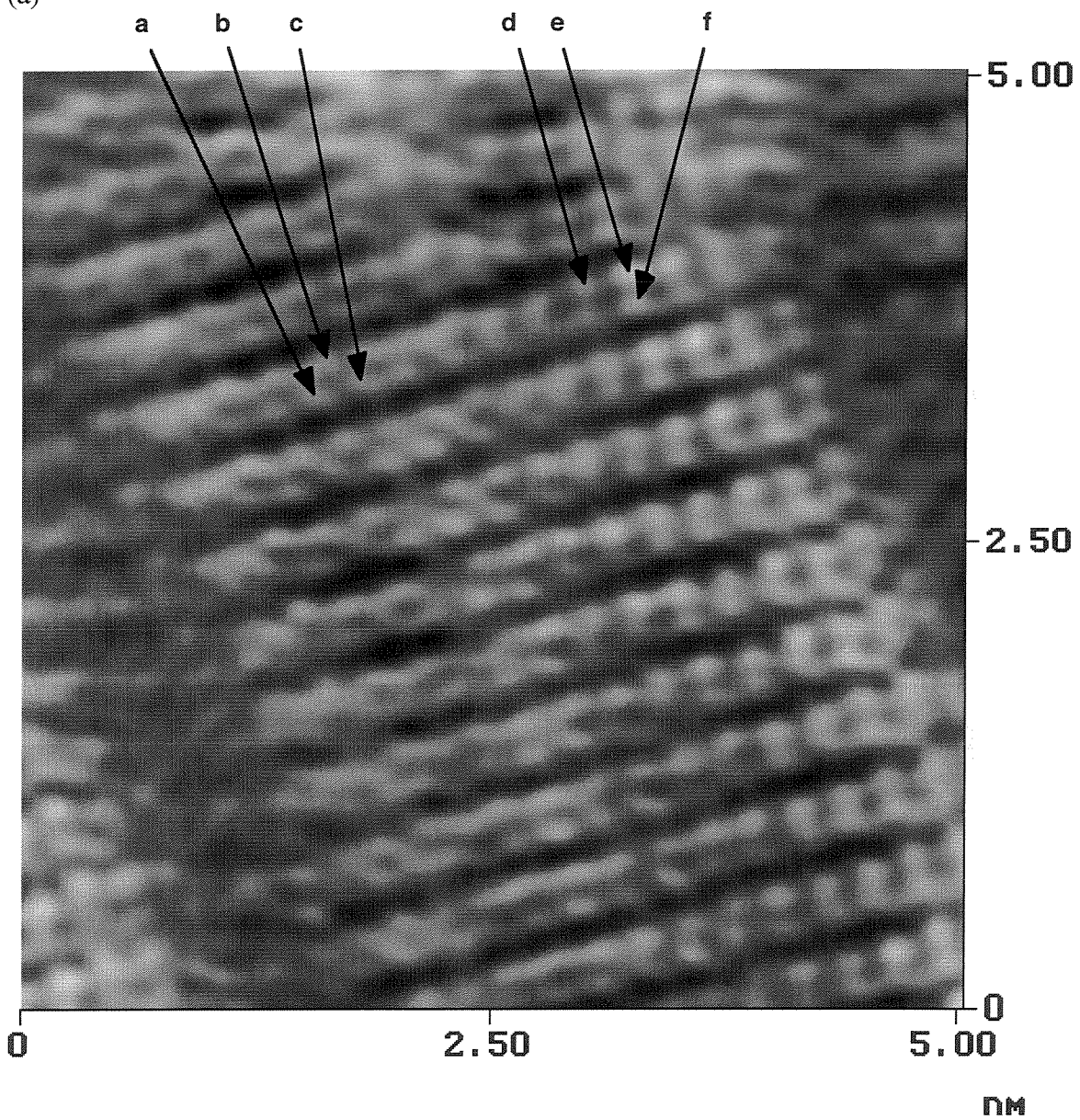

(B) Vertical $CH_3(CH_2)_7CH_3$ at $-1.0\ eV$ Constant current

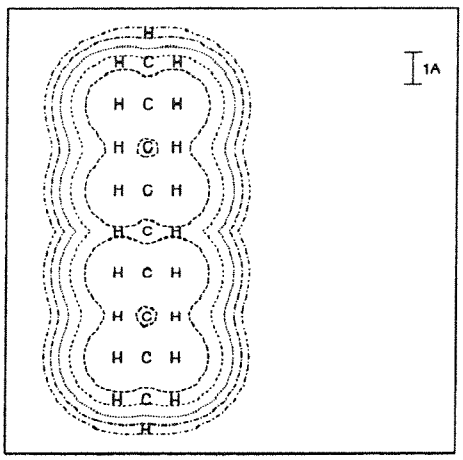

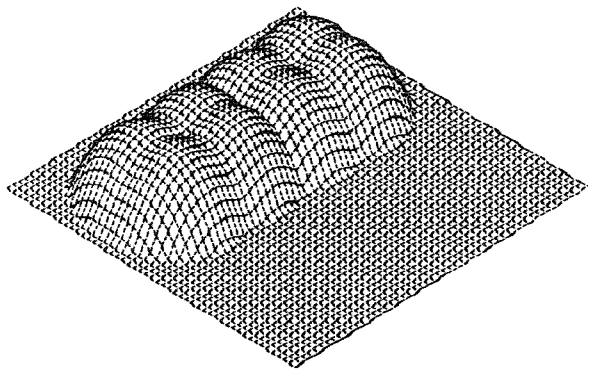

(C) Flat $CH_3(CH_2)_6CH_3$ at $-1.0\ eV$ Constant current

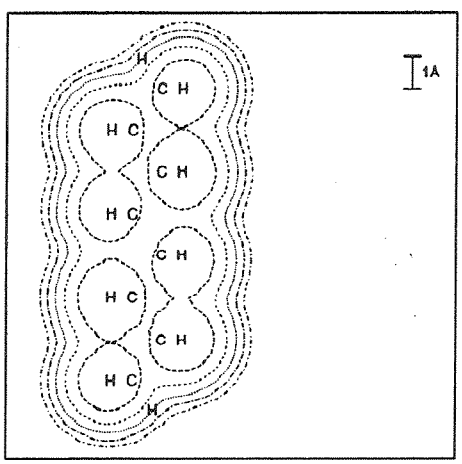

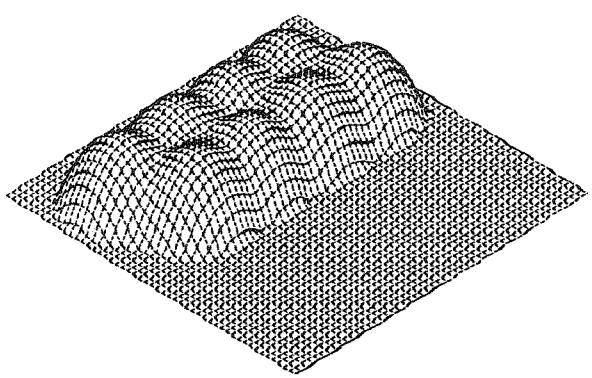

Figure 1. (a) Constant current STM image of a monolayer of 17, 18-pentatriacontadiene, $H_3C(CH_2)_{15}C{=}C{=}C(CH_2)_{15}CH_3$, molecules adsorbed on a graphite surface (V=1.023 volt, I=500 pA. The image is dominated by the topography of the adsorbate molecules, with the individual bright spots corresponding to the upward-facing hydrogen atoms in the alkyl chains on either side of the allene functionality. On the left-hand side of the adsorbed molecules, the bright spots appear to alternate in a pattern and spacing similar to that of an alkane adsorbed in a flat orientation. On the right-hand side of the molecules, the bright spots are ordered in a rectangular pattern, and the alkyl chain on this side of the molecule appears to be adsorbed in a perpendicular orientation. (b) Computed constant current STM images of an alkane molecule adsorbed onto the graphite surface in a flat and (c) vertical orientation. The contour levels are at 1/6, 2/6, 3/6, 4/6, and 5/6 of the maximum peak of each plot, and 3-D plots are shown to the right of the contour plots.

molecules appears to change on either side of the allene functionality that is located in the center of the molecule. On the left-hand side of the molecules, the bright spots are separated by a mean distance of 2.56 ± 0.05 Å in the direction along the molecule (a to c) and the distance between these spots was 2.36 ± 0.05 Å (a to b and b to c). The distance between alternating spots in adjacent molecules was 2.66 ± 0.05 Å. On the right-hand side of the molecules, the bright spots are separated by a mean distance of 2.56 ± 0.05 Å in the direction along the molecule (d to e) while the distance between these spots was 1.57 ± 0.05 Å (e to f). The distance between rows of spots in adjacent molecules was 2.56 ± 0.05 Å.

Previous STM measurements on alkane and alkanol molecules have assigned the bright spots within individual molecules to the hydrogen atoms nearest the tip.[1] This hypothesis is also supported by the allene experiment -- the alkyl chains on either side of the allene functionality are forced to be twisted by 90° with respect to one another, and this is reflected in the spot pattern that is observed within individual allene molecules. This assignment implies that the alkyl chain to the left of the allene functionality in this image is oriented such that the plane containing the carbon-carbon skeleton lies parallel to the graphite surface plane, while the alkyl chain to the right of the allene functionality is oriented such that the plane containing the carbon-carbon skeleton lies perpendicular to the graphite surface plane.

Figure 1 b and c are the computed constant current STM images of an alkane molecule adsorbed onto the graphite surface in a vertical and flat oriention.[2] The calculated images show spots corresponding to the hydrogen atoms closest to the tip, leading to a rectangular pattern for the vertical orientation and an alternating spot pattern for the flat orientation. These calculated images are in excellent agreement with the experimental image of the allene. In the constant current simulation, the average distance between spots in the vertical orientation is 2.59 Å along the backbone and 1.57 Å between nearest neighbors. For the flat orientation the average distance between spots

along the direction of the molecule is 2.56 Å and 2.61 Å between subsequent spots along the alkane chain. The positions of the spots observed experimentally are not in exact agreement with those in the simulation presumably due to the approximations contained in both the model and the computation.

2. STM Image of Tetradecanol on MoS_2

Figure 2 displays an image of a monolayer of tetradecanol molecules ($C_{14}H_{29}OH$) adsorbed on the surface MoS_2. The average molecular length of 19.8 ± 0.1 Å is in good agreement with the molecular length of 19.2 Å obtained from molecular modeling using Cerius 2 software for the all-*trans*-conformation of the molecule. Similar to the previous high-resolution images of tetradecanol molecules on graphite,[1] a series of alternating bright spots within individual tetradecanol molecules is observed. The bright spots are separated by a mean distance of 2.55 ± 0.05 Å in the direction along the molecule (a to c) and the distance between these spots was 2.35 ± 0.05 Å (a to b and b to c). The distance between alternating spots in adjacent molecules was 2.75 ± 0.05 Å. These data are nearly identical to those measured previously for alkanol and alkane monolayers adsorbed on graphite[1] and provide further evidence that the positions of the bright spots in STM images of the alkyl chains are dominated by the locations of individual hydrogen atoms on methylene units in a *trans*-alkane chain.

A previous argument has been made that these images cannot be explained in terms of enhanced imaging of graphite lattice atoms by the presence of the adsorbed alkane or alkanol. Specifically, the observed distances do not correspond to the lattice spacing of graphite.[1] The distance between adjacent β site carbon atoms in a graphite lattice is 2.46 Å,[7] and the origin of the bright spots in the STM data therefore cannot be explained in terms of enhanced imaging of graphite lattice atoms. This argument is further supported by the observation of nearly identical spot patterns and metrics for the STM image of tetradecanol molecules adsorbed on MoS_2, which has a lattice constant of 3.16 Å.[7]

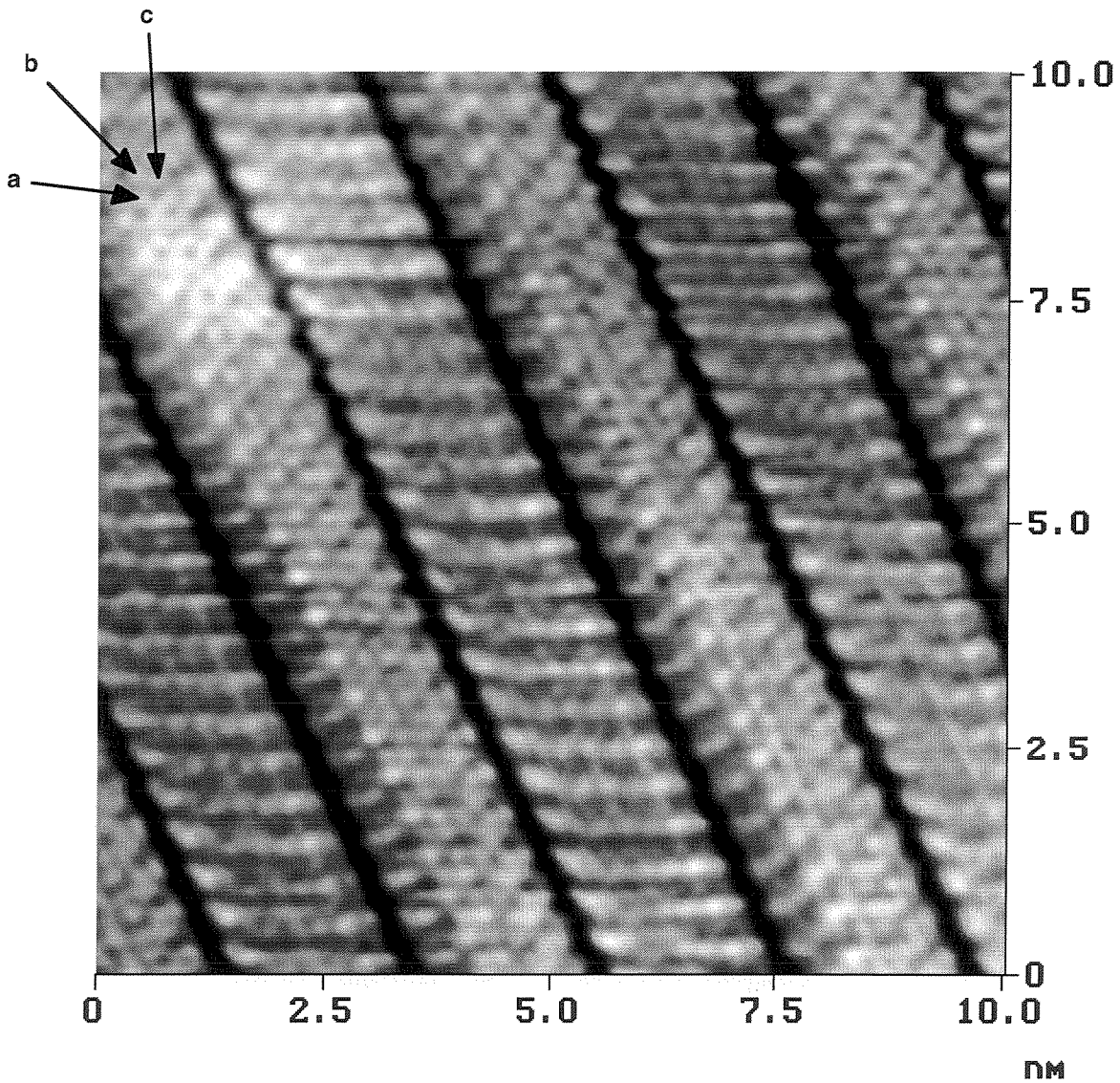

Figure 2. High-resolution STM image of tetradecanol molecules on MoS_2 (V=1.866 volts, I=300 pA). Similar to the images observed of tetradecanol molecules on graphite, the individual tetradecanol molecules contain alternating bright spots which correspond closely to the locations of the hydrogen atoms nearest the tip.

3. STM Image of an Internal Bromo Diol

The STM image of 10-bromo-1, 20-eicosanediol, $HO(CH_2)_9CHBr(CH_2)_{10}OH$, is shown in Figure 3a. The molecules appear to order in the normal herringbone fashion associated with alkanols and have a molecular packing angle $\theta=23°$. The average length of the molecules is 28.4 ± 0.2 Å, which is in excellent agreement with the length of 28.3 Å obtained from molecular modeling for the all-*trans*-conformation of this molecule. The terminal hydroxyl groups are identifiable as troughs of length 3.5 ± 0.1 Å and depth -0.61 ± 0.05 Å (black arrows), and the bright feature that is attributed to the bromine atom (white arrows) correlates well with its asymmetric location in the molecule--the feature appears 14.7 Å from one end of the molecule and 13.5 Å from the other (Figure 3a, b). For comparison, molecular modeling of an all-*trans*-conformation predicts the bromine atom to be located 14.8 Å from one end of the molecule and 13.5 Å from the other, which compares well with experimental observations. The bright feature attributed to the bromine atom has an average length of 8.8 ± 0.2 Å and height of 3.11 ± 0.05 Å.

This result is in contrast to that obtained for 12-bromo-dodecanol, where the bromine heteroatom was observed to be dark relative to the contrast of the methylene groups with an average length of 4.1 ± 0.1 Å and height of -0.41 ± 0.05 Å.[1] Calculations suggest that this is a consequence of molecular geometry,[2] and the current experiment supports this conclusion. The simulated images for a terminal bromine in the *trans* and *gauche* conformations with respect to the carbon chain is shown in Figure 4 c and d. For the *trans* conformation, the bromine atom is dark, but for the *gauche* conformation, the bromine atom is bright. These results are in excellent agreement with experimental data.

4. STM Images of Internal Hydroxy-, Methyl-, and Bromo- Functionalized Alkanes

Figure 5 presents the image of an alkane with an internal hydroxyl functionality, 18-hydroxy-pentatriacontane, $H_3C(CH_2)_{16}CHOH(CH_2)_{16}CH_3$. The molecules order in a parallel arrangement similar to other alkanes with $\theta=0°$. The average length of the

(a)

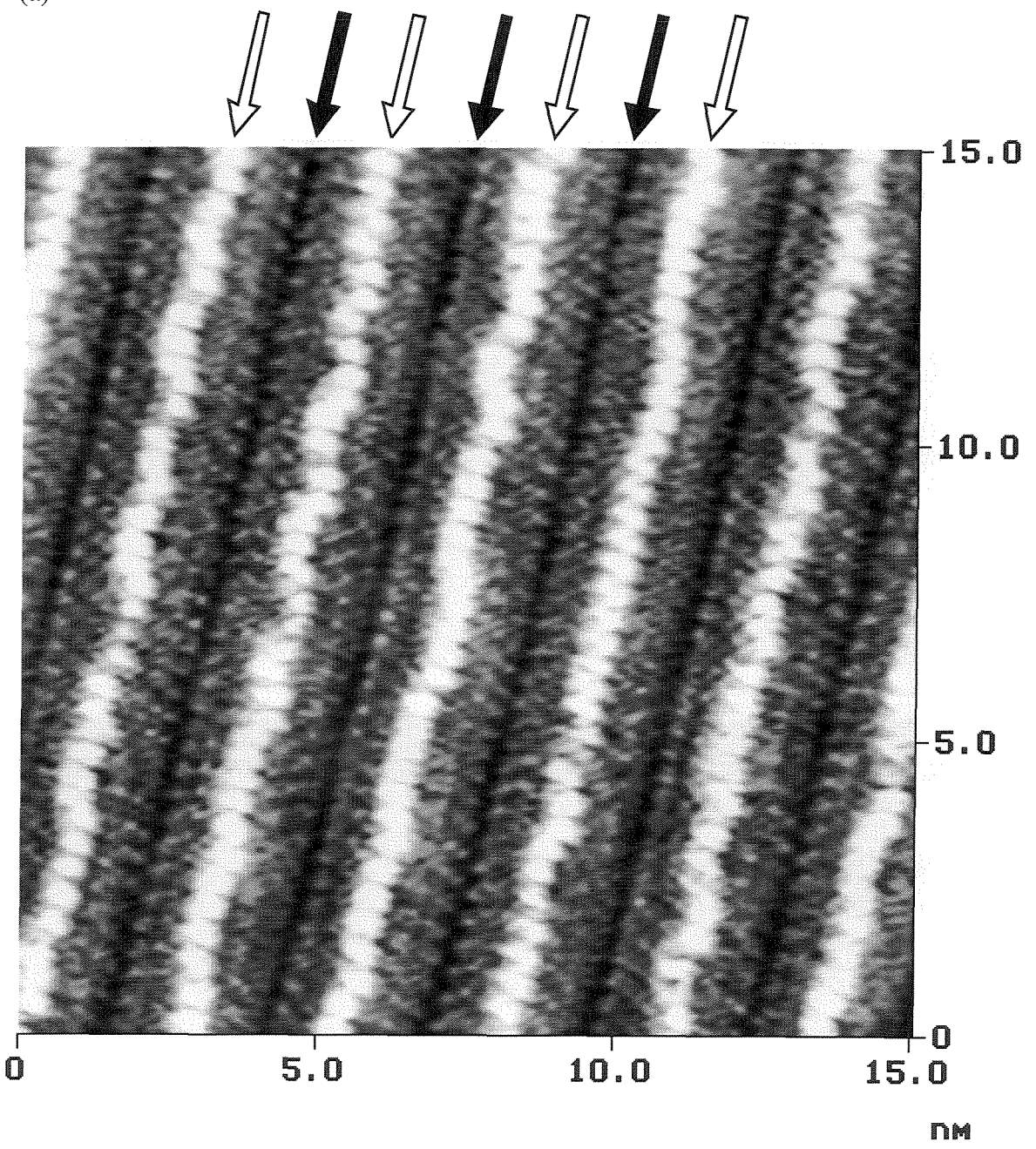

(b)

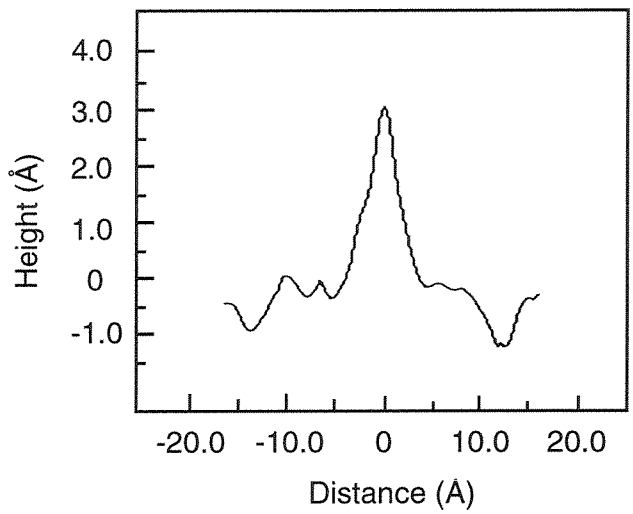

Figure 3. (a) STM image of $HO(CH_2)_9CHBr(CH_2)_{10}OH$ molecules on graphite (V=1.061 volts, I=200 pA). The black arrows indicate the dark troughs associated with the terminal hydroxyl groups, and the bright regions (white arrows) are assigned to the internal bromine atoms. (b) Single line scan along the length of the molecule; note the asymmetric location of the peak assigned to the bromine atom relative to the location of the troughs assigned to the terminal hydroxyl groups.

(A) $CH_3(CH_2)_3Br$

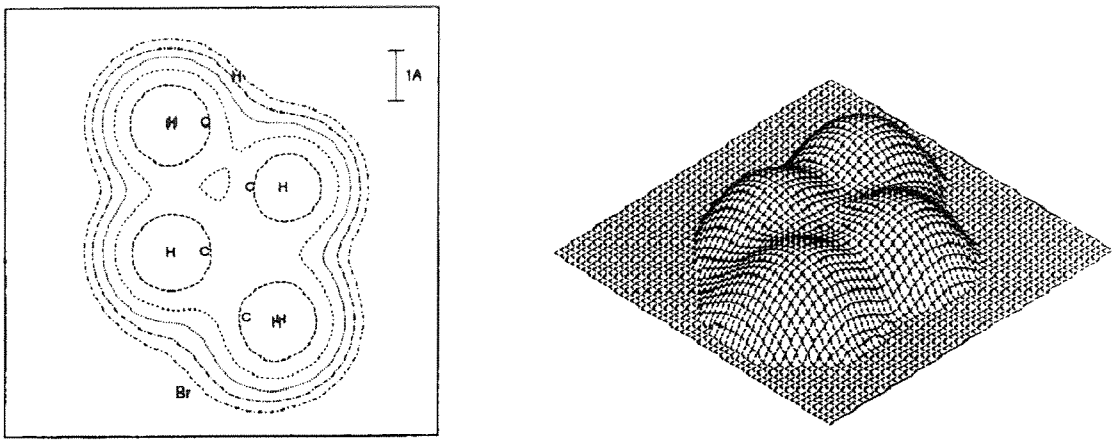

(B) $CH_3(CH_2)_3Br$ *Br* up

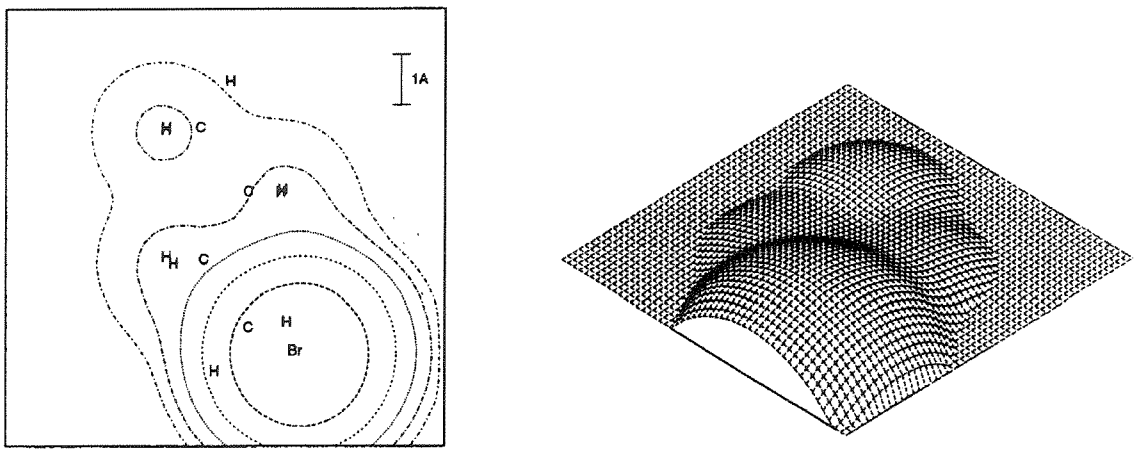

Figure 4. (a) Calculated constant current STM image for a terminal bromine atom in a position *trans* to the alkyl chain (flat on the graphite) and (b) *gauche* to the alkyl chain (pointing away from the graphite).

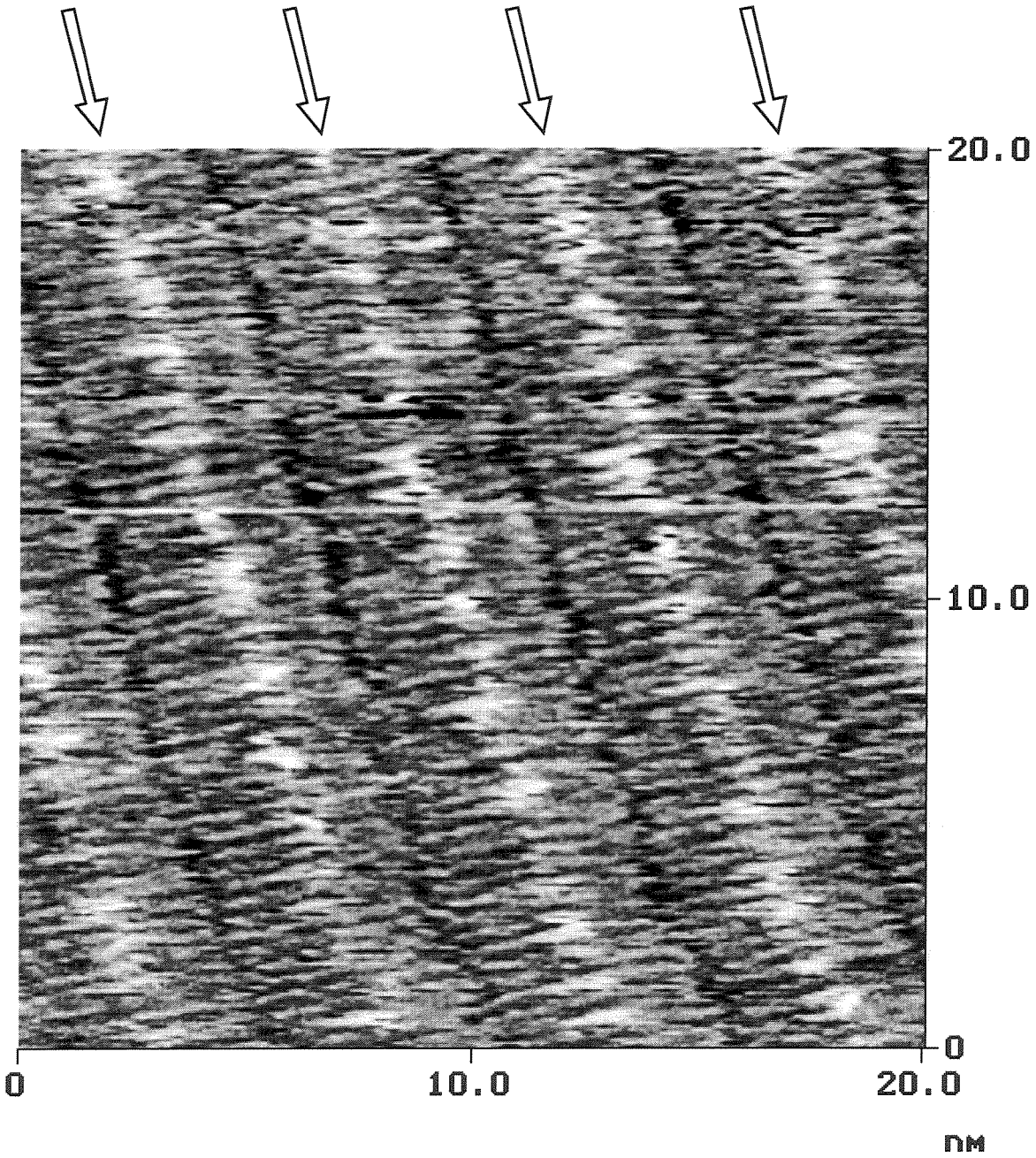

Figure 5. STM image of $H_3C(CH_2)_{16}CHOH(CH_2)_{16}CH_3$ molecules on graphite (V=1.210 volts, I=200 pA). The bright region in the middle of the molecular rows is assigned to the hyroxyl functionality (white arrows).

molecules is 46.7 ± 0.5 Å, as compared to the predicted length of 45.5 Å from molecular modeling. The hydroxyl groups (white arrows) appear bright relative to the methylene units, with an average length of 9.0 ± 0.5 Å and height 0.30 ± 0.05 Å. Similar to the bromine heteroatom discussed previously, the hydroxyl group contrast depends sensitively on its geometric orientation in the molecule. Previous experiments of alcohol functionalities that were located in terminal regions of the molecule are thought to lie in a flat orientation on the graphite surface (*trans* to the alkyl chain) and are observed to be dark in the STM images, in accord with the calculated STM images in this orientation (Figure 6a).[2] However, the calculated images of the OH group pointing away from the graphite (*gauche* to the alkyl chain) show the OH group to be slightly brighter than the surrounding methylene units (Figure 6b). This is in excellent agreement with the experimental observations.

The STM image of an alkane with an internal methyl functionality, 18-methyl-pentatriacontane, $H_3C(CH_2)_{16}CHCH_3(CH_2)_{16}CH_3$, is shown in Figure 7. The molecules pack in a different arrangement than the typical alkane molecules, presumably because of steric interactions caused by the bulky methyl functionality; however, the packing angle is the same as other alkanes with $\theta=0°$. Molecules in adjacent rows do not stagger by half a molecular width as they normally do in alkane monolayers, rather the molecules are in line across adjacent rows. The proposed packing scheme is shown in Figure 8. The average length of the molecules is 46.3 ± 0.5 Å, which is in good agreement with the expected length of 45.6 Å obtained for the all-*trans*-configuration from molecular modeling. The bright features in the image are attributed to the internal methyl groups, and have an average length of 10.9 ± 0.5 Å and height of 0.74 ± 0.05 Å.

Figure 9 presents the STM image of an alkane with an internal bromo heteroatom, 18-bromo-pentatriacontane, $H_3C(CH_2)_{16}CHBr(CH_2)_{16}CH_3$. The molecules pack in an arrangement different than the typical alkane molecules, and order in a slightly different fashion than the similar molecule $H_3C(CH_2)_{16}CHCH_3(CH_2)_{16}CH_3$ discussed above.

$CH_3(CH_2)_3OH$ Constant current

(A) Flat

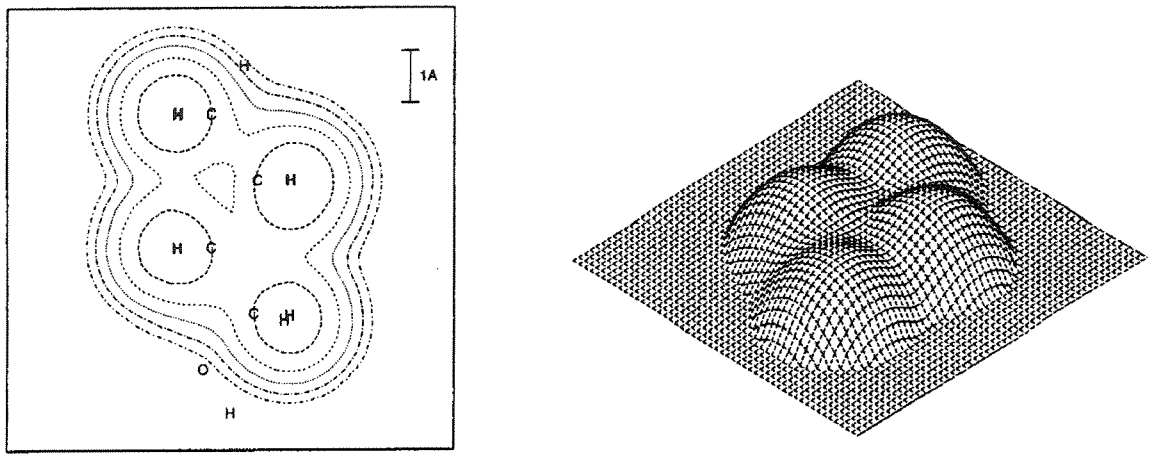

(B) $-OH$ up

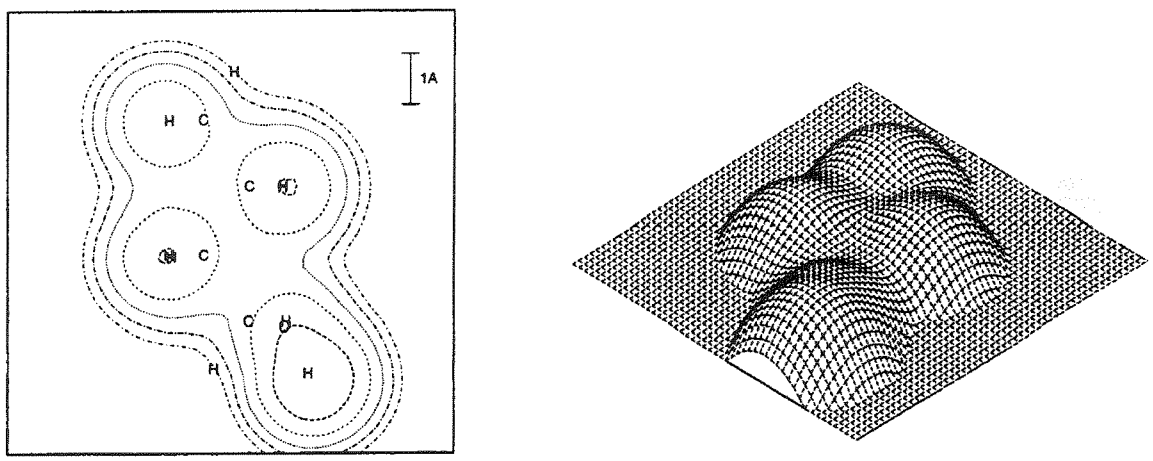

Figure 6. (a) Calculated constant current STM image for an alcohol molecule laid flat on the graphite surface with the terminal OH group in a position *trans* to the alkyl chain (flat on the graphite) and (b) *gauche* to the alkyl chain (pointing away from the graphite).

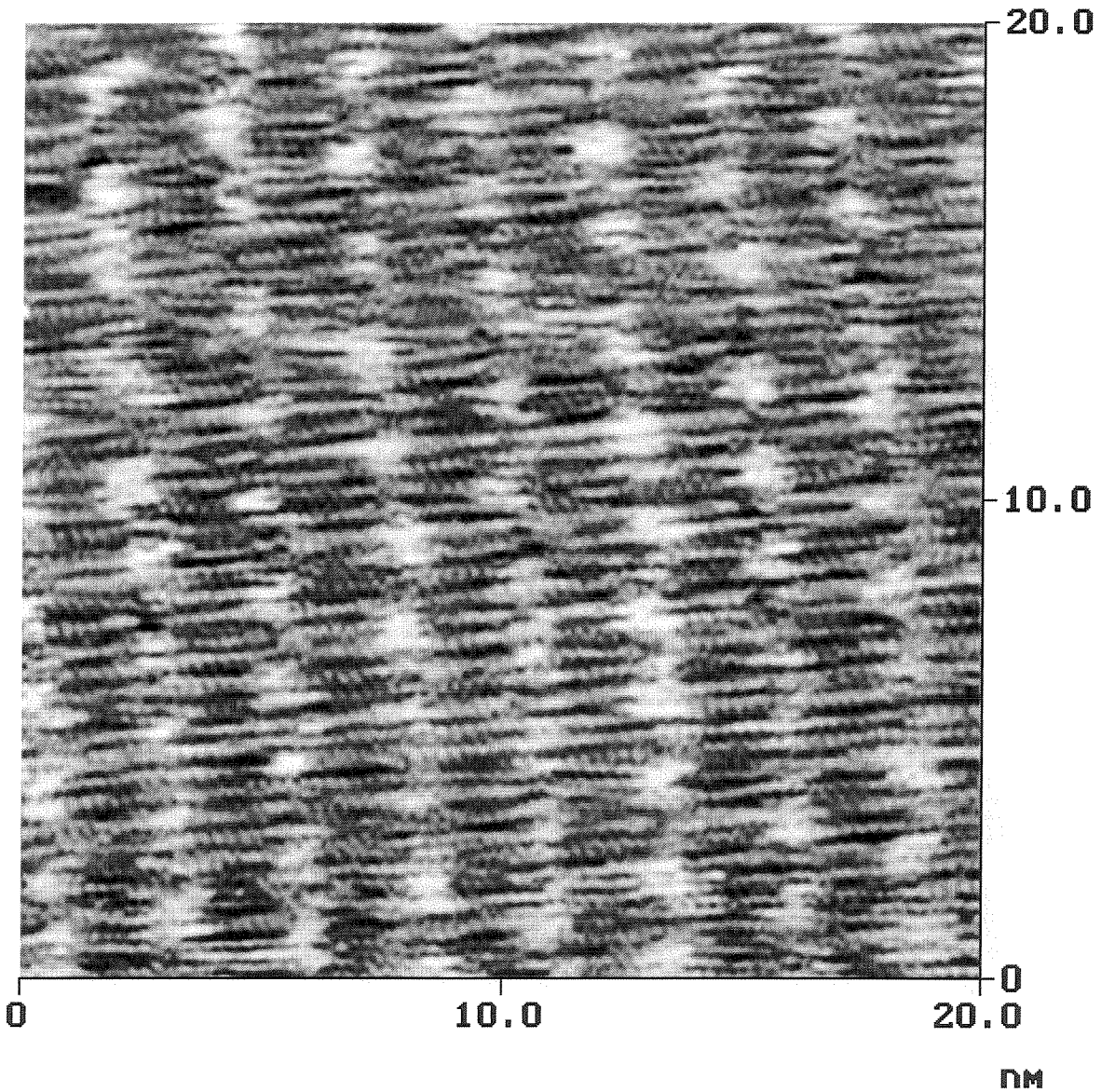

Figure 7. STM image of $H_3C(CH_2)_{16}CHCH_3(CH_2)_{16}CH_3$ molecules on graphite (V=1.351 volts, I=200 pA). The bright regions are assigned to the methyl groups.

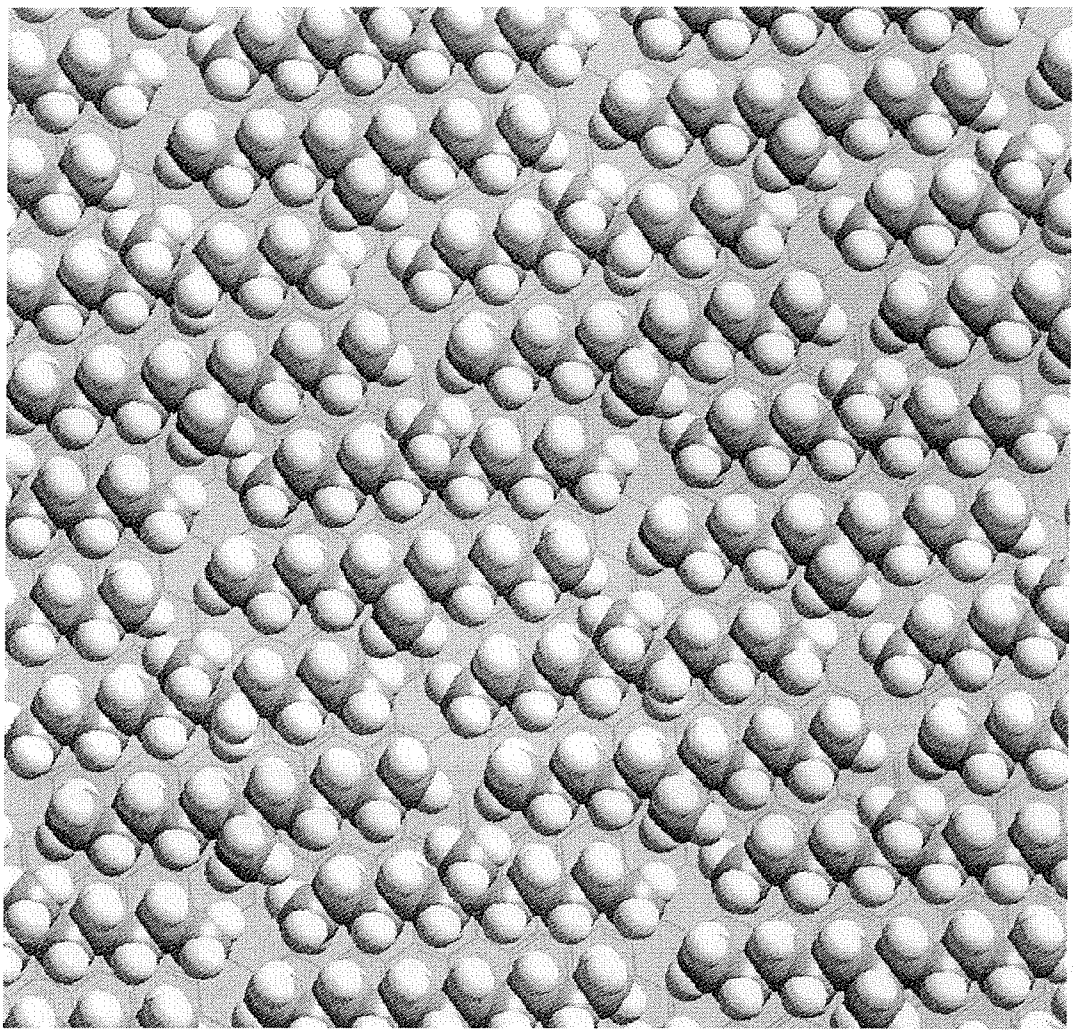

Figure 8. Schematic diagram of the proposed packing of the methyl-alkane molecules; $H_3C(CH_2)_4CHCH_3(CH_2)_4CH_3$ molecules are shown for clarity. Note that the packing angle θ is 0° in this configuration.

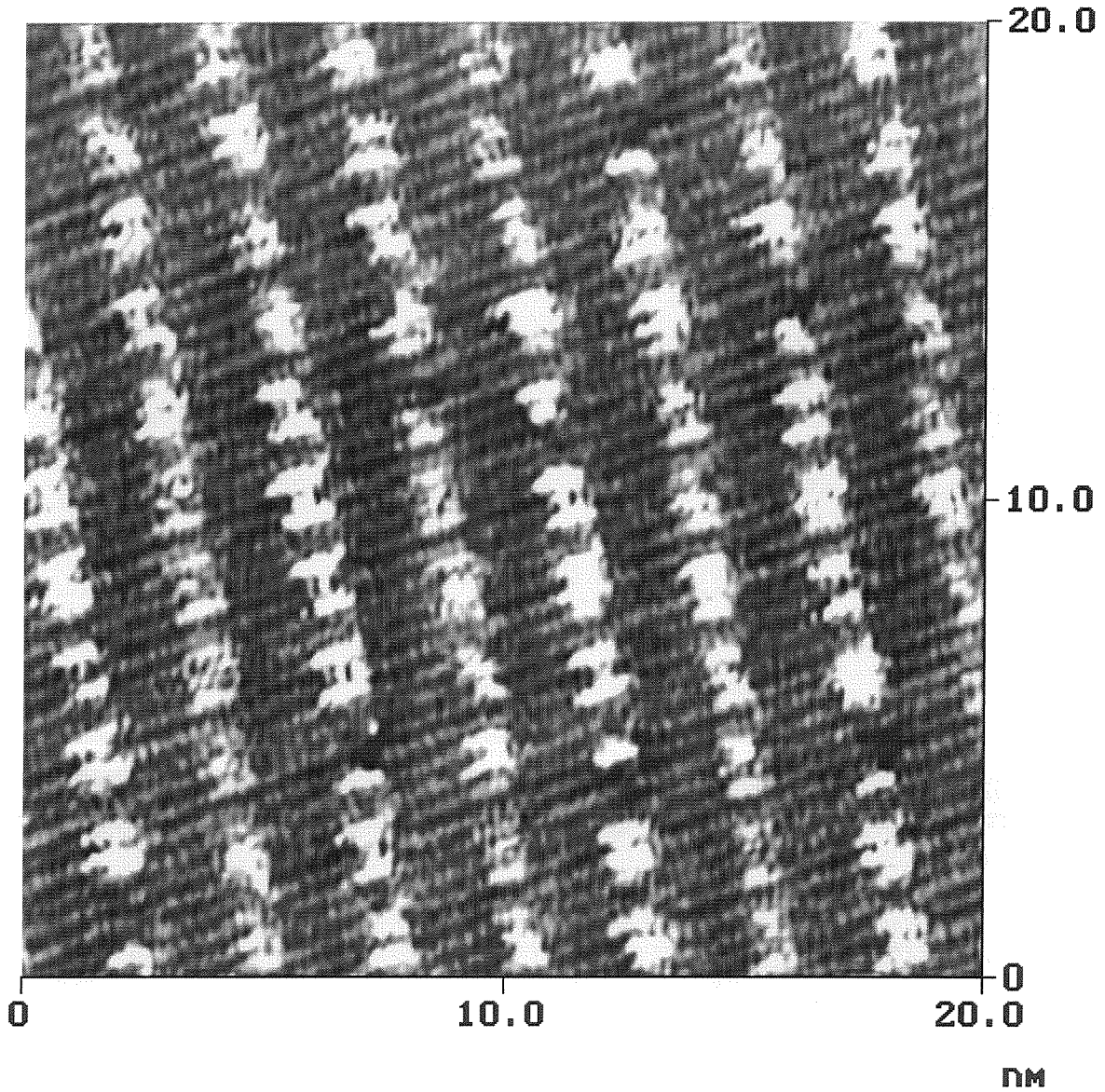

Figure 9. STM image of $H_3C(CH_2)_{16}CHBr(CH_2)_{16}CH_3$ molecules on graphite (V=1.304 volts, I=200 pA). The bright regions correspond to the bromine heteroatoms.

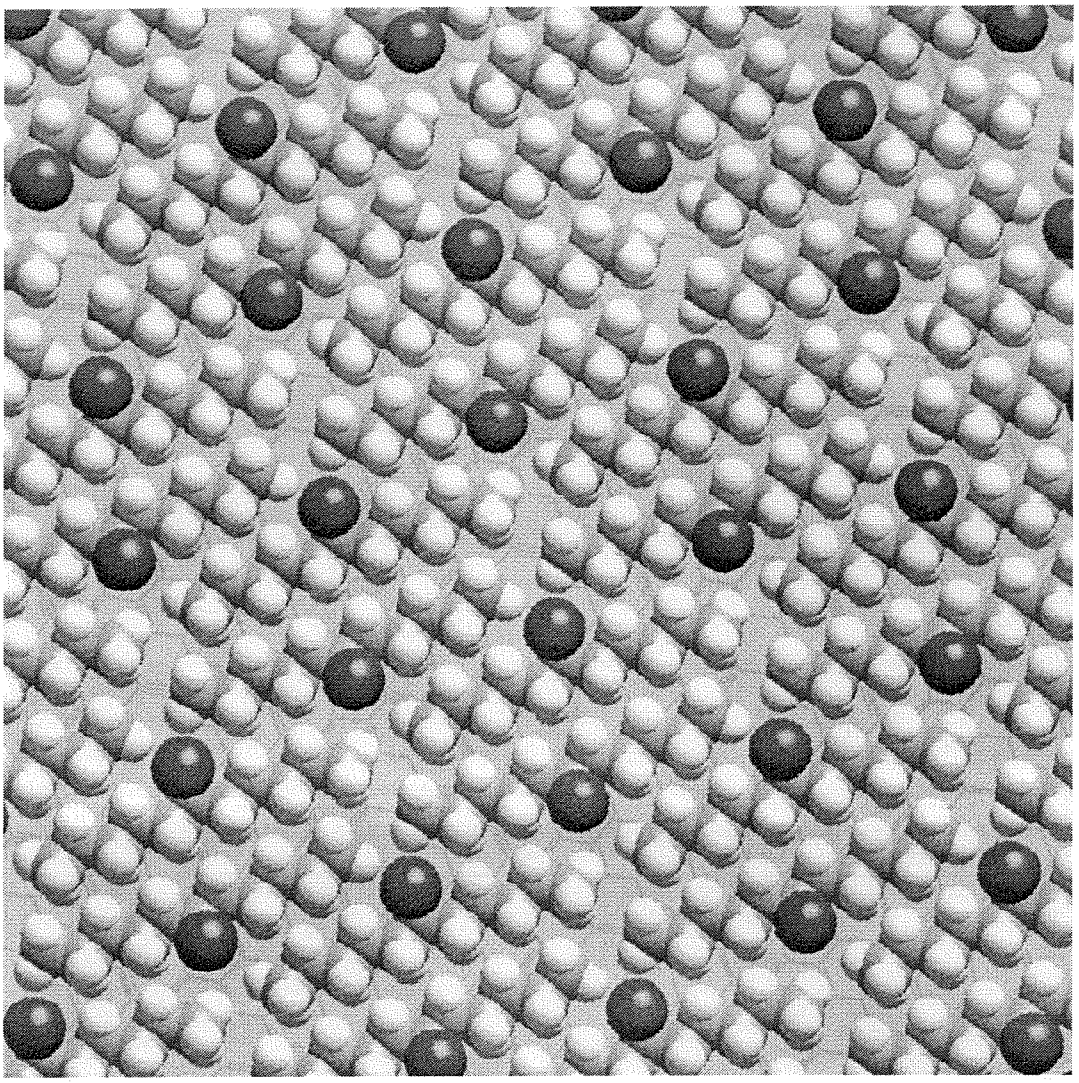

Figure 10. Schematic diagram of the proposed packing of the bromo-alkane molecules; $H_3C(CH_2)_4CHBr(CH_2)_4CH_3$ molecules are shown for clarity. Note that the packing angle θ is 8° in this configuration.

Again, this is most likely a consequence of steric interactions caused by the large bromine heteroatoms located in the center of the molecules. Like the methyl derivative, molecules in adjacent rows are in line rather than staggered by half a molecular width as they do in many of the previously observed alkane monolayers, but unlike the methyl derivative the packing angle θ is observed to be 8° rather than 0°. The proposed packing scheme is shown in Figure 10. The average molecular length is 48.8 ± 0.5 Å, compared to the expected length of 45.5 Å obtained from molecular modeling of the all-*trans*-configuration of the molecule. The bright features in the image are attributed to the internal bromine heteroatoms, and have an average length of 10.6 ± 0.1 Å and height of 2.86 ± 0.05 Å. As with the internal bromo-alkanediol, the theoretical calculations are in excellent agreement with the experimental results (Figure 4 a, b).

IV. Discussion

1. Topography and Orientation of the Alkane and Alkanol Overlayers on Graphite and MoS_2 Surfaces.

Previous arguments have been made that the hydrogen atoms on the methylene chains in alkane and alkanol monolayers dominate the observed STM spot pattern based on extended Hückel calculations and the close agreement between the measured spot distances in the STM images and those expected for the molecules adsorbed in the flat orientation.[1] The experiments presented herein provide additional support for this conclusion. First, the prediction that the spot pattern should change from an alternating to rectangular pattern for an alkyl chain adsorbed in the vertical orientation has been observed in the experiment of the allene molecule. Second, the observation of identical spot patterns and metrics for tetradecanol molecules adsorbed on graphite and MoS_2, which have lattice spacings of 2.46 Å and 3.16 Å respectively, provide further evidence that the spot patterns reflect the topography of the adsorbed molecules rather than enhanced substrate sites. These experiments also provide additional evidence that the

molecules adsorb in the flat orientation, unless forced to do otherwise, as in the case of the allene.

2. The Relative Importance of Molecular Geometry and Topography on STM Image Contrast.

Both topographic and electronic coupling factors are important in determining the STM image contrast. The observation that the contrast over the methylene units is dominated by the positions of the hydrogen atoms underscores the importance of topography in defining the image contrast of these regions. However, for some of the functional groups observed previously,[1] the electronic coupling factors appear to dominate the image contrast. For example, even though CF_3 groups are large relative to methyl groups, they appear dark because of electronic effects; that is, the occupied orbitals describing the wavefunctions in the fluorine region are computed to be very strongly bound, while the virtual orbitals are very far above the vacuum level. Similarly, the amine functionality appears bright even though it is small relative to the methyl groups. Here again, electronic effects dominate the topography--the predicted brightness is due to the fact that the HOMO, which is localized on the amine, is in the conduction region. However, for functionalities that do not have overwhelming electronic effects, orbital diffuseness and the proximity of the tip appear to play a dominant role in the STM image contrast.

This idea is reinforced in these experiments. Functionalities that do not have overwhelming electronic effects can be bright or dark because of topographic effects. For example, when the bromine atom is *trans* to the alkyl chain (therefore further from the tip), it is observed to be dark, but when it points towards the tip in the *gauche* position, the bromine atom becomes bright. The simulated and experimental results presented here for bromine are in agreement with the image-contrast reversal that has been reported for bromide groups after sustained imaging of alkyl bromide overlayers on graphite.[8]

V. Conclusions

We have provided additional evidence with the experimental images of the allene on graphite and tetradecanol on MoS_2 surfaces that topographic factors dominate the STM image contrast over the alkyl regions of the adsorbed molecules and the observed bright spots are determined by the positions of the hydrogen atoms on the methylene units of the alkyl chains. Furthermore, the simple model based on perturbation theory was used to successfully predict and understand the effects of different molecular orientations on STM image contrast. Although the theoretical predictions are mainly qualitative, they have provided significant insight into understanding and predicting the experimental STM images of a wide range of functionalized alkanes and alkanols adsorbed on graphite.

VI. Acknowledgments

We acknowledge the NSF, grants CHE-9202583 (NSL), CHE-95-22179 (WAG), and ASC-92-17368 (WAG) for partial support of this work.

VII. References

(1) Claypool, C. L.; Faglioni, F.; Goddard, W. A., III; Gray, H. B.; Lewis, N. S.; Marcus, R. A. *J. Phys. Chem. B* **1997**, *101*, 5978.

(2) Faglioni, F.; Claypool, C. L.; Lewis, N. S.; Goddard, W. A., III *J. Phys. Chem. B* **1997**, *101*, 5996.

(3) Bard, A. J.; Chang, H. J. Am. Chem. Soc. **1990**, *112*, 4698.

(4) Brummond, K. M.; Dingess, E. A.; Kent, J. L. *J. Org. Chem.* **1996**, *61*, 6097.

(5) Gilchrist, J. le G. *Chem. Phys.* **1987**, *115*, 307-317.

(6) Zambelli, A.; Gatti, G. *Macromolecules.* **1978**, *11*, 485-489.

(7) *CRC Handbook of Chemistry and Physics*, Weast, R. C.; Lide, D. R.; Astle, M. J.; Beyer, W. H., ed.; CRC Press: Boca Raton, 1989.

(8) Venkataraman, B.; Flynn, G. W.; Wilbur, J. L.; Folkers, J. P.; Whitesides, G. M. *J. Phys. Chem.* **1995**, *99*, 8684. Cyr, D. M.; Venkataraman, B.; Flynn, G. W.; Black, A.; Whitesides, G. M. *J. Phys. Chem.* **1996** *100*, 13747. Cyr, D. M.; Venkataraman, B.; Flynn, G. W. *Chem. Mater.* **1996** *8*, 1600.